Regulation des Energiehaushalts von Kleinsäugern unter besonderer Berücksichtigung saisonaler Stoffwechseladaptionen des Dsungarischen Zwerghamsters, *Phodopus sungorus*.

Dissertation

zur

Erlangung des Doktorgrades

der Naturwissenschaften

(Dr. rer. nat.)

dem Fachbereich Biologie

der Philipps-Universität Marburg

vorgelegt von

Luzie Julia Braulke

aus Scherzingen (Schweiz)

Marburg/Lahn 2010

Diese Arbeit wurde vom Fachbereich Biologie der Philipps-Universität Marburg als Dissertation am 12.10.2010 angenommen.

Erstgutachter: Herr Prof. Dr. Gerhard Heldmaier

Zweitgutachter: Herr Dr. Christian Wegener

Tag der mündlichen Prüfung am 05.11.2010

INHALTSVERZEICHNIS

1. ZUSAMMENFASSUNG

1.1. Einleitung

Vögel und Säugetiere sind zur endogenen Wärmebildung (Endothermie) befähigt. Dies erlaubt ihnen, ihre Körpertemperatur weitgehend unabhängig von der Außentemperatur auf konstant hohem Niveau zu halten, was zu einer optimalen Reaktionskinetik verschiedenster Stoffwechselprozesse und somit zu konstant hoher Aktivität und Leistungsfähigkeit führt. Dieser Vorteil der Endothermie wird allerdings mit einem sehr hohen Energiebedarf bezahlt, was eine präzise Regulationsfähigkeit des Energiehaushalts zugunsten einer optimierten Energieausbeute unabdingbar macht. Wenngleich sich im letzten Jahrzehnt immenses Wissen über die den Energiehaushalt kontrollierenden, komplexen Regelkreise zwischen peripheren Hormonen und dem zentralen Nervensystem (ZNS) angesammelt hat, stehen wir trotzdem erst am Beginn der Aufklärung dieser komplexen Zusammenhänge.

Zur weiteren Charakterisierung dieser Zusammenhänge eignen sich Tiere mit ausgeprägter Saisonalität, da diese in der Regel natürliche Änderungen des Energiestoffwechsels beinhaltet. Besonders markant sind diese Anpassungen in gemäßigten und arktischen Klimazonen, die durch starke jahreszeitliche Schwankungen der Temperatur und des Nahrungsangebotes gekennzeichnet sind und somit die Befriedigung eines hohen Energiebedarfs schwierig werden lassen. Diese Problematik wird durch energiesparende Maßnahmen gelöst, die sich in enorm vielfältiger saisonaler Anpassungsfähigkeit von Verhalten, Morphologie und Physiologie äußern.

Während viele Vögel einer saisonal unwirtlichen Situation durch Migration „entfliegen“ können, sind die meisten Säuger saisonal gezwungen ihren Energiebedarf adäquat zu adaptieren oder gegebenenfalls zu reduzieren. Dies gelingt ihnen zum Beispiel durch eine Reduktion des Wärmeverlustes an die Umgebung durch verbesserte Fellisolation oder die Einstellung der energetisch aufwendigen Reproduktion und Aufzucht der Jungen im Winter. Das wohl wichtigste und gleichzeitig zuverlässigste Umweltsignal für die Steuerung der meisten saisonalen Anpassungen ist die Photoperiode, d.h. die Änderung der Tageslichtlänge. Bei vielen Tierarten werden saisonale Rhythmen und physiologische Anpassungen ausschließlich durch die Veränderungen der Tageslichtlänge reguliert (Bradshaw & Holzapfel, 2010).

Eine erhebliche Rolle in der saisonalen Regulation des Energiehaushaltes spielt die saisonale Körpergewichtsregulation. Während die meisten größeren Säuger eine Gewichtszunahme durch die Anlage von Energiespeichern in Form von Fettdepots für die kalte, nahrungsarme Zeit zeigen, ist bei den meisten winteraktiven Kleinsäugern, die weniger als 1 kg wiegen, ein gegenteiliges Phänomen zu beobachten (Heldmaier, 1989). Die Körpermasse steigt

mit länger werdenden Tagen im Sommer und sinkt mit kürzer werdenden Tagen im Winter. Die Körpergewichtsreduktion im Winter scheint zunächst keine sinnvolle Maßnahme zur Energieeinsparung zu sein, da die in Relation zum Körpergewicht steigende Körperoberfläche eine erhöhten Wärmeverlust zur Folge hätte und damit einen relativ höheren Energieumsatz erforderte. Betrachtet man dieses Phänomen allerdings am Beispiel des saisondimorphen Dsungarischen Zwerghamsters, so zeigt sich, daß die vermeintlich steigende Wärmeabgabe durch das ungünstigere Oberflächen-Volumen-Verhältnis bereits mit einer höheren Fellisolation kompensiert wird. Auf diese Weise sinkt der Gesamtenergiebedarf des Tieres durch die Reduktion des bei Kältebelastung zu erwärmenden Gewebes.

Saisonale Änderungen des Körpergewichts beinhalten sowohl Änderungen im Körperfettgehalt, als auch in fettfreier Körpermasse (Wade & Bartness, 1984; Klingenspor et al., 2000). Die regulativen Mechanismen hinter diesem Phänomen sind jedoch nur teilweise bekannt. Die Entdeckung des Leptins, einem Hormon, welches von weißen Fettgewebszellen produziert wird, hat das Wissen über die Körpergewichtsregulation erheblich vorangebracht. Es wird proportional zum Körperfettgehalt produziert und signalisiert dem ZNS den energetischen Zustand des Körpers. Die Leptinrezeptoren sind im Hypothalamus lokalisiert und die Stärke des Leptinsignals wird dann über die Aktivität von Orexigenen bzw. Anorexigenen (Neuropeptide, die die Nahrungsaufnahme regulieren) in erhöhte oder gesenkte Futteraufnahme umgesetzt (Mercer et al., 1997; Reddy et al., 1999).

Mit dieser Gegebenheit wäre zu erwarten, daß höhere Leptinlevel in „fetteren“ Sommerhamstern zu einer Senkung der Futteraufnahme und einem gesteigerten Verbrauch der Fettreserven führen, während die niedrigen Leptinlevel in schlanken Wintertieren eine gesteigerte Futteraufnahme und einen reduzierten Energieverbrauch zur Folge haben. Das Gegenteil ist der Fall, was sich unter anderem mit einer saisonal unterschiedlichen Leptinsensitivität erklären läßt (Mercer & Tups, 2003; Adam & Mercer, 2004). So haben kurztagakklimatisierte Hamster eine hohe Leptinsensitivität, während langtagakklimatisierte Hamster unempfänglich für Leptin sind.

Die Gewichtsreduktion der Kleinsäuger im Winter ist bis zu 30% auf die fettfreie Trockenmasse (lean mass), die auch die Muskelmasse beinhaltet, zurückzuführen (Niggemann, 1998). Die endokrine Kontrolle saisonaler Änderungen der fettfreien Gewebe ist gänzlich unbekannt. Hierbei könnte Myostatin eine Rolle spielen. Myostatin, auch bekannt als GDF-8 (growth and differentiation factor-8), ist ein Mitglied der TGF-β-Superfamilie. Es ist ein evolutiv stark konserviertes Hormon, wird im Skelettmuskel produziert, zirkuliert im Blut und inhibiert das Muskelwachstum und die Muskelzelldifferenzierung in konzentrationsabhängiger Weise

(Matsakas & Diel, 2005). Störungen des Myostatin-Signalwegs oder des Gens selbst führen zu einer überdimensionalen (~200%) Muskelentwicklung in Form von Hyperplasie, einer Zunahme der Muskelzellzahl, und Hypertrophie, einer Zunahme des Zellvolumens (Lee & McPherron, 2001).

Eine andere, unter Kleinsäugern weit verbreitete, saisonale Adaption, die der saisonalen Energieeinsparung dient, ist die Fähigkeit, energetisch rentable, „torpide“ Zustände, wie Winterschlaf oder täglichen Torpor, zu erreichen. Diese Zustände zeichnen sich durch einen massiv reduzierten Stoffwechsel mit einhergehend reduzierter Körpertemperatur aus (Heldmaier et al., 2004). Während die hypometabolen und hypothermen Phasen des Winterschlafs für mehrere Tage bis Wochen andauern, beschränken sich die des täglichen Torpors in der Regel auf einige Stunden während der circadianen Ruhephase der Tiere. Die Stoffwechselrate torpider Tiere erreicht Werte, die um 60 bis 90 % unter dem Basalstoffwechsel liegen (Heldmaier et al., 2004). Sind bei anhaltenden torpiden Phasen die Glukosespeicher erschöpft, wird der Stoffwechsel auf Lipidmetabolismus umgestellt (Heldmaier et al., 1999), was sich dann in einer Reduktion des respiratorischen Quotienten äußert. Entgegen der veralteten Annahme, daß der niedrige Stoffwechsel eine passive Folge der niedrigen Körpertemperatur sei, sprechen viele Befunde für eine aktive Inhibition des Stoffwechsels. So findet beispielsweise die rasche Reduktion des Stoffwechsels bei Eintritt in den torpiden Zustand schon vor der Reduktion der Körpertemperatur statt (Elvert & Heldmaier, 2005). Die neuronalen oder endokrinen Mechanismen, die das Auslösen und den Verlauf des täglichen Torpors kontrollieren, sind gänzlich unbekannt.

Vermutlich spielt das autonome Nervensystem eine entscheidende Rolle bei der Regulation des Torporverhaltens. Bei Eintritt in den Torpor ist, parallel zur Stoffwechselreduktion und vor erkennbarer Reduktion der Körpertemperatur, eine starke Drosselung der Herz- und Atemfrequenz unter Erhalt der Vagus-bedingten, natürlichen Herzarrhythmien und ventilatorischen Tachykardien zu beobachten (Milsom et al., 1999; Lyman & O’Brien, 1963; Morhardt, 1970; Strumwasser, 1960). Dies spricht für eine gesteigerte Aktivität des parasympathischen Tonus und eine reduzierte sympathische Aktivität während des Eintritts in den torpiden Zustand. Das Erwachen aus dem Torpor (Arousal) scheint dagegen auf einer Aktivierung des Sympathikus zu beruhen, da die Herz- und Atemfrequenz und die endogene Wärmebildung während des Arousals innerhalb kürzester Zeit auf Spitzenwerte gesteigert werden, während die Körpertemperatur noch weit unter 20°C liegen kann (Heldmaier et al., 2004).

Einen weiteren Ansatz zur Untersuchung der Regulation des Torpors bietet ein neuentdecktes, endogen vorkommendes Schilddrüsenhormonderivat, das 3-Iodothyronamin (T1AM). Bei Mäusen löst es nach Injektion torporähnliche Reaktionen, wie Hypothermie, Bradykardie und den Verlust der Herzschlagvariabilität, aus (Scanlan et al., 2004). Man vermutet, daß das T1AM aus der enzymatischen Deiodierung und Decarboxylierung des Thyroxins hervorgeht. In vivo konnte es in allen bislang untersuchten Säugern, wie Meerschweinchen, Ratten, Mäusen und Menschen, sowie allen untersuchten Geweben, wie Herz, Leber, Gehirn und Blut detektiert werden. Diese Verbreitung in Spezies und Organen verspricht eine fundamentale Funktion in der Physiologie der Säugetiere.

Ein weiterer Regelmechanismus für die Energiebalancierung von Säugern verspricht das Endocannabinoidsystem zu sein. Neben vielfältigen Funktionen, wie z.B. in der Schmerzempfindung, bei Lern- und Gedächtnisprozessen und in Emotionalität, ist es auch bei der Kontrolle der Nahrungsaufnahme und Nahrungsverwertung beteiligt (Piomelli, 2003; Steiner & Lutz, 2006; Moreira & Lutz, 2008). Der Cannabinoidrezeptor 1 (CB1) gehört im Gehirn zu den am stärksten exprimierten Rezeptoren. Die Expression ist aber nicht auf das Gehirn beschränkt; auch periphere Organe, wie Muskel, Leber oder Fettgewebe, exprimieren diesen Rezeptor zu einem zwar geringeren, aber vermutlich funktionell wichtigen Maß. Ein CB1-Knockout führt bei Mäusen zu reduziertem Körpergewicht und Körperfettgehalt und einer Adipositas-Resistenz (Cota et al., 2003; Ravinet-Trillou et al., 2004). Die Art und Weise, wie das Endocannabinoidsystem in die Regulation des Essverhaltens und der Energiebalance eingreift, ist bislang unklar. Da der CB1-Rezeptor sowohl im zentralen Nervensystem als auch in nicht-neuronalen peripheren Organen exprimiert ist (z.B. in Leber, Fettgewebe, Pankreas), stellt sich die Frage nach der Bedeutung dieses Rezeptors in den verschiedenen Organsystemen.

1.2. Zielsetzung

Ziel dieser Arbeit war es, verschiedene Mechanismen, die an der Regulation des Energiehaushaltes von Kleinsäugern beteiligt sind, zu finden und ihre Rolle bzw. ihre Funktionalität zu charakterisieren:

- Welchen Anteil haben die verschiedenen Organsysteme bei der saisonalen Körpergewichtsentwicklung und welche Rolle spielt dabei die Muskulatur als Teil der fettfreien Trockenmasse?

- Wird das die Muskelmasse regulierende Hormon Myostatin saisonal reguliert und nimmt somit Einfluß auf die saisonale Körpergewichtsentwicklung?

- Liegt der Senkung der Nahrungsaufnahme, die einen erheblichen Anteil an der Körpergewichtsreduktion im Winter hat, eine saisonal differentielle Modifikation anorexigener Neuroendokrine, wie dem Proopiomelanocortin, zugrunde?

- Kann das endogen vorkommende 3-Iodothyronamin als *das* torporeinleitende Signal in Betracht gezogen werden, ist es also in der Lage, eine Stoffwechseldepression zu induzieren, die der eines natürlichen Torpors entspricht? Wie läßt sich die beobachtete, durch Thyronamin ausgelöste Hypothermie erklären?

- Besteht eine Notwendigkeit parasympathischer und/oder sympathischer Aktivitäten für das Auftreten natürlicher hypometaboler Zustände? Ist also einer der vegetativen Zweige essentiell für das Abspielen eines natürlichen Torporbouts?

- Welche Bedeutung haben die zentralen Endocannabinoidrezeptoren für die bereits bekannte Einflußnahme des Endocannabinoidsystems auf Körpergewicht, Futteraufnahme und diätinduzierte Adipositas? Welche Mechanismen und Signalwege stehen hinter den Auswirkungen des Endocannabinoidsystems auf den Energiehaushalt?

1.3. Methoden

Versuchstiere und Haltungsbedingungen

Phodopus sungorus. Die in dieser Arbeit verwendeten Dsungarischen Zwerghamster, *Phodopus sungorus sungorus* (PALLAS, 1773), stammten aus der institutseigenen Zucht der Philipps-Universität Marburg bei konstanter Umgebungstemperatur von 23±1°C und natürlicher Photoperiode (Marburg 50°49' N) oder künstlich langer Photoperiode (L:D 16:8). Jungtiere wurden in einem Alter von 3 Wochen einzeln in Makrolonkäfigen Typ II (16 cm × 21 cm × 13 cm) mit Holzspaneinstreu gehalten und erhielten Hamsterzuchtdiät (ssniff® Ha) und Wasser ad libitum.

Zur Untersuchung photoperiodisch bedingter physiologischer Adaptionen, wurden Hamster im Alter von 2-3 Monaten verschiedenen Lichtverhältnissen, nämlich künstlichem Kurztag (L:D 8:16), künstlichem Langtag (L:D 16:8) oder natürlicher Photoperiode (Marburg 50°49' N), ausgesetzt. Bei jeder versuchsbedingten Aufteilung von Tieren in verschiedene Gruppen wurde auf eine ausgewogene Geschlechterverteilung und auf ein ähnliches Alter geachtet.

Mus musculus. Bei allen verwendeten Mäusen handelte es sich um ausschließlich männliche Tiere. C57BL/6-Mäuse wurden über Charles River Laboratories (Sandhofer Weg 7, 97633 Sulzfeld) bezogen. *CB_1*-KO und CaMK-*CB_1*-KO-Mäuse (Deletion des CB_1 Rezeptors der Ca^{2+}/Calmodulin-Kinase-IIα-exprimierenden Hauptneurone des Vorderhirns) und ihre Wildtyp-Wurfgeschwister mit dem genetischen Hintergrund C57BL/6 stammten aus der institutseigen Erzeugung und Zucht (Marsicano et al., 2002; Marsicano et al., 2003) der Universität Bordeaux (NeuroCentre Magendie, U862 INSERM Université Bordeaux 2, Bordeaux, Frankreich).

Alle Mäuse wurden einzeln in Makrolonkäfigen Typ II (16 cm × 21 cm × 13 cm) mit Holzspaneinstreu bei konstanter Umgebungstemperatur von 24±1°C und konstanten Lichtverhältnissen (L:D 12:12) gehalten und erhielten Futter (ssniff® M-Z, ssniff Spezialdiäten GmbH, Soest, Deutschland; oder Piccioni-48 vs. Piccioni-HFD, „Laboratorio Dott. Piccioni", Milano, Italy) und Wasser ad libitum.

Messung der Körperzusammensetzung

Zur Erfassung der Körperzusammensetzung wurden die Tiere dem noninvasiven DEXA-Verfahren (Dual Energy X-Ray Absorbtiometry) mittels eines Lunar PIXImus Mouse Densitometers (GE Medical Systems Deutschland GmbH & CoKG, Solingen) unterzogen. Die Datenerhebung und Analyse erfolgt dabei automatisch. Um völlige Bewegungslosigkeit während

der Aufnahme zu gewährleisten, wurden die Tiere für wenige Minuten mit Inhalationsnarkotikum 1-4 Vol% Isofluran (Forene, Abbott, Wiesbaden, Deutschland) betäubt.

Erfassung der Körpertemperatur

Zur Erfassung der Körperkerntemperatur (T_b) wurden den Versuchstieren eingekapselte, wachsummantelte und kalibrierte Temperatur-Transmitter (Mini-Mitter, Model X, Sunriver, Oregon, USA) intraperitoneal implantiert. Die Implantation erfolgte unter Anästhesie durch Ketaminhydrochlorid (Ketavet, Pharmacia Upjohn GmbH, Erlangen, Deutschland, 50 $mg*kg^{-1}$) und 1-2% Isofluran (Forene, Abbott, Wiesbaden, Deutschland). Die im Mittelwellenbereich gesendeten, temperaturabhängigen Transmittersignale (T (°C) = A+B* log (t)) wurden mit Hilfe eines Radio-Receiver-Systems (ZN 416 E, AM-Radio-Receiver, Gehäuse Dp8) unter den Tierkäfigen kontinuierlich detektiert und anschließend durch ein Mikrocomputersystem in Temperaturwerte umgewandelt (Heldmaier & Ruf, 1992).

Erfassung der Stoffwechselrate

Die Stoffwechselrate (VO_2) wurde durch die indirekte Kalorimetrie ermittelt (dabei wird der tatsächliche Energieumsatz indirekt über den Sauerstoffverbrauch und die Kohlendioxidabgabe eines Tieres gemessen). Während der Messung wurden die Tiere einzeln in geschlossenen Makrolonkäfigen Typ II (s.o.) innerhalb eines Klimaschranks gehalten, der die Einstellung konstanter Lichtverhältnisse (L:D 16:8; L:D 12:12; L:D 8:16) und Außentemperaturen erlaubt. Der Luftfluß durch die Tierkäfige wurde auf ca. 45 $l*h^{-1}$ eingestellt und kontinuierlich mit Flußmessern (FM 360, Tylan, München, Deutschland) überwacht. Die zu messende Luft wurde gefriergetrocknet (M&C Cooler, EPC, Ratingen, Deutschland) und an die Analysatoren weitergeleitet. Der O_2-Verbrauch wurde mittels eines Ein-Kanal-O2-Analysators (S3AII, Ametek, Sunnyvale USA) und die CO_2-Produktion mittels eines 2-Kanal-CO2-Analysators (UNOR 6N, Maihak AG, Hamburg, Deutschland) bestimmt. Dabei wurde die Meßluft konstant mit einer Referenzluft aus dem Klimaschrank verglichen. Ein computergesteuertes Magnetventilsystem erlaubte die simultane Messung von bis zu 6 Käfigen. Ein leerer Käfig diente immer als Nullpunktausgleich. Der Energieumsatz eines Tieres wurde dann nach folgender Gleichung berechnet: VO_2 [ml O_2*h^{-1}] = Δ Vol% O_2 × Flow [$l*h^{-1}$] ×10. Der RQ ergibt sich aus dem Verhältnis zwischen produziertem CO_2 zum konsumierten O_2.

Ketonkörperanalyse des Urins

Zur Urinsammlung wurden die Versuchstiere in speziell angefertigten Stoffwechselkäfigen (Ø18 cm × 12 cm), die Teil eines automatischen Versuchsaufbaus waren, gehalten (Stieglitz et al., 1995). Die Käfige waren mit einem Plastikgitterboden mit einer Maschenweite von 4×4 mm und mit einem Plastikhäuschen (Ø6 cm × 10 cm) als Rückzugsmöglichkeit ausgestattet. Der Zugang zu Futter und Wasser war konstant gewährleistet. Zusätzlich bekamen die Tiere Gurke ad libitum, um die Harnproduktion zu stimulieren. Der Urin lief über ein Trichtersystem ab und wurde in 4-Stunden-Intervallen abgesogen. Die Urinproben wurden für 5 Minuten bei 2500g und 25°C zentrifugiert und der Ketonkörpergehalt mit Ketostix (Bayer HealthCare, Mishawaka, USA) bestimmt.

Kälteexposition

Zur Bestimmung der Thermogeneseleistung der CB_1-KO-, CaMK-CB_1-KO- und C57BL/6-Mäuse wurden die Stoffwechselrate und die Körpertemperatur unter Kälteexposition bestimmt. Diese Analyse erfolgte zunächst bei einer 24-stündigen Außentemperatur von 15°C. Eine Woche später erfolgte die Kurzzeitexposition von einer Stunde bei 6°C Außentemperatur. Der Zugang zu Futter und Wasser war konstant gewährleistet.

Pharmazeutika

6-Hydroxydopamin (6-OHDA). Zur Inhibition des sympathischen Nervensystems Dsungarischer Zwerghamster wurde 6-OHDA (Sigma (Fluka), Deisenhofen, Deutschland) einmalig in einer Dosis von 200mg/kg intraperitoneal injiziert. Das 6-OHDA wurde in physiologischer Kochsalzlösung (0.9% NaCl, pH 7,4) gelöst und in einem Endvolumen von 100µl appliziert. Reine physiologische Kochsalzlösung (0.9% NaCl, pH 7,4, 100µl) diente als Kontrollinjektion.

Atropin. Zur Inhibition des parasympathischen Nervensystems Dsungarischer Zwerghamster wurde Atropin (Sigma (Fluka), Deisenhofen, Deutschland) verabreicht. Dies erfolgte durch die Implantation einer speziellen Atropin-haltigen (0.25mg) Tablette mit einer biologisch abbaubaren Matrix, die eine konstante Freisetzung des Atropins über 21 Tage gewährleistet (≈0,48 mg/kg/Tag) (Innovative Research of America, Sarasota, FL). Die Tablette wurde mit einer Kanüle (10-gauge trochar, Innovative Research of America) subkutan, lateral des Nackens injiziert. Eine Placebotablette diente als Kontrollbehandlung.

3-Iodothyronamin (T1AM). Zur Beschreibung der physiologischen Eigenschaften des neuentdeckten Schildrüsenhormonderivats, T1AM (Scanlan et al., 2004; Departments of Pharmaceutical Chemistry and Cellular & Molecular Pharmacology, University of California-San Francisco, San Francisco, California, USA), wurde es winter- und sommerakklimatisierten Hamstern sowie Mäusen einmalig intraperitoneal injiziert (50mg/kg). Dafür wurde das T1AM in 60% Dimethylsulfoxid (DMSO) und 40% physiologischer Kochsalzlösung (0.9% NaCl, pH 7,4) gelöst und in einem Gesamtvolumen von 100µl appliziert. Reine physiologische Kochsalzlösung (0.9% NaCl, pH 7,4, 100µl) diente als Kontrollinjektion.

Rimonabant. Zur Antagonisierung der peripheren CB1-Rezeptoren von Mäusen wurde Rimonabant (Inserm U 862, Institut Francois Magendie, Bordeaux, Frankreich) einmalig intraperitoneal in einer Dosis von 10 mg/kg injiziert. Die Vehikellösung setzte sich aus 1 Tropfen Tween-80 und 3 ml 2,5% Dimethylsulphoxid zusammen. Die Dosierung orientierte sich an den Angaben der Studie von Osei-Hyiaman et al. (2008) bei Mäusen. Als Kontrollbehandlung diente die Vehikellösung ohne Rimonabant. Insgesamt wurden rund 20 ml Vehikel- bzw. Rimonabantlösung pro kg Körpergewicht verabreicht.

Organentnahmen

Für die Organentnahmen wurden die Versuchstiere mit CO_2-Begasung betäubt und anschließendem Herzschnitt getötet. Entnommen wurden Blut, Gehirn, Muskeln, suprasternales braunes Fettgewebe (BAT), inguinales weißes Fettgewebe (WAT), Herz, Leber und Milz.

Das Blut wurde direkt nach dem Herzschnitt aus dem Brustraum abgesaugt, in ein Eppendorf-Cup mit 30µl 2% EDTA überführt und auf Eis kaltgestellt. Zum Erhalt des Blutserums wurden die Zellbestandteile der Probe einmalig für 10 Minuten bei 4500 RPM und 4°C abzentrifugiert. Das präparierte Gehirn wurde zunächst auf Trockeneis gefroren. Die Präparation der Muskeln, Musculus quadriceps, Musculus gastrocnemius und Musculus tibialis anterior erfolgte nach anatomischen Bildern aus „Anatomy of the Rat“ (Green, 1935).

Alle Proben wurden in Flüssigstickstoff schockgefroren und für weitere Analysen bei -80°C aufbewahrt.

RNA Isolation

Gesamt-RNA wurde mit TRIzol (Invitrogen, Karlsruhe, Deutschland) nach Herstellerangaben (Chomczynski & Sacchi, 1987) isoliert. Die RNA wurde zusätzlich in einer Lösung, bestehend aus 6.3 M Guanidiniumthiocyanat, 40 mM Natriumcitrat (pH 7), 0.8% Sarcosyl, 8 mM 2-Mercaptoethanol, resuspendiert, mit 1% Vol. Isopropanol gefällt, mit 75%

Ethanol gewaschen und in DEPC-behandeltem Wasser gelöst. Anschließend wurde die Gesamt-RNA bei 260 nm photometrisch quantifiziert und bei –80°C gelagert.

Dotblot-Analyse

Zur Quantifizierung der relativen RNA-Expression wurde der Versuchsaufbau einer Dotblot-Apparatur (hergestellt von der institutseigenen Werkstatt der Philipps-Universität Marburg) genutzt. Da die RNA-Proben für diesen Aufbau nicht elektrophoretisch getrennt werden, wurde zuvor die benötigte Spezifität der zu verwendenden cDNA-Sonde per Northernblot verifiziert. Jeweils 2 µg RNA jeder Probe wurden in 30µl Denaturierungslösung (2,2M Formaldehyd, 50% Formamid 0,5×-MOPS) 15 Minuten bei 68°C denaturiert, auf Eis abgekühlt und mit 20×-SSC auf 60µl verdünnt. Die aufbereiteten Proben wurden auf die Dotblot-Apparatur pipettiert, mittels einer Wasserstrahlpumpe durch eine Lochplatte auf eine mit Wasser und 10×-SSC-hydrierte Nylonmembran (Hybond N, Amersham) gesaugt und anschließend auf der Membran mittels UV-Strahlung fixiert (UV-Stratalinker, Stratagene).

Radioaktive Hybridisierung

Spezifische Myostatin-cDNA-Fragmente (25ng) wurden mit [α-^{32}P]dCTP (Rediprime DNA labeling system, Amersham) radioaktiv markiert und nach 30-minütiger Inkubation bei 37°C über eine G-50 Sepharonsäule (beta-Schield Device System, Stratagene) aufgereinigt. Die Nylonmembran wurde für eine Stunde in BSA-Lösung (0,5M Na_2PO_4/NaH_2PO_4, pH 7,0; 1 mM EDTA, pH 8,0; 7% SDS, 1% BSA) bei 63°C prähybridisiert und dann über Nacht bei 63°C mit der ^{32}P-markierten Sonde hybridisiert. Anschließend wurde der Blot mit SDS-haltiger SSC-Lösung abnehmender Stringenz und zunehmender Konzentration bei Raumtemperatur gewaschen (15 Min. 2x SSC/0,1% SDS; 15 Min. 1x SSC/0,1% SDS; 10 Min. 0,5x SSC/0,1% SDS; 10 Min. 0,1x SSC/0,1% SDS bei 60°C). Die komplementär an die Myostatin-RNA gebundene radioaktive cDNA wurde mittels PhosphorScreens (Molecular Dynamics) und „Phosphor Imaging“ (Storm 860, Molecular Dynamics) autoradiographisch detektiert und die Signalstärke mit ArrayVision 7.0 (Imaging Research) quantifiziert. Der Normalisierung diente die Hybridisierung mit ß-Actin. Zwischen aufeinanderfolgenden Hybridisierungen wurde die Membran gewaschen (20 Min. bei 64°C nach Zugabe kochender 0.1x SSC).

Auswertung und Statistik

Die Torpordauer wurde als die Zeit definiert, die die Tiere mit einer Körpertemperatur von unter 32°C verbrachten. Die ultradiane Rhythmik der Körpertemperatur wurde mit Hilfe der Chi-Quadrat-Periodogramm-Analyse und einer Sinuskurvenpassung analysiert.

Alle statistischen Auswertungen erfolgten mit dem Programm SigmaStat für Windows (Version 3.5, Systat Software, Inc.). Sämtliche Daten wurden zunächst auf Normalverteilung und Varianzhomogenität geprüft. Daten, die dieser Prüfung nicht standhielten, wurden log10-transformiert und erneut geprüft. Der Varianzanalyse mehrerer Stichproben diente je nach Anzahl der Einflußfaktoren die ein- bis mehr-faktorielle ANOVA. Bei Meßwiederholungen von Stichprobengruppen und je nach Anzahl der Einflußfaktoren wurde die ein- bis mehr-faktorielle RM ANOVA genutzt. Multiple Vergleiche wurden *post hoc* mit der Fisher LSD Methode durchgeführt. Die Abhängigkeit verschiedener Daten wurde mit dem Pearson-Test auf Korrelation geprüft und mit dem Korrelationskoeffizienten beschrieben. Das Signifikanzniveau wurde bei einer Irrtumswahrscheinlichkeit von $p<0,05$ festgelegt.

Alle durchgeführten Tierversuche wurden nach § 8 Abs. 1 des Deutschen Tierschutzgesetzes beantragt und genehmigt.

1.4. Ergebnisse und Diskussion

Nahezu alle Organe unterliegen einer saisonalen Reorganisation

Um die Beteiligung verschiedener Körperkomponenten an der saisonalen Körpergewichtsänderung genauer zu beleuchten, wurde der Effekt konstant langer, konstant kurzer und sich natürlich ändernder Photoperiode auf die Körperzusammensetzung Dsungarischer Zwerghamster untersucht. Wie erwartet reduzieren die Hamster in Reaktion auf konstant und natürlich kurze Photoperiode ihr Körpergewicht. Die Reduktion des Körpergewichtes um 7-8 g ergab sich aus der Reduktion des Körperfettgehaltes um 4-5 g und der Reduktion der fettfreien Körpermasse um 2-3 g.

Die Analyse einzelner Organe, wie Leber, Milz, braunem Fettgewebe und der Beinmuskulatur (Gemisch aus Musculus quadriceps, Musculus gastrocnemius und Tibialis anterior) zeigte einen nichtsignifikanten Trend des Gewichtsverlustes im natürlichen Kurztag. Verglichen mit gleichaltrigen, langtagadaptierten Hamstern jedoch sind Leber, Milz, braunes Fettgewebe und die Beinmuskeln kurztagadaptierter Tiere signifikant leichter. Frühere Studien zeigten, daß auch der Intestinaltrakt in kurztagadaptierten Hamstern signifikant weniger wiegt, als der langtagadaptierter Hamster (Wiesinger, 1989). Die Herzmasse zeigte sich in keinster Weise durch natürlich kurze Photoperiode beeinflusst und entsprach derjenigen, der langtagadaptierten Hamster. Hingegen stieg der Knochenmineralgehalt der Hamster sowohl bei sich natürlich ändernder Photoperiode, als auch bei konstant langer Photoperiode kontinuierlich an. Diese gegensätzlichen Veränderungen der verschiedenen Organe veranschaulichen, wie komplex die saisonale Reorganisation der Gewebe und deren regulative Mechanismen sind, die sich letztendlich in der saisonalen Körpergewichtsveränderung äußern. Im Weiteren wurde die an der saisonalen Körpergewichtsregulation beteiligte Muskelmasse und deren Regulation genauer betrachtet.

Das Muskelwachstum ist saisonal eingeschränkt

Diese Arbeit zeigt, daß die Muskelmasse des Oberschenkelmuskels, Musculus quadriceps, der Dsungarischen Zwerghamster trotz kürzer werdender Tage im Winter mit etwa 75 mg konstant bleibt. Dieser Umstand spiegelt in keiner Weise den Verlauf der Körpermasse wieder, die mit kürzer werdenden Tagen sinkt. So liegt es zunächst nahe, zu behaupten, die Muskelmasse leiste keinen Beitrag zur saisonalen Körpergewichtsentwicklung. Betrachtet man allerdings die Entwicklung der Muskelmasse der gleichaltrigen, im Langtag verbliebenen Hamster, so zeigt sich ein signifikantes und konstantes Wachstum. Dies hat zur Konsequenz, daß es einen

signifikanten Unterschied in der Muskelmasse zwischen kurztag- und langtagadaptierten Hamstern gibt, was auch schon in einer früheren Studie beobachtet wurde (Klingenspor et al., 2000). Unsere Longitudinalstudie demonstriert, daß die Muskulatur im Kurztag nicht reduziert wird, sondern das Wachstum der Muskeln saisonal, in Reaktion auf eine kurze Photoperiode, eingeschränkt ist. Die Muskelmasse ist also nicht an der Reduktion der Körpermasse im Kurztag beteiligt, vereinfacht aber das Erreichen eines energetisch günstigen geringen Körpergewichtes im Winter durch ein reduziertes Wachstum.

In der Regel kann man annehmen, daß je schwerer ein Körper ist, desto ausgeprägter die Skelettmuskulatur ist, die den Körper tragen muß. Demnach korreliert die Muskelmasse im Normalfall positiv mit dem Körpergewicht (Biewener, 1991). Die langtagadaptierten Hamster dieser Studie zeigen diese positive Relation zwischen der Muskelmasse, in diesem Fall der Masse präparierter Quadricepsmuskeln, und dem Körpergewicht. Diese Korrelation konnte nicht bei Hamstern festgestellt werden, die an den natürlichen Kurztag adaptiert waren. Insgesamt sprechen die Befunde, also das fehlende Muskelwachstum und die nicht vorhandene Relation zwischen Muskelmasse und Körpergewicht im natürlichen Kurztag, für eine photoperiodenabhängige differentielle Regulation der Muskelmasse.

Die Myostatin-Expression unterliegt einer saisonalen Regulation

Myostatin ist bekannt als *das* Hormon, welches als Inhibitor des Wachstums der Skelettmuskulatur fungiert (Matsakas & Diel, 2005). Es ist also naheliegend eine Beteiligung dieses Hormons am saisonal eingeschränkten Muskelwachstum im Dsungarischen Hamster zu vermuten, weshalb im Weiteren der Einfluß der Photoperiode auf die mRNA-Expression des Myostatins untersucht wurde.

Natürlicher Kurztag resultierte in einer signifikanten Steigerung der Myostatin-mRNA der Oberschenkelmuskulatur Dsungarischer Zwerghamster. Hamster, die im künstlichen Langtag verblieben, zeigten keine Änderung in der Myostatin-mRNA Expression. Dies spricht für eine photoperiodenabhängige saisonale Regulation des Myostatins. Es kann also durchaus angenommen werden, daß die gesteigerte Myostatin-Expression im Kurztag dem reduzierten oder gar eingestellten Muskelwachstum im Kurztag zugrunde liegt.

Eine Korrelationsanalyse zwischen der Expression der relativen Myostatin-mRNA und der Muskelmasse einzelner Individuen weist darauf hin, daß neben der Expression auch die Funktion des Myostatins saisonal verändert ist. Denn während im natürlichen Kurztag die Expression der Myostatin-mRNA mit der Muskelmasse des jeweiligen Hamsters negativ korreliert und so das Myostatin seiner Rolle als negativer Regulator der Muskelmasse gerecht wird, fehlt diese

Relation bei Hamstern aus langer Photoperiode. Sowohl im artifiziellen als auch im natürlichen Langtag ist keinerlei Beziehung zwischen der Myostatin-mRNA und der Muskelmasse zu detektieren. Dies läßt vermuten, daß Myostatin im Langtag ein geringeres Potential als Inhibitor des Muskelwachstums hat, als im Kurztag. Eine saisonal veränderte Sensitivität gegenüber diesem Hormon, mit einer hohen Sensitivität im Kurztag und einer niedrigen im Langtag, ähnlich wie es für Leptin bekannt ist, könnte hierfür eine plausible Erklärung bieten. Für Myostatin ist aber auch bekannt, daß es zunächst als inaktives Vorläuferhormon synthetisiert wird, welches dann in Propeptid und aktiven Liganden proteolysiert wird (Matsakas & Diel, 2005). Demnach wäre es auch denkbar, daß das Myostatin-Vorläufermolekül saisonal unterschiedlichen posttranslationalen Modifikationen unterliegt, welche dann zu den saisonal verschiedenen Relationen zwischen Myostatin-mRNA und der Muskelmasse führen.

Die posttranslationale Modifikation des Proopiomelanocortin ist photoperiodisch reguliert, zugunsten appetithemmender Signale im Kurztag

Es ist naheliegend, zu vermuten, daß die freiwillige saisonale Reduktion der Futteraufnahme und somit des Körpergewichts Dsungarischer Zwerghamster im Kurztag auf einer gesteigerten Aktivität von appetithemmenden Anorexigenen beruht. Hierbei bietet das Melanozyten-stimulierende Hormon (α-MSH) einen guten Ansatzpunkt, da es eine fundamentale Funktion als anorexigenes Signal im Nucleus arcuatus (ARC), dem wohl wichtigsten hypothalamischen Kerngebiet zur Integration appetitregulierender Signale, hat (Wynne et al., 2005). Dementsprechend kontraproduktiv erscheint es dann zunächst, daß die Genexpression des Proopiomelanocortin (POMC), einem Vorläuferhormon, aus dem das α-MSH durch postranslationale Prozessierung hervorgeht, im Kurztag reduziert ist (Reddy et al., 1999; Mercer et al., 2000). Die reduzierte POMC-mRNA im Kurztag hat jedoch keine reduzierten Proteingehalte zur Folge, da immunhistochemische Untersuchungen unserer Studie keine quantitativen Unterschiede bei POMC-positiven Neuronen im ARC zwischen kurztag- und langtagakklimatisierten Hamstern ergaben. Offensichtlich unterliegt also die POMC-Biosynthese neben der transskriptionalen auch einer translationalen Kontrolle.

Hypothetisch könnten höhere α-MSH-Level im Kurztag erreicht werden, wenn es z.B. eine photoperiodische Regulation der Prohormonkonvertasen 1 (PC1/3) und 2 (PC2), die für die posttranslationale Prozessierung des POMC zuständig sind, gibt. Die PC1/3 spaltet POMC zunächst in die größeren Zwischenprodukte Adrenocorticotropin (ACTH) und Lipotropin. Anschließend werden diese von der PC2 in α-MSH bzw. β-Endorphin gespalten (Benjannet et al., 1991).

Im ARC konnte keine photoperiodenabhängige Änderung der Genexpression der PC1/3 festgestellt werden und auch die Protein-Level der PC1/3 zeigten keinen Unterschied zwischen kurztag- und langtagakklimatisierten Hamstern. Dies bedeutet, daß die PC1/3 nicht primär durch die Photoperiode reguliert ist und es somit auch keine Unterschiede in ihrer Spaltaktivität zwischen kurztag- und langtagadaptierten Hamstern gibt. Diese Vermutung wird dadurch gestützt, daß sich der Gehalt des PC1/3-Spaltproduktes ACTH im Kurztag und Langtag nicht voneinander unterschied. Wenngleich dem ACTH eine anorexigene Wirkung zugeschrieben wird (Al-Barazanji et al., 2001), so scheint es dennoch keine entscheidende Bedeutung für die *saisonale* Reduktion der Nahrungsaufnahme und des Körpergewichts zu haben.

Im Gegensatz zur PC1/3 war die Genexpression der PC2 nach 14 Wochen Kurztag signifikant hochreguliert, was sich auch in höheren PC2-Proteingehalten widerspiegelte. Weiterhin führte ein Transfer vom Kurztag in den Langtag wieder zu einer Reduktion der PC2-

Expression, die sich bereits nach 2 Wochen nicht mehr von der langtagadaptierter Hamster unterschied. Erwartungsgemäß und einer gesteigerten PC2-Aktivität im Kurztag entsprechend, konnten im ARC auch signifikant mehr β-Endorphin-positive Zellen sowie vermehrt α-MSH-positive Nervenfasern im Kurztag nachgewiesen werden.

Diese Ergebnisse, also die photoperiodenabhängige Änderung der PC2-Expression einhergehend mit der im Kurztag beobachteten Steigerung der Anorexigene α-MSH und β-Endorphin, die bereits vor Änderungen des Körpergewichts auftraten, sprechen für eine wichtige Rolle der PC2-Aktivität bei der Integration photoperiodischer Informationen und der Umsetzung saisonal veränderter Energiebalancierung.

Thyronamin induziert keinen natürlichen Torpor

Befunde einer durch Thyronamin (T1AM) induzierten Hypothermie und Bradykardie bei Mäusen (Scanlan et al., 2004) ließen dieses Hormon als torporeinleitendes Signal in Frage kommen. Nach intraperitonealer Injektion des Thyronamins war zwar sowohl bei kurztag- als auch bei langtagadaptierten Hamstern sowie bei Mäusen eine sofortige Reduktion der Stoffwechselrate, der Körpertemperatur und des respiratorischen Quotienten zu beobachten. Die Verläufe dieser Parameter unterscheiden sich jedoch wesentlich von denen eines natürlichen Torporereignisses:

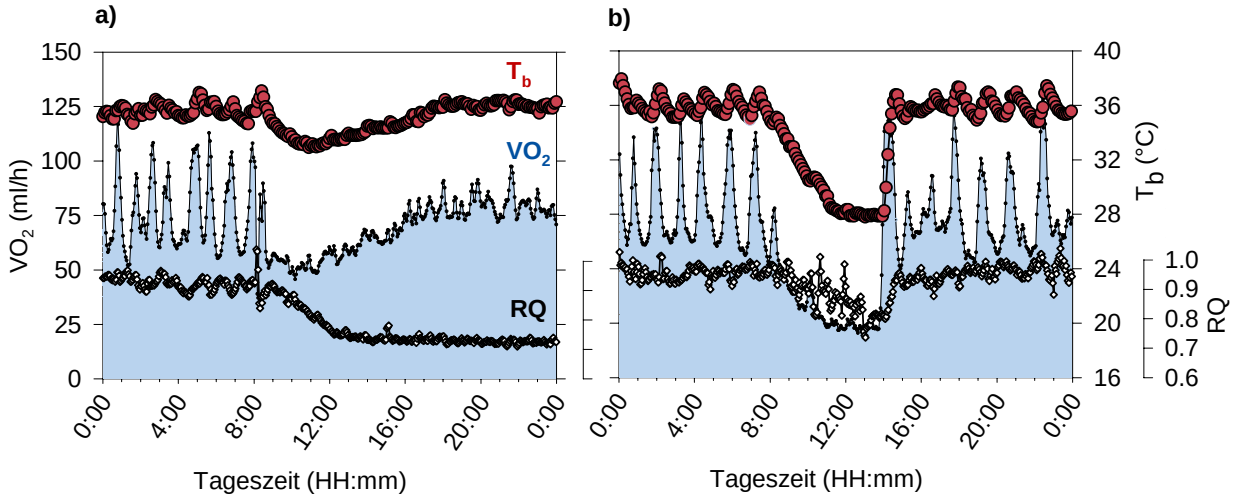

Abb. 1 Verlauf der Körpertemperatur (T_b), der Stoffwechselrate (VO_2) und des respiratorischen Quotienten (RQ) nach T1AM-Injektion (a) und während eines natürlichen Torporbouts (b). Die T1AM-Injektion erfolgte um 8:00 Uhr.

Die durch T1AM ausgelöste Stoffwechseldepression findet deutlich schneller statt, als die bei Eintritt in den Torpor. So wird eine Reduktion des Sauerstoffverbrauches um 25 ml O_2 pro Stunde innerhalb von 9 Minuten nach T1AM Injektion und innerhalb von 19 Minuten bei Eintritt in den Torpor erreicht. Ein weiterer Unterschied zeigt sich in den Zeiten, die die Tiere benötigen, um wieder normometabole Werte zu erlangen. Ausgehend von den niedrigsten Stoffwechselwerten wird die Rückkehr zur Normometabolie nach T1AM-Behandlung über einen Zeitraum von nahezu 8 Stunden vollzogen, während das Arousal aus dem Torpor nur wenige Minuten dauert. Darüberhinaus ist die Tiefe der durch T1AM ausgelösten Hypometabolie und Hypothermie deutlich weniger ausgeprägt als im natürlichen Torpor, obwohl sie insgesamt länger anhält als im Torpor. Auch und besonders der extreme und nachhaltige Effekt des

Thyronamins auf den RQ, der sofort auf 0,7 sinkt, spiegelt in keiner Weise die eher moderaten Änderungen des RQs während des Torpors wider.

Die Auswirkung des Thyronamins, also die Dauer und Tiefe der metabolen Depression, der Körpertemperatur- und RQ-Senkung, sind bei Mäusen ausgeprägter als bei Hamstern und bei langtagakklimatisierten Hamstern ausgeprägter als bei kurztagakklimatisierten Hamstern. Dies widerspricht der Funktion des T1AM als torporeinleitendes Signal, da unter natürlichen Umständen ausschließlich kurztagakklimatisierte Hamster Torpor zeigen und aufgrund dieser Torporneigung der Effekt des T1AM bei eben diesen Tieren den größten Effekt zeigen sollte. Warum die Hypometabolie bei kurztagadaptierten Hamstern am geringsten ausfällt, darüber kann bislang nur spekuliert werden. Da die Tiefe der durch T1AM ausgelösten Hypometabolie mit dem Körpergewicht korreliert und die Regressionskurve auf Körpergewichtswerte extrapoliert, die typisch für die fettfreie Körpermasse der beiden Spezies sind, kann man annehmen, daß der Effekt vom Körperfettgehalt oder von körperfettgehaltsassoziierten Faktoren abhängig ist.

Diente das Thyronamin als endokrines Torporsignal, könnte man annehmen, daß man höhere endogene Level dieses Hormons in torpiden, als in normometabolen Hamstern vorfindet. Die Analyse des Blutserums kurztagadaptierter Hamster zeigte, daß sich die endogenen T1AM-Level torpider Tiere mit 0,80 ± 0,11 nM nicht von denen der normometabolen Hamster mit 0,91 ± 0,21 nM unterscheiden (P = 0,64).

Die in allen T1AM behandelten Tieren ausgelöste Hypometabolie und Hypothermie zeigen zwar, daß Thyronamin als metaboler Inhibitor agiert, allerdings ist es mit den aufgeführten Vergleichen fraglich, ob es *diejenigen* torporinduzierenden Stoffwechselwege anstößt, die zu der kontrollierten Stoffwechseldepression des Torpors führen. Zu klären bleibt zunächst die Frage, auf welche Weise das T1AM den Stoffwechsel inhibiert.

Thyronamin blockiert den Kohlenhydratstoffwechsel

Wie bereits erwähnt induziert i.p. appliziertes T1AM neben mehrstündiger Hypometabolie und Hypothermie eine drastische Senkung des respiratorischen Quotienten von 0,9 auf 0,7 in Dsungarischen Zwerghamstern und Mäusen. Stöchiometrisch bedingt liefert der respiratorische Quotient (das Verhältnis von produziertem Kohlendioxid zu verbrauchtem Sauerstoff) aussagkräftige Informationen über die Substratverstoffwechselung eines Tieres. Die durch T1AM ausgelöste sofortige Reduktion des RQ impliziert eine sofortige Einstellung des vor Injektion überwiegenden Kohlenhydratstoffwechsels (RQ≈0,9) und eine rasche Umstellung auf Lipidstoffwechsel (RQ≈0,7). Die Annahme eines gesteigerten Fettstoffwechsels durch T1AM wird von weiteren Befunden gestützt. So entwickeln T1AM-behandelte Tiere 8 Stunden nach

Injektion eine ausgeprägte Ketourie. Desweiteren war durch die Analyse der Körperzusammensetzung ein signifikanter Verlust an Körperfett nachzuweisen, was für eine Mobilisierung und den Verbrauch von Körperlipiden spricht. Insgesamt deuten diese Ergebnisse darauf hin, daß Thyronamin den Kohlenhydratstoffwechsel blockiert und somit der Energiebedarf der Tiere ausschließlich durch die Verstoffwechselung von Lipiden befriedigt werden muß. Die Dauer der durch T1AM ausgelösten Hypometabolie und Hypothermie spiegelt somit die Dauer wider, die die Tiere benötigen, um ihre Stoffwechselmaschinerie so umzustellen, daß sie ihren gesamten Stoffwechselbedarf über Lipidmetabolismus befriedigen können.

Die Hypothese eines durch Thyronamin massiv gestörten Zuckerstoffwechsels wird von einer kürzlich veröffentlichen Arbeit gestützt. Dort konnte gezeigt werden, daß sowohl periphere als auch zentrale Thyronamingabe bei Ratten und Mäusen zu Hyperglykämie und gesteigerten Glucagonwerten führt, während die adäquate Insulinantwort darauf fehlt (Klieverik et al., 2009). Entgegen der Erwartung einer gesteigerten Insulinantwort auf den hohen Blutzucker wird eine Hypoinsulinämie beobachtet, welche wiederum in Einklang mit den Befunden dieser Arbeit steht, da Hypoinsulinämie zu einer gesteigerten Lipolyse und der Bildung von Ketokörpern führt.

Sympathische Kontrolle des Torpors

Es ist bekannt, daß die Aktivitäten des vegetativen Nervensystems Einfluß auf das kardiorespiratorische System während des Torpors haben. Es wird angenommen, daß Aktivitäten des Parasympathikus eine Schlüsselrolle in der Torporeinleitung spielen. So konnte gezeigt werden, daß durch akute parasympathische Inhibition oder Vagotomie bei Torporeintritt die typische Depression der Ventilation und Herzfrequenz umgekehrt und Herzarrhythmien gemildert werden können (Milsom et al., 1999; Milsom et al., 1993; Lyman & O'Brien, 1963; Morhardt, 1970; Zosky, 2002). Ob sie aber für das Auftreten und die grundsätzliche Kontrolle des Torpors verantwortlich sind, ist bislang nicht beantwortet worden. Um die Notwendigkeit der vegetativen Aktivitäten für das Auftreten eines Torporereignisses zu evaluieren, wurde der Effekt mehrtägiger sympathischer und parasympathischer Blockade auf das Torporverhalten kurztagakklimatisierter Hamster untersucht.

Wäre für das Einleiten eines Torporereignisses die gesteigerte Aktivität des parasympathischen Tonus ursächlich, so sollte die in dieser Studie durchgeführte Blockade des Parasympathikus durch Atropin (kompetitive Hemmung der muscarinergen Acetylcholinrezeptoren) das Torporverhalten aufhalten oder zumindest einschränken. Kurztagadaptierte Hamster, denen ein Atropin-Implantat appliziert wurde, welches eine Gesamtdosis von 0,25 mg über einen Zeitraum von 21 Tagen konstant entließ, zeigten keine Veränderung in ihrem Torporverhalten. Sie wurden in der gleichen Frequenz, Dauer und Tiefe torpid, wie es vor der Behandlung zu beobachten war. Obwohl der parasympathische Tonus eine Rolle in der transienten Phase des Torporeintritts spielt, spricht der Befund dieser Studie dafür, daß er nicht essentiell für das Auslösen oder Auftreten des natürlichen Torpors ist und die bisherige Vorstellung über eine parasympathische Dominanz als Ursache für den Übergang in die torpide Stoffwechsellage überdacht werden muß.

Auf der anderen Seite führte die reversible Zerstörung sympathischer Nervenendigungen durch 6-OHDA-Injektion zu einer mehrtägigen Blockade des Torporverhaltens Dsungarischer Zwerghamster. So war bei 6-OHDA-behandelten Hamstern für einen Zeitraum von mindestens einer Woche kein Torpor detektierbar, was bedeutet, daß für das Auftreten natürlichen Torpors ein intakter peripherer Sympathikustonus erforderlich ist. Dieses Ergebnis paßt zu Studien von Swoap et al. (2006; 2008), die zeigten, daß Dopamin-Hydroxylase-knock-out-Mäuse, denen die Fähigkeit zur Noradrenalin und Adrenalin Synthese fehlt, keinen hungerinduzierten Torpor zeigen. Spritzt man diesen Mäusen einen β3-adrenergen spezifischen Agonisten, wird diese Unfähigkeit zum fasteninduzierten Torpor aufgehoben.

Der kausale Zusammenhang zwischen der Notwendigkeit eines intakten peripheren sympathischen Tonus und dem Auftreten von Torpor wird aufgrund der Komplexität vegetativer Regulationsmechanismen nicht leicht zu entschlüsseln sein. Bei vielen Spezies kann kurz vor Eintritt in den Torpor eine metabolische Erregungsphase beobachtet werden, in der Ventilation, Herz- und Stoffwechselrate kurzzeitig Spitzenwerte erreichen (Elvert & Heldmaier, 2005; Ortmann & Heldmaier, 2000; Morris et al., 1994; Song et al., 1997), was für eine hohe sympathische Aktivität spricht. Es wäre denkbar, daß diese vermutlich adrenerg kontrollierte Erregungsphase essentiell auf die direkt folgende Stoffwechseldepression vorbereitet, jedoch durch 6-OHDA unterbunden wurde und deshalb kein Torpor mehr stattfand.

Das vegetative Nervensystem ist an der Generierung der ultradianen Rhythmik beteiligt

Ein zusätzlicher Befund nach Inhibition des sympathischen oder parasympathischen Tonus ergab sich in Hinblick auf die ultradiane (<24 Stunden) Rhythmik der Körpertemperatur Dsungarischer Zwerghamster. Ultradiane Rhythmen sind ein verbreitetes Charakteristikum von Säugern und für Aktivität, Körpertemperatur und Sauerstoffverbrauch vieler Spezies gut beschrieben (Refinetti & Menaker, 1992). Über die Generierung und Bedeutung dieser Rhythmen war bislang nichts bekannt, was Grundlage vieler Spekulationen war.

Sowohl nach Atropin-, als auch nach 6-OHDA-Applikation kam es unmittelbar zu einem Verlust der ultradianen Rhythmik der Körpertemperatur. Die Rückkehr zu einer normalen Oszillation der Körpertemperatur mit einer Periodenlänge von ca. 3 Stunden wurde rund 24 Stunden nach Atropingabe und erst wieder 2-6 Tage nach 6-OHDA-Injektion erreicht. Diese Ergebnisse lassen darauf schließen, daß sowohl adrenerge, als auch cholinerge Signalwege für die Entstehung ultradianer Rhythmen notwendig sind.

Eine aktuell erschienene Studie an Ratten zeigte, daß die ultradianen Rhythmen der motorischen Aktivität, der braunen Fett- (BAT), Gehirn- und Körpertemperatur, des Blutdrucks und der Herzfrequenz, sowie die rhythmischen Gehirnaktivitäten (per EEG gemessene Thetawellen (5-8Hz)) phasenverschoben miteinander gekoppelt sind. Die Analyse der Phasenverschiebungen belegt, daß die ultradianen Steigerungen der hippocampalen Aktivität die ultradianen Spitzen der Herzfrequenz, des Blutdrucks und der BAT-Temperatur zur Folge haben und erst dann die ultradiane Erwärmung des Körpers und des Gehirns erfolgt (Ootsuka et al., 2009).

Diese ultradianen Rhythmen finden auch ohne vorausgehende Änderungen der verschiedenen physiologischen Parameter, also völlig autonom, statt. Das macht deutlich, daß Tiere zum Erhalt eines stabilen physiologischen Zustandes nicht auf exakte Sollwerte regulieren,

sondern episodisch vom Sollwert abweichen, was sie befähigt ihr Potential bei akut vorherrschenden Umweltbedingungen genau abschätzen zu können.

Zum gegenwärtigen Zeitpunkt ist unklar, welche Gehirnregionen und genregulierten Clock-Mechanismen an der Entstehung dieser autonomen, phasengekoppelten ultradianen Rhythmen beteiligt sind, aber offensichtlich sind die absteigenden vegetativen Signalwege, die unter anderem die Herzfrequenz oder die sympathisch innervierte BAT-Thermogenese kontrollieren, von entscheidender Bedeutung für die Entstehung ultradianer Rhythmen in Kleinsäugern.

Für den Einfluß des Endocannabinoidsystems (ECS) auf den Energiehaushalt sind die Neurone des Vorderhirns und Sympathikus von entscheidender Bedeutung.

CB1-Knockout-Mäuse (CB1-KO) haben einen schlanken Phänotyp und sind resistent gegenüber Adipositas (Cota et al., 2003; Ravinet-Trillou et al., 2004). Da der Cannabinoidrezeptor 1 (CB1) sowohl im zentralen Nervensystem als auch in nicht-neuronalen peripheren Organen exprimiert ist (z.B. in Leber, Fettgewebe, Pankreas), stellte sich die Frage nach der Bedeutung des CB1-Rezeptors im ZNS bei der Entwicklung dieses Phänotyps. Aus diesem Grund wurden konditionale Mausmutanten (CaMK-CB1-KO) generiert, denen der CB1-Rezeptor ausschließlich in Neuronen Energiebalance-regulierender Zentren (Hypothalamus und Nucleus tractus solitarii) des Vorderhirns fehlt. Diese Mäuse wiesen jedoch auch eine partielle, 60%ige Deletion des Rezeptors in sympathischen Neuronen der oberen Zervikalganglien auf.

Die CaMK-CB1-KO-Mäuse entwickelten bei Standarddiät wie die CB1-KO-Mäuse ein geringeres Körpergewicht als die Wildtyp-Mäuse. Behandlung mit dem CB1-Antagonisten Rimonabant hatte keinerlei Effekte bei CaMK-CB1-KO-Mäusen, während es bei Wildtypmäusen zu einer Reduktion des Körpergewichts und des respiratorischen Quotienten führte. Nach chronischer Fütterung einer hochkalorischen Diät (HFD), was bekanntlich die Endocannabinoidproduktion steigert (Kunos et al., 2008), wiesen die Körperfettanteile und Plasmagehalte verschiedener energiebalancerelevanter Metabolite, wie Leptin, Insulin, Glucose, freie Fettsäuren und Triglyceriden, keine Unterschiede zwischen CaMK-CB1-KO und CB1-KO-Mäusen auf. Verglichen mit Mäusen unter Standarddiät waren diese Parameter unter HFD bei CaMK-CB1-KO und CB1-KO-Mäusen unverändert, während sie bei Wildtyp-Mäusen massiv stiegen. Diese Ergebnisse zeigen, daß zusätzliche CB1-Antagonisierung der Peripherie keinen Einfluß auf den Phänotyp von CaMK-CB1-KO-Mäusen hat und diese wie die CB1-KO-Mäuse gegenüber diätinduzierter Adipositas (DIO) resistent sind. Dies läßt die Schlußfolgerung zu, daß das Endocannabinoidsystem seinen Einfluß auf die Energiebalancierung maßgeblich über Neurone des Vorderhirns und/oder des Sympathikus ausübt.

CB1-Deletionen in Neuronen des Vorderhirns und Sympathikus führen zu vermehrter Fettverbrennung und gesteigerter Thermogeneseleistung des braunen Fettgewebes (BAT).

Die einfache Rechnung, den schlanken und DIO-resistenten Phänotyp der CaMK-CB1-KO-Mäuse mit einem gesteigerten Stoffwechsel und/oder einer reduzierten Futteraufnahme zu erklären, geht leider nicht auf. CaMK-CB1-KO- und Wildtyp-Mäuse zeigen bei Raumtemperatur keine signifikanten Unterschiede, weder in Sauerstofferbrauch und Körpertemperatur, noch in der Energieaufnahme über das Futter. Allerdings weisen die CaMK-CB1-KO-Mäuse in der

aktiven Phase (des Nachts) einen signifikant niedrigeren RQ als die Wildtyp-Mäuse auf, was bedeutet, daß die Mutanten einen höheren Anteil an Lipiden verstoffwechseln.

Ein Teil der geringeren Futtereffizienz (Körpergewichtszunahme/aufgenommene Energie) der CaMK-CB1-KO-Mäuse gegenüber den Wildtypen läßt sich mit einer reduzierten metabolisierten Energie erklären. So scheiden die CaMK-CB1-KO-Mäuse einen höheren Anteil aufgenommener Energie über die Fäzes aus, als es bei den Wildtypen der Fall ist.

Wenngleich die Thermogeneseleistung der Mäuse bei moderaten Temperaturen nicht signifikant verändert zu sein scheint, wurden dennoch Hinweise für gesteigerte Stoffwechselaktivitäten und thermogenetische Kapazitäten des braunen Fettgewebes in CaMK-CB1-KO-Mäusen gefunden. Diese beinhalten gesteigerte Expressionslevel wichtiger Regulatoren der Mitochondrienbiogenese (Coaktivator 1α des Peroxisom-Proliferator-aktivierten Rezeptoren γ und die Transkriptionsfaktoren NRF-1 und Tfam) und Komponenten der Atmungskette (Cytochrom c, Cyotochrom c-Oxidase und das für die Wärmeproduktion wichtige Entkopplerprotein UCP1), sowie insgesamt mehr mitochondriale DNA und gesteigerte Aktivität der Citrat-Synthase. Tatsächlich führte eine Kälteexposition (6°C) bei CaMK-CB1-KO-Mäusen zu signifikant höherem Sauerstoffverbrauch und höheren Körpertemperaturen als bei Wildtyp-Mäusen. Desweiteren zeigte die Positronen-Emissions-Tomographie, daß die 2-Deoxy-2-[^{18}F]-Fluoro-D-Glukose-Aufnahme im suprascapularen BAT bei Kältebelastung in CaMK-CB1-KO-Mäusen signifikant höher ist als bei Wildtyp-Mäusen. Rimonabant wiederum hatte keinen Einfluß auf die Glukose-Aufnahme der CaMK-CB1-KO-Mäuse, aber steigerte die der Wildtyp-Mäuse auf Werte der CaMK-CB1-KO-Mäuse.

All diese Befunde sprechen dafür, daß eine eingeschränkte CB1-Signaltransduktion auf Ebene des Vorderhirns und des Sympathikus der DIO entgegenwirkt, indem es zu einer Reduktion der metabolisierbaren Energie, einer Steigerung der Lipidoxidation und einer höheren Energievergeudung durch gesteigerte thermogenetische Aktivitäten des BATs kommt.

Der Einfluß des ECS auf den Energiehaushalt wird sympathisch vermittelt.

Es ist bekannt, daß die Aktivierung der präsynaptischen CB1-Rezeptoren die Noradrenalin(NE)-Ausschüttung inhibiert und somit zu einer Senkung des sympathischen Tonus peripherer Organe führt (Kunos et al., 2008). Im Umkehrschluß kann man vermuten, daß eine Reduktion der Aktivität des ECS zu einer Steigerung des sympathischen Tonus führt und die beobachteten Änderungen des Energiehaushalts, wie der verbesserten Thermogenesefunktion des BAT der CaMK-CB1-KO-Mäuse sympathisch moduliert sind.

Tatsächlich waren gegenüber den Wildtypen in CaMK-CB1-KO- und CB1-KO-Mäusen unter HFD sowohl höhere NE-Level im Plasma als auch eine gesteigerte NE-Aufnahme im BAT nachweisbar. Diese Unterschiede zwischen Wildtypen und CaMK-CB1-KO- und CB1-KO-Mäusen konnten durch Kälteexposition, die bekanntlich die BAT-Thermogenese über das sympathische Nervensystem stimuliert, sogar noch vergrößert werden. Desweiteren war es möglich, den NE-Umsatz im BAT der Wildtypen durch CB1-Antagonisierung mit Rimonabant auf Level der CaMK-CB1-KO- und CB1-KO-Mäuse zu steigern. Diese Ergebnisse sprechen also dafür, daß die zentralen CB1-Rezeptoren die Aktivität des peripheren sympathischen Tonus modulieren und so auch ihren Einfluß auf die Thermogeneseleistung des braunen Fettgewebes ausüben. Diese Annahme wird durch die Tatsache untermauert, daß die beobachtete höhere Glukoseaufnahme und Thermogenese des BAT in CaMK-CB1-KO-Mäusen und in mit Rimonabant behandelten Wildtypmäusen sowohl durch chemische Sympathektomie mit 6-OHDA als auch durch sympathische Denervierung des BAT aufgehoben werden kann.

Es kann also angenommen werden, daß im Gegensatz zur HFD-induzierten gesteigerten Aktivität des ECS und somit der Abdämpfung sympathischer Aktivitäten, die zu Energiespeicherung in Form von Fettdepots führen, die Inhibition von CB1-Signalwegen zu einer sympathischen Überaktivität führt, die sich im schlanken Phänotypus der CaMK-CB1-KO-Mäuse äußert.

1.5. Fazit

Die präzise Kontrolle und Anpassungsfähigkeit des Energiehaushalts sind Voraussetzung für das Ermöglichen eines „energetisch hohen Lebensstandards“. Diese Arbeit veranschaulicht, wie komplex und vielfältig die regulatorischen Instanzen für einen den Umständen angemessenen Energiestoffwechsel von Endothermen sind. Sie finden sich auf Ebene der

- Genexpression in der Peripherie, wie z.B. bei der in dieser Studie demonstrierten saisonalen Regulation der Myostatin-Expression. Hier dient sie der Regulation der Organgröße über die Inhibition des Muskelwachstums zugunsten eines geringen Körpergewichtes in jahreszeitlich bedingten Energieversorgungsengpässen im Winter.

- posttranslationalen Prozessierung von Neuropeptiden im Zentralnervensystem, wie es für den Neuropeptidvorläufer POMC gezeigt wurde. So ist die Genexpression und Proteinbiosynthese der an der posttranslationalen Prozessierung des POMC beteiligten PC2 im Kurztag zugunsten appetitsenkender Wirkung hochreguliert, was mit einem gesteigerten Vorkommen der anorexigenen POMC-Spaltprodukte α-MSH und β-Endorphin einhergeht.

- endokrinen Kontrolle über die Art der Substratverstoffwechselung, in der offensichtlich das endogen vorkommende Schilddrüsenhormonderivat Thyronamin eine Rolle übernimmt, da es hemmend auf den Glukosestoffwechsel wirkt und zu einer Umstellung auf Lipidstoffwechsel führt.

- Signaltransduktion des autonomen Nervensystems. So sind die parasympathischen und sympathischen Aktivitäten an der Generierung ultradianer Rhythmen beteiligt, die eine flexible und schnell reaktionsfähige Regulation physiologischer Prozesse ermöglichen. Desweiteren zeigte sich, daß eine intakte Neurotransmission des Sympathikus für das Auftreten der natürlichen Stoffwechseldepression des täglichen Torpors benötigt wird.

- Signaltransduktion in spezialisierten Zentren des ZNS, wie über die CB1 Rezeptoren des Endocannabinoidsystems. So führt deren Fehlen zu einer sympathisch vermittelten Reduktion der metabolisierten Energie, einer Steigerung der Lipidoxidation und einer gesteigerten Thermogenese, was in einem niedrigen Körpergewicht und einer Resistenz gegenüber diätinduzierter Adipositas resultiert.

Diese Studien über die Regulation extremer Stoffwechselphänomene wie des täglichen Torpors und ausgeprägter Änderungen des Körpergewichts sind nicht nur von Bedeutung für das Verständnis und die Aufklärung der metabolischen Organisation von Säugern. Sie bieten auch Ansätze zu weitreichenden Anwendungsmöglichkeiten in klinischen Bereichen. So könnten etwa induzierte hypometabole Zustände als lebensverlängernde Maßnahmen beim Transport von Schwerverletzten genutzt werden oder in der Transplantationsmedizin die Lebenszeiten von Spenderorganen außerhalb des Körpers verlängern. Der Erkenntnisgewinn über die Regulation des Körpergewichts könnte bei der Aufklärung pathologischer Zustände, wie z.B. der in unserer Gesellschaft mittlerweile weit verbreiteten Eßsucht bzw. Adipositas oder der krankhaften Muskeldystrophie, helfen.

Abschließend sei jedoch betont, daß bei jeder weiterführenden Forschung, unabhängig von Zielrichtung und Anwendung, eines nicht aus dem Blickfeld geraten sollte: die immense Komplexität physiologischer Regelmechanismen, die in den vorliegenden Einzeluntersuchungen aus neuen Perspektiven beleuchtet werden konnte.

1.6. Literatur

Adam CL, Mercer JG (2004). Appetite regulation and seasonality: implications for obesity. Proc Nutr Soc 63(3):413-419.

Al-Barazanji KA, Miller JE, Rice SQ, Arch JR, Chambers JK (2001). C-terminal fragments of ACTH stimulate feeding in fasted rats. Horm Metab Res 33(8):480-5.

Benjannet S, Rondeau N, Day R, Chrétien M, Seidah NG (1991). PC1 and PC2 are proprotein convertases capable of cleaving proopiomelanocortin at distinct pairs of basic residues. Proc Natl Acad Sci U S A 88(9):3564-8.

Biewener AA (1991). Musculoskeletal design in relation to body size. J Biomech 24 Suppl 1:19-29.

Bradshaw WE, Holzapfel CM (2010). Light, time, and the physiology of biotic response to rapid climate change in animals. Annu Rev Physiol 72:147-66. Review.

Chomczynski P, Sacchi N (1987). Single-step method of RNA isolation by acid guanidinium thiocyanate-phenol-chloroform extraction. Anal Biochem 162: 156–159.

Cota D, Marsicano G, Tschöp M, Grübler Y, Flachskamm C, Schubert M, Auer D, Thöne-Reinecke C, Ortmann S, Cervino C, Linthorst A, Pasquali R, Lutz B, Stalla GK, Pagotto U (2003). Decreased fat mass in mice deficient for cannabinoid receptor 1 is due to decreased orexigenic drive and impaired adipocyte differentiation. J Clin Invest 112:423-431.

Elvert R, Heldmaier G (2005). Cardiorespiratory and metabolic reactions during entrance into torpor in dormice, *Glis glis*. J Exp Biol 208(Pt 7):1373-83.

Green EC (1935). *Anatomy of the Rat*. Haffner Publishing, New York.

Heldmaier G (1989). Seasonal acclimization of energy requirements in mammals: functional significance of body weight control, hypothermia, torpor and hibernation. In: Wieser W, Gnaiger E (eds) Energy Transformations in Cells and Organisms. Georg Thieme, Stuttgart, pp 130-139.

Heldmaier G, Klingenspor M, Werneyer M, Lampi BJ, Brooks SP, Storey KB (1999). Metabolic adjustments during daily torpor in the Djungarian hamster. Am J Physiol 276(5 Pt 1):E896-906.

Heldmaier G, Ortmann S, Elvert R (2004). Natural hypometabolism during hibernation and daily torpor in mammals. Respir Physiol Neurobiol. 2004 Aug 12;141(3):317-29. Review.

Heldmaier G, Ruf T (1992). Body temperature and metabolic rate during natural hypothermia in endotherms. J Comp Physiol [B] 162(8), 696-706.

Klieverik LP, Foppen E, Ackermans MT, Serlie MJ, Sauerwein HP, Scanlan TS, Grandy DK, Fliers E, Kalsbeek A (2009). Central effects of thyronamines on glucose metabolism in rats. J Endocrinol. 201(3):377-86.

Klingenspor M, Niggemann H, Heldmaier G (2000). Modulation of leptin sensitivity by short photoperiod acclimation in the Djungarian hamster, *Phodopus sungorus*. J Comp Physiol B 170(1):37-43.

Kunos G, Osei-Hyiaman D, Liu J, Godlewski G, Bátkai S (2008). Endocannabinoids and the control of energy homeostasis. J Biol Chem 283(48):33021-5.

Lee SJ, McPherron AC (2001). Regulation of myostatin activity and muscle growth. Proc Natl Acad Sci USA 98(16):9306-9311.

Lyman CP und O'Brien RC (1963). Autonomic control of circulation during the hibernating cycle in ground squirrels. J Physiol 168 477-499.

Marsicano G, Goodenough S, Monory K, Hermann H, Eder M, Cannich A, Azad SC, Cascio MG, Gutiérrez SO, van der Stelt M, et al. (2003). CB1 cannabinoid receptors and on-demand defense against excitotoxicity. Science *3*, 84-88.

Marsicano G, Wotjak CT, Azad SC, Bisogno T, Rammes G, Cascio MG, Hermann H, Tang J, Hofmann C, Zieglgänsberger W, et al. (2002). The endogenous cannabinoid system controls extinction of aversive memories. Nature *418*, 530-534.

Matsakas A, Diel P (2005). The growth factor myostatin, a key regulator in skeletal muscle growth and homeostasis. Int J Sports Med 26(2):83-89.

Mercer JG, Tups A (2003). Neuropeptides and anticipatory changes in behaviour and physiology: seasonal body weight regulation in the Siberian hamster. Eur J Pharmacol 7;480(1-3):43-50.

Mercer JG, Moar KM, Rayner DV, Trayhurn P, Hoggard N (1997). Regulation of leptin receptor and NPY gene expression in hypothalamus of leptin-treated obese (ob/ob) and cold-exposed lean mice. FEBS Lett 3;402(2-3):185-8.

Mercer JG, Moar KM, Ross AW, Morgan PJ (2000). Regulation of leptin receptor, POMC and AGRP gene expression by photoperiod and food deprivation in the hypothalamic arcuate nucleus of the male Siberian hamster (Phodopus sungorus). Appetite 34(1):109-11.

Milsom WK, Burlington RF, Burleson ML (1993). Vagal influence on heart rate in hibernating ground squirrels, J Exp Biol 185 25-32.

Milsom WK, Zimmer MB, Harris MB (1999). Regulation of cardiac rhythm in hibernating mammals. Comp Biochem Physiol A Mol Integr Physiol. 124(4) 383-391.

Moreira FA, Lutz B (2008). The endocannabinoid system: emotion, learning and addiction. Addict Biol 13:196-212.

Morhardt JE (1970). Heart rates, Breathing rates and the effect of Atropine and Acetycholine on white-footed mice (*Peromyscus sp.*) during daily torpor. Comp Biochem Physiol 33 441-457.

Morris S, Curtin AL, Thompson MB (1994). Heterothermy, torpor, respiratory gas exchange, water balance and the effect of feeding in Gould's long-eared bat Nyctophilus gouldi. J Exp Biol 197:309-35.

Niggemann H (1998), Diplomarbeit, Philipps Universität Marburg.

Ootsuka Y, de Menezes RC, Zaretsky DV, Alimoradian A, Hunt J, Stefanidis A, Oldfield BJ, Blessing WW (2009). Brown adipose tissue thermogenesis heats brain and body as part of the brain-coordinated ultradian basic rest-activity cycle. Neuroscience 164(2):849-61.

Ortmann S, Heldmaier G (2000). Regulation of body temperature and energy requirements of hibernating alpine marmots (Marmota marmota). Am J Physiol Regul Integr Comp Physiol 278(3):R698-704.

Osei-Hyiaman D, Liu J, Zhou L, Godlewski G, Harvey-White J, Jeong WI, Bátkai S, Marsicano G, Lutz B, Buettner C, Kunos G (2008). Hepatic CB1 receptor is required for development of diet-induced steatosis, dyslipidemia, and insulin and leptin resistance in mice. J Clin Invest 118(9):3160-9.

Piomelli D (2003). The molecular logic of endocannabinoid signalling. Nat Rev Neurosci 4:873-84.

Ravinet Trillou C, Delgorge C, Menet C, Arnone M, Soubrié P (2004). CB1 cannabinoid receptor knockout in mice leads to leanness, resistance to diet-induced obesity and enhanced leptin sensitivity. Int J Obes Relat Metab Disord 28(4):640–648.

Reddy AB, Cronin AS, Ford H, Ebling FJ (1999). Seasonal regulation of food intake and body weight in the male Siberian hamster: studies of hypothalamic orexin (hypocretin), neuropeptide Y (NPY) and pro-opiomelanocortin (POMC). Eur J Neurosci 11(9):3255-64.

Refinetti R, Menaker M (1992). The circadian rhythm of body temperature. Physiol Behav 51(3):613-37. Review.

Scanlan TS, Suchland KL, Hart ME, Chiellini G, Huang Y, Kruzich PJ, Frascarelli S, Crossley DA, Bunzow JR, Ronca-Testoni S, Lin ET, Hatton D, Zucchi R, Grandy DK (2004). 3-Iodothyronamine is an endogenous and rapid-acting derivative of thyroid hormone. Nat Med 10(6):638-42.

Song X, Körtner G, Geiser F (1997). Thermal relations of metabolic rate reduction in a hibernating marsupial. Am J Physiol 273(6 Pt 2):R2097-104.

Steiner M, Lutz B (2006). Endocannabinoid-System und zentrales Nervensystem. Ed. Schusdziarra V. Das Endocannabinoid-System. UNI-MED Verlag Bremen. pp 25-44 Moreira & Lutz 2008.

Stieglitz A, Spiegelhalter F, Klante G, Heldmaier G (1995). Urinary 6-sulphatoxymelatonin excretion reflects pineal melatonin secretion in the Djungarian hamster (Phodopus sungorus). J Pineal Res 18(2):69-76.

Strumwasser F (1960). Some physiological principles governing hibernation in Citellus beecheyi, Bulletin of the Museum of Comparative Zoology 124 (1960) 285-320.

Swoap SJ, Gutilla MJ, Liles LC, Smith RO, Weinshenker D (2006). The full expression of fasting-induced torpor requires beta 3-adrenergic receptor signaling. J Neurosci 4;26(1):241-5.

Swoap SJ, Weinshenker D (2008). Norepinephrine controls both torpor initiation and emergence via distinct mechanisms in the mouse, PLoS One 3(12):e4038.

Wade GN, Bartness TJ (1984). Effects of photoperiod and gonadectomy on food intake, body weight and body composition in Siberian hamsters. Am J Physiol 246:26-30.

Wiesinger H (1989). Kälteakklimation beim Djungarischen Zwerghamster, *Phodopus sungorus*. Dissertation, Philipps Universität Marburg.

Wynne K, Stanley S, McGowan B, Bloom S (2005). Appetite control. J Endocrinol 184(2):291-318. Review.

Zosky GR (2002). The parasympathetic nervous system: Its role during torpor in the fat-tailed dunnart (Sminthopsis crassicaudata), J Comp Physiol [B] 172(8) 677-684.

2. MANUSKRIPTE UND PUBLIKATIONEN

RESEARCH ARTICLE

Seasonal Changes of Myostatin Expression and Its Relation to Body Mass Acclimation in the Djungarian Hamster, *Phodopus sungorus*

JOURNAL OF EXPERIMENTAL ZOOLOGY
PART A
ECOLOGICAL GENETICS AND PHYSIOLOGY
A Journal of Integrative Biology

L. J. BRAULKE[1]*, G. HELDMAIER[1], DIAZ M. BERRIEL[2], J. ROZMAN[3], AND C. EXNER[1]
[1]Department of Biology, Philipps-University Marburg, Marburg, Germany
[2]Emmy Noether and Marie Curie Research Group Molecular Metabolic Control, DKFZ-ZMBH Alliance, German Cancer Research Center (DKFZ) Heidelberg, Heidelberg, Germany
[3]Helmholtz Zentrum München, Institute of Experimental Genetics, Munich/Neuherberg, Germany

ABSTRACT

The Djungarian hamster is an animal that is prominent for distinct seasonal adaptations. Cued by shortening day length in autumn they spontaneously exhibit reductions in food intake, body mass (BM), fat mass and also in lean mass (LM). The mechanisms behind the seasonal regulation of body composition are only partly resolved. Although most studies focused on the participation of body fat in seasonal body weight regulation, we addressed the influence of LM, moreover of muscle mass (MM) on seasonal BM changes. Therefore, we analyzed body composition, MM and the expression of myostatin, a hormone negatively regulating muscle growth and differentiation, in Djungarian hamsters in response to naturally changing photoperiod in winter compared to long photoperiod (LP). Winter-acclimated hamsters upregulated myostatin mRNA when compared with hamsters adapted to natural and artificial LP, whereas MM remained unchanged when compared with natural LP. Moreover, in natural short photoperiod, individual myostatin expression levels were negatively correlated with MM. These results suggest that myostatin is under seasonal control in order to regulate MM and hence contributes to the overall LM and therefore BM changes in seasonal mammals. *J. Exp. Zool. 313A, 2010.* © 2010 Wiley-Liss, Inc.

How to cite this article: Braulke LJ, Heldmaier G, Berriel DM, Rozman J, Exner C. 2010. Seasonal changes of myostatin expression and its relation to body mass acclimation in the Djungarian hamster, *Phodopus sungorus*. J. Exp. Zool. 313A:[page range].

The Djungarian hamster *Phodopus sungorus*, a small cricetid rodent weighing 25 to 45 g, which mainly inhabits the Djungarian steppe, shows a variety of seasonal adjustments cued by day length (Hoffmann, '81; Steinlechner and Heldmaier, '82). The day length is converted into a biochemical signal via the nightly secretion of melatonin from the pineal gland (Hoffmann, '73; Axelrod, '74; Goldman and Darrow, '83; Stieglitz et al., '95). A photoperiod below 12 hr (critical photoperiod) induces the winter adaption (Hoffmann, '82), which includes reductions of food intake (Wade and Bartness, '84) and body mass (BM) (Heldmaier and Steinlechner, '81a), a reduction of the reproductive organs,

Abbreviations: BM, body mass; DEXA, dual energy X-ray absorption; FM, fat mass; GDF-8, growth and differentiation factor-8; Myostatin; LM, lean mass; LP, long photoperiod; MM, muscle mass; NP, natural photoperiod; SP, short photoperiod.

*Correspondence to: L. J. Braulke, Department of Biology, Philipps-University Marburg, Karl von Frisch Str.8, 35032 Marburg, Germany.
E-mail: braulkel@staff.uni-marburg.de

Received 10 December 2009; Revised 31 March 2010; Accepted 17 May 2010
Published online in Wiley InterScience (www.interscience.wiley.com). DOI: 10.1002/jez.626

a change in fur color from the brown summer state to snow-white winter acclimatized condition (Figala et al., '73), an increase in fur density (Heldmaier and Steinlechner, '81a; Heldmaier and Lynch, '86), and alterations in energy metabolism, such as lower thermoneutral zones, decreased basal metabolic rates, increased cold tolerance, and the ability to display spontaneous daily torpor (Heldmaier et al., '89; Heldmaier and Klingenspor, 2003 for review). All these measures, including the reduction of BM, reduce individual energy requirements in winter-acclimatized small mammals (Heldmaier and Steinlechner, '81a; Heldmaier, '89). Under natural conditions, the hamsters' winter status is reversed to the summer status during February and March in parallel with increasing day lengths. However, the return to the summer status (recrudescence) does not necessarily require an exposure to long photoperiod (LP) but may also occur spontaneously after 5 months exposure to short photoperiod (SP) (Heldmaier and Lynch, '86 for review).

The seasonal change in body weight is modulated in response to environmental cues and/or endogenous circannual rhythms (Steinlechner et al., '83; Dark and Zucker, '84). Fasting-refeeding and lipectomy experiments during the transition from summer to winter state showed that Djungarian hamsters are able to adjust their BM at any intermediate level of the transition (Steinlechner et al., '83; Mauer and Bartness, '94). Photoperiodic control of seasonal changes in BM include changes in body fat content as well as in lean mass (LM), including muscle mass (MM) (Wade and Bartness, '84; Klingenspor et al., 2000). The mechanisms regulating these seasonal changes of body composition are only partly resolved. A central role for the control of lipid storage is played by leptin, especially by seasonal changes in leptin sensitivity. Compared with LP-adapted hamsters, circulating leptin levels are significantly decreased in SP-acclimated hamsters but as they have a high sensitivity for leptin they can respond to leptin by a reduction of food intake and BM, whereas LP-acclimated hamsters with a high body fat content and high leptin levels are refractory toward leptin (Klingenspor et al., 2000; Mercer and Tups, 2003; Adam and Mercer, 2004).

The endocrine control for seasonal changes in LM is not known at all. Myostatin, also known as GDF8 (growth and differentiation factor-8) is a member of the tumor growth factor-β family, is produced by skeletal muscle, circulates in the blood, and acts as a potent inhibitor of skeletal muscle growth and differentiation in a concentration-dependent manner (see review Matsakas and Diel, 2005). These properties of myostatin are precisely those hypothesized by Bullough ('62, '65) for molecules that act to regulate tissue size, and to be consistent with the terminology that he proposed, myostatin should be considered to be a muscle chalone (Lee, 2004). Disruption of the myostatin gene or signaling, for example by inhibition of circulating myostatin with follistatin or by expression of a dominant-negative form of the myostatin receptor ActRIIB, in mice induces a dramatic increase in MM caused by a combination of hypertrophy and hyperplasia (Lee and McPherron, 2001). Besides massively increased MM and hence increased BM, a lack of the myostatin gene results in increased in bone density, content, and strength (Elkasrawy and Hamrick, 2010).

Hypothetically one could expect that seasonal reduction in BM is combined with a seasonal reduction in MM and hence an increased myostatin expression. Therefore, we analyzed whether myostatin, most relevant for muscle growth and differentiation, is under seasonal control, in order to regulate MM and hence contributes to the overall LM and therefore BM changes in seasonal mammals. To confirm this hypothesis, we studied body compositions by non-invasive dual energy X-ray absorption (DEXA) scanning and measured MM and myostatin expression of Djungarian hamsters kept in seasonally changing photoperiod and artificial LP.

ANIMALS, MATERIALS, AND METHODS

Animals

One hundred twenty-eight Djungarian hamsters (*Phodopus sungorus*) were bred and raised at the University of Marburg under natural photoperiod (NP) (according to geographic coordinates: 50° 49′ 0″ N, 8° 46′ 0″ E) and a constant ambient temperature (T_a) of 24 ± 1°C. Postweaning hamsters were housed individually in makrolon-cages type II (16 cm × 21 cm × 13 cm) with wood shavings and were constantly supplied with water and food (ALTROMIN 7014) ad libitum. At the age of 10 weeks, hamsters were transferred either into SP ($n = 12$); LD 8:16; light on: 08:00 h, light off: 1600 h; $T_a = 24 \pm 1$°C), into LP ($n = 56$); LD 16:8; light on: 0400 h, light off: 2000 h; $T_a = 24 \pm 1$°C), or remained in NP ($n = 60$); LD naturally changing, according to geographic coordinates: 50° 49′ 0″ N, 8° 46′ 0″ E; $T_a = 24 \pm 1$°C).

Body Weight and Body Composition

To detect the influence of constant short (SP, $n = 12$; mean birth date: 8th April ± 2.36 days), constant long (LP, $n = 14$; mean birth date: 3rd May ± 0.98 days) or NP ($n = 12$; mean birth date: 13th June ± 3.27 days) on BM and body composition, such as LM and fat mass (FM), hamsters were analyzed every 2–3 weeks, starting with transfer to different photoperiods (i.e. 10 weeks after birth, for NP at 28th August), using a DEXA scanner (PIXIMUS2 scanner, software version 1.46.007; GE Medical Systems, Madison, WI). The DEXA scans were performed under 4% Isoflurane anesthesia (Forene; Abbott, Wiesbaden, Germany).

Tissue Sampling

An additional cohort of hamsters kept at constant long (LP, $n = 42$; mean birth date: 10th June ± 2.55 days) or natural changing photoperiod (NP, $n = 42$; mean birth date: 9th June ± 2.45 days) was used for analysis of MM and myostatin expression. Every 3 weeks, six hamsters of each photoperiod were killed and the heart, liver, spleen, suprasternal brown adipose tissue (BAT), musculus quadriceps, musculus gastrocnemius and

musculus tibialis anterior were dissected and weighed. Bone mineral content (BMC) was analyzed by using DEXA. Data were pooled and presented in three periods. The first sampling period includes the data from tissues gathered when NP was longer than the critical value of about 12 hr light per day (between mid August and mid September; NP-summer). The second period contains data from tissues gathered in winter (between mid October and mid January; NP-winter). The third sampling period comprises data from tissues during recrudescence of NP hamsters (between mid February and mid March; NP-spring).

RNA Isolation

Total RNA was isolated from musculus quadriceps. This was performed with TRIzol (Invitrogen) according to the manufacturer's protocol (Chomczynski and Sacchi, '87). As an additional step, the RNA pellet was redissolved in a solution containing 6.3 M guanidinium thiocyanate, 40 mM sodium citrate pH 7, 0.8% sarcosyl, 8 mM 2-mercaptoethanol, precipitated with 1 vol isopropanol, washed in 75% ethanol, and finally dissolved in DEPC-treated water. Total RNA was photometrically quantified at 260 nm and stored at −80°C.

RNA-Dot Blotting

This method was used because it allowed analyzing all RNA samples in one blot. As RNA samples are not separated by electrophoresis, premise for this method is the use of a highly specific prime-labeled cDNA. All used cDNA probes had previously been tested for specificity using Northern blot hybridization. Two micrograms of RNA was denatured, blotted to a nylon membrane (Hybond N, Amersham) using a dot-blot filtration manifold (Phillips-University Marburg, Germany), and UV cross-linked (UV-Stratalinker, Stratagene).

Cloning of a *Phodopus sungorus* Myostatin cDNA Fragment

Total RNA from the gastrocnemius muscle of *Phodopus sungorus* was reverse transcribed into cDNA using the Superscript™ II Reverse Transcriptase (Invitrogen). A 503 bp-fragment of the myostatin (GDF8) cDNA was amplified by RT-PCR using the following primers designed based on a mouse and rat consensus sequence: forward, 5′-TGTGGAAAAAGAGGGGCTGTGTAA-3′; reverse, 5′-AGTGCCTGGGCTCATGTCAAGTTT-3′. The amplified cDNA fragment was cloned into the pGEM-T vector, verified by sequencing and subsequently used as template for the synthesis of labeled myostatin cDNA probes.

Radioactive Hybridization

Specific cDNA fragments were random prime-labeled with [α-^{32}P]dCTP (Rediprime DNA labeling system; Amersham). Nylon membrane was prehybridized at 63°C with BSA solution (0.5 M Na_2PO_4/NaH_2PO_4, pH 7.0, 1 mM EDTA, pH 8.0, 7% SDS, 1% BSA) for at least 1 hr and hybridized overnight at 63°C with the ^{32}P-labeled probe. After hybridization, the blots were washed with 2 × SSC/0.1% SDS for 15 min, 1 × SSC/0.1% SDS for 15 min, and 0.5 × SSC/0.1% SDS for 10 min at room temperature. The stringency of washing was subsequently increased to 0.1 × SSC/0.1% SDS for 10 min at 60°C. Signal intensities were monitored by exposure to a PhosphorScreen (Molecular Dynamics) and then detected by phosphor imaging (Storm 860; Molecular Dynamics). ArrayVision 7.0 (Imaging Research) was used for quantifying the signal intensities.

The blot was hybridized with probes corresponding to the cDNA sequences of hamster myostatin (GDF8). Hybridization with a probe detecting β-actin was used for normalization. In between subsequent hybridizations, membranes were stripped by shaking for 20 min at 64°C after addition of boiling 0.1 × SSC.

Relative myostatin expression levels are presented as relative to an internal standard myostatin mRNA, which was extracted from six animals in August.

Statistics

Data are presented as mean ± standard error. The effect of photoperiod on body compositions in male and female hamsters was evaluated by two-way repeated measures analysis of variance (Two-way RM ANOVA), with gender and days of exposure as factors. The effect of sampling period in NP and LP on tissue masses was assessed by two-way analysis of variance (Two-way ANOVA). Multiple comparisons post-hoc were performed by Fisher LSD Method. Relations between data were detected using the Pearson product moment correlation procedure and described by correlation coefficient. All data were tested for normality and homogeneity of variance and were log10-transformed and reanalyzed if these assumptions were not met. All statistical analyses were conducted using SigmaStat for Windows (version 3.5; Systat Software, Inc.). Statistical significance was determined at $P<0.05$, unless stated otherwise.

All experiments were done in accordance with approved guidelines for the use and care of animals by the German animal welfare law (Deutsches Tierschutzgesetz).

RESULTS

Body Composition

Long-term effects of different photoperiodic regimes (i.e. constant long (LP), naturally changing (NP) and constant SP) on changes in body composition in *Phodopus sungorus* are illustrated in Figure 1. The time course of the response to SP and NP is similar in parameters studied, except for FM in females, which tend to be higher in NP when compared with SP. Until mid of January in NP or the 20th week in SP, both male NP and SP hamsters constantly lost BM by about 7.5 g, FM by 4–5 g, and LM by about 2–3 g (Fig. 1A–C). Female NP and SP hamsters also reduced their BM until mid of January in NP or the 20th week in SP, but to a lesser extent by only 4.5 g when compared with male hamsters (Two-way RM ANOVA; $P = <0.001$ for NP and SP; Fig. 1D). FM in female

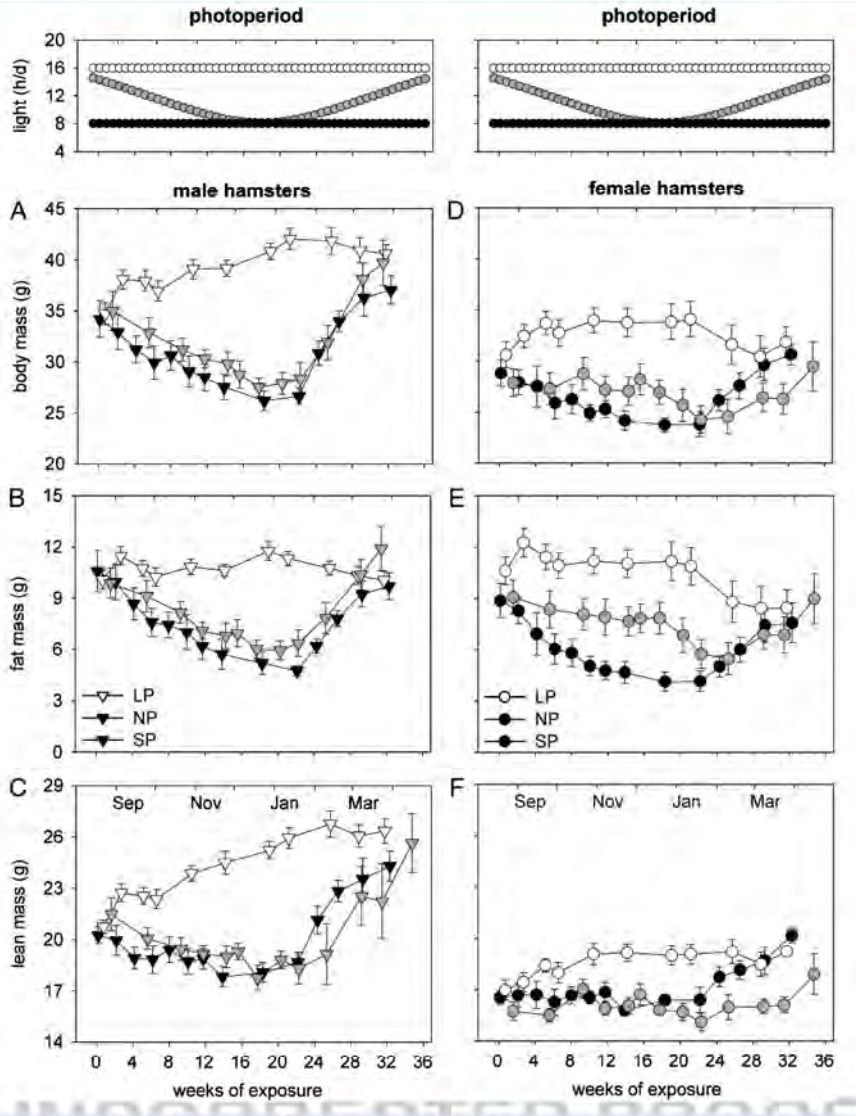

Figure 1. Changes of body mass (A, D), fat mass (B, E) and lean mass (C, F) of male (triangles) and female (circles) hamsters in response to constant LP (white symbols), changing NP (gray symbols), and constant SP (black symbols). LP, long photoperiod; NP, natural photoperiod; SP, short photoperiod.

hamsters was reduced by about the same amount as observed in male hamsters (Fig. 1E). In contrast to male hamsters which reduced their LM, female hamsters maintained a constant LM during winter until the end of January (Two-way RM ANOVA; for NP: $P = < 0.001$; for SP: $P = 0.043$) (Fig. 1F). By the end of January in NP and after 22 weeks exposure to constant SP, male and female NP and SP hamsters started to become recrudescent and rapidly increased BM, fat, and LM. Within the following 2 months these animals reached values for BM, fat content, and LM identical to hamsters of the same age kept in constant LP.

In constant LP male hamsters continually increased their BM throughout the entire observation period of 34 weeks. This was accompanied by a continuous increase in LM, whereas FM remained constant (Fig. 1A–C). Female LP hamsters increased their BM within the first 5 weeks, remained constant for the following 16 weeks, and then decreased to near initial values of about 32 g. A similar pattern was detected in FM. LM of these hamsters increased by about 2–3 g in the first 11 weeks in LP and then remained constant until the end of observation.

Table 1. Tissue masses of Djungarian hamsters exposed to constant LP or natural changing photoperiod.

	Sampling period 1		Sampling period 2		Sampling period 3	
Tissue (mg)	LP (n = 12)	NP-summer (n = 12)	LP (n = 18)	NP-winter (n = 18)	LP (n = 12)	NP-spring (n = 12)
Heart	198 ± 11.47	185 ± 9.88	214 ± 9.03	195 ± 5.52	214 ± 7.11	188 ± 8.93
Liver	1,336 ± 69.76	1,198 ± 52.44	1,466 ± 53.52	1,169 ± 35.82[a]	1,466 ± 56.74	1,193 ± 49.95[a]
Spleen	67 ± 5.74	63 ± 5.73	87 ± 7.31	52 ± 1.52[a]	95 ± 20.06	72 ± 4.34
BAT	241 ± 25.21	209 ± 15.46	247 ± 8.31	171 ± 14.15[a]	208 ± 16.17	209 ± 21.97
Muscle[b]	127 ± 8.11	125 ± 7.82	149 ± 8.39[c]	118 ± 3.87[a]	159 ± 7.03[c]	135 ± 6.40[a]
BMC	370 ± 13.20	349 ± 13.40	427 ± 15.90[c]	397 ± 18.92[d]	462 ± 18.01[c]	385 ± 16.52[a]

Mean ± SEM are given. Significant differences ($P < 0.05$) were evaluated by two-way ANOVA; post-hoc by all pairwise multiple comparison procedure (Fisher LSD method). LP, long photoperiod; NP, natural photoperiod; BMC, bone mineral content; BAT, suprasternal brown adipose tissue.[a]Significant difference when compared with values of LP in the same sampling period.[b]The sum of muscle masses of musculus tibialis anterior, musculus gastrocnemius, and musculus quadriceps.[c]Significant difference when compared with values of LP in sampling period 1.[d]Significant difference when compared with values of NP-summer in sampling period 1.

To elucidate the participation of specific tissues in the seasonal reorganization of BM, masses of heart, liver, spleen, BMC, limb muscles, and BAT were analyzed during natural changing photoperiod when compared with constant LP (Table 1). Tissue samples were pooled and presented in three periods as described in the methods. Two-way ANOVA (post-hoc Fisher LSD; $P > 0.05$, each) revealed no difference between these tissue masses of male and female hamsters and therefore data were pooled for further analysis. No substantial change in heart mass was caused by changing photoperiod. Furthermore, no difference between heart masses of NP and LP hamsters was detected during any sampling period. In addition, no significant changes in masses of liver, spleen, BAT, and muscle were detected in response to NP. Yet these tissue masses were significantly higher in LP hamsters during the second sampling period when compared with NP hamsters in winter (Two-way ANOVA, post-hoc Fisher LSD; $P < 0.05$, each). Interestingly, NP hamsters showed enhanced BMC in winter when compared with NP hamsters in summer. In LP hamsters, BMC and MM were increased in second and third sampling periods when compared with the first sampling period.

MM and Myostatin Expression

MM of musculus quadriceps and relative myostatin mRNA expression of LP and NP hamsters were analyzed and presented in Figure 2. Tissue samples were obtained in three periods as mentioned above. Hamsters in NP maintained their quadriceps MM constant during winter and slightly, yet not significantly, increased it during spring (Fig. 2B). In contrast, hamsters kept in LP significantly increased their quadriceps MM from 77.42 ± 5.74 to 102.58 ± 4.85 mg over the observation period of 7 months (Two-way ANOVA, post-hoc Fisher LSD; $P = 0.001$). NP hamsters in winter had a lower MM (75.11 ± 2.74 mg) when compared with LP hamsters with a MM of 94.00 ± 5.83 mg (Two-way ANOVA, post-hoc Fisher LSD; $P = 0.006$) (Fig. 2B-2). In addition, in spring, the muscles of NP hamsters weighed significantly less than those of their LP counterparts during the third sampling period (Two-way ANOVA, post-hoc Fisher LSD; $P = 0.047$; Fig. 2B-3).

NP hamsters' relative myostatin mRNA was increased in winter and differed significantly from the myostatin expression of muscles sampled in LP (Two-way ANOVA, post-hoc Fisher LSD; $P = 0.003$) (Fig. 2C-2). In LP hamsters, myostatin expression remained unchanged in the second sampling period but was increased in the third sampling period (Two-way ANOVA, post-hoc Fisher LSD; $P = 0.032$) (Fig. 2C). No difference between myostatin expression of NP hamsters in spring and LP hamsters of the third sampling period was detected (Two-way ANOVA, post-hoc Fisher LSD; $P = 0.43$) (Fig. 2C-2).

NP hamsters adapted to winter did not show any correlation between MM of musculus quadriceps and body weight. In contrast, MM of musculus quadriceps in LP hamsters significantly correlated with BM (Pearson correlation: $r = 0.78$; $P = < 0.001$) (Fig. 3). The largest male hamster with a BM of 46.4 g had a MM of 135 mg, whereas the smallest female hamster with 29.2 g BM had a quadriceps MM of 60 mg. No difference between male and female hamsters with regard to the slope of the regression in the relation between BM and MM was detected.

The relationship between relative myostatin mRNA expression and MM is presented in Figure 4. Relative myostatin mRNA was negatively correlated with MM in NP hamsters adapted to winter (Pearson correlation: $r = -0.636$; $P = 0.0046$) (Fig. 4B). In NP hamsters, this correlation was neither observed during summer nor during spring (data not shown). Relative myostatin mRNA does not correlate with MM of hamsters kept at constant LP (Fig. 4A).

DISCUSSION

Male and female Djungarian hamsters responded to natural and artificial SP by decreasing BM and FM, which is in accordance

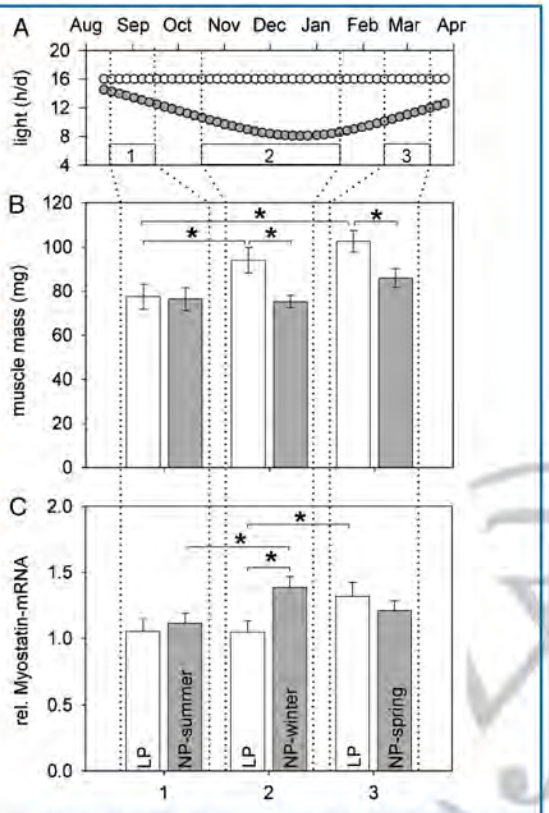

Figure 2. Means (±SE) of muscle mass (B) and its relative myostatin mRNA (C) of hamsters sacrificed at different times of the year. (Sampling period 1: between mid August and mid September; sampling period 2: between mid October and mid January; sampling period 3: between mid February and mid March.) Samples derived from hamsters either kept in constant LP (white symbols) or natural changing photoperiod (gray symbols). Myostatin expression is presented as relative to an internal standard myostatin-mRNA, which was extracted from six animals in August.

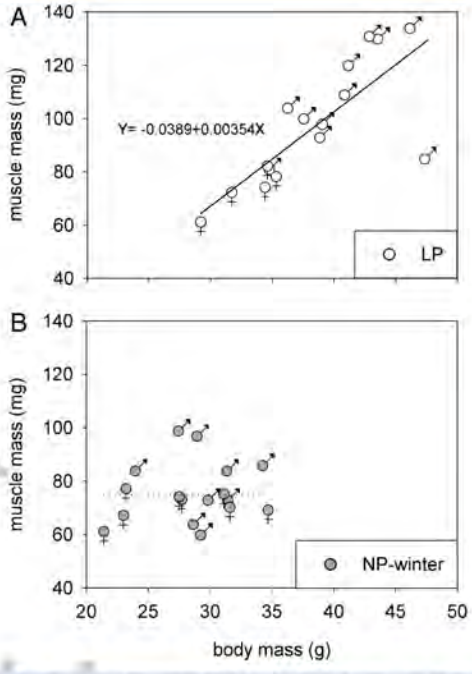

Figure 3. Relation between BM and muscle mass of musculus quadriceps of male (♂) and female (♀) hamsters adapted to constant LP (A; white symbols) and hamsters adapted to natural SP/NP-winter (B; gray symbols). Muscle mass significantly correlates with BM in LP ($r = 0.78$; $P < 0.05$) but not in natural SP. (For LP, data are presented from LP hamsters of the same age and dissected in the same sampling period as hamsters adapted to natural SP). LP, long photoperiod, NP, natural photoperiod; SP, short photoperiod; BM, body mass.

with previous observations (for review see Bartness and Wade, '85). This seasonal reduction was also accompanied by a reduction in LM by about 2–3 g in male hamsters, but no significant changes were observed in females. However, female hamsters exposed to continuous LP showed a greater LM when compared with female hamsters exposed to continuous SP and natural SP. This indicates that LM of females also responds to seasonal changes in photoperiod. Furthermore, LM of adult females is always less than LM of adult male hamsters with the same BM.

Previous studies either did not observe seasonal changes in LM or did not consider gender differences in this response (Wade and Bartness, '84; Bartness and Wade, '85; Klingenspor et al., 2000). Our present findings were obtained by a new non-invasive method for analysis of body composition (DEXA-scanning), which allowed repeated high-resolution measurements in the same individuals. The gender-specific decrease in LM can partly be explained by gonadal regression. Although female hamsters lose only about 100 mg of ovary pair mass and uterine mass in SP (Moffatt-Blue et al., 2006), gonadal regression is more pronounced in male hamsters by reduction of testis weight by up to 800 mg (Hoffmann, '73; Steinlechner and Puchalski, 2002). The analysis of changes in additional organs such as heart, liver, spleen, muscle, and BMC in response to natural SP did not show any significant gender-specific differences in this study. Therefore, the further causes of gender-specific difference in LM changes cannot be specified at the moment, but will require further studies.

Tissue masses of liver, spleen, BAT, and muscles were significantly less during natural SP when compared with tissues of hamsters kept in constant LP. Compared with the hamsters from natural LP in summer, only a trend in reduction of these tissues was observed. Previous studies showed that intestine is also reduced in SP when compared with LP hamsters (Wiesinger, '89). Heart mass remained constant throughout the exposure to natural changing photoperiod in this study and

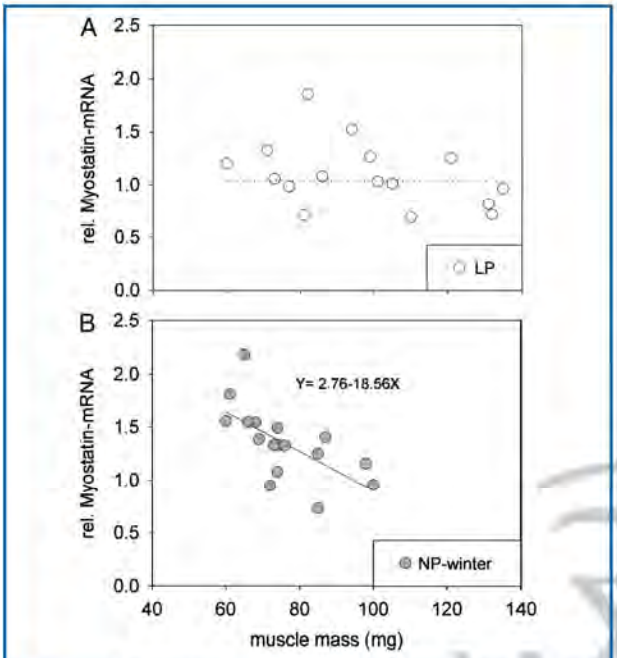

Figure 4. Relation between muscle mass of musculus quadriceps and relative myostatin mRNA of hamsters adapted to constant LP (A; white symbols) and hamsters adapted to natural SP/NP-winter (B; gray symbols). Relative myostatin expression significantly correlates with muscle mass in natural SP ($r = -0.64$; $P < 0.05$) but not in LP. (For LP, data are presented from LP hamsters of the same age and dissected in the same sampling period as hamsters adapted to natural SP). LP, long photoperiod; NP, natural photoperiod; SP, short photoperiod.

corresponded to heart masses in constant LP. In contrast, BMC was increased in NP hamsters in winter and in LP hamsters. In addition, fur density is increased in response to SP (Heldmaier and Lynch, '86). These partly contradictory findings demonstrate the complexity in seasonal reorganization of tissues and the regulating mechanisms behind. We concentrated on the contribution of MM and its regulation to seasonal LM and therefore BM changes.

MM of musculus quadriceps remained constant in NP hamsters during winter, i.e. in response to natural SP (Fig. 3) and does not contribute to seasonal reductions of BM. Hamsters maintained in LP increased their MM. This is in accordance with earlier observations where a greater mass of hind leg femoral muscle was observed in LP-acclimated hamsters when compared with SP-acclimated hamsters (Klingenspor et al., 2000). Our data suggest that MM contributes to low BM in SP by reduced muscle growth rather than by a decrease of MM.

In mammals, MM or performance increases during training and is diminished during long-term resting conditions. This muscle wasting indicates that the maintenance of MM and power is energetically rather costly. Djungarian hamsters remain active during the entire winter season. They do not hibernate but show only daily torpor during their diurnal resting period and are active outside their burrows even in cold winter nights (Flint, '66; Heldmaier and Steinlechner, '81b). This requires the maintenance of physical performance and thus it seems reasonable to maintain a constant MM. Muscle is also an important site of thermoregulatory heat production. It has been shown that the capacity for shivering thermogenesis is maintained constant during winter and non shivering thermogenesis is enhanced. This is also in agreement with a constant MM.

According to the common assumption that skeletal MM is related to BM in most species (Biewener, '91), a positive relationship between MM and BM was observed in hamsters adapted to LP. Surprisingly, no such correlation between MM and BM was detected in hamsters adapted to natural SP. This indicates a BM independent and therefore differential regulation of MM in response to SP.

Indeed, in NP hamsters, relative myostatin mRNA was significantly upregulated in winter when compared with spring or LP hamsters, concluding a seasonal regulation of myostatin. The fact that relative myostatin mRNA is negatively correlated with MM in winter underlines its function as a negative regulator of MM as proposed by others (Lee and McPherron, '99; Matsakas and Diel, 2005). However, this correlation was neither observed in constant LP nor in NP-summer or -spring. This suggests either that myostatin is not used as a negative regulator for muscle growth in LP or low MM in winter may be achieved by increased sensitivity to myostatin. A similar change in sensitivity as it is shown for leptin, which acts as a negative regulator of lipid accumulation (Klingenspor et al., 2000; Mercer and Tups, 2003; Adam and Mercer, 2004). Myostatin is synthesized as a precursor protein, which is then proteolysed in propeptide and active 12.5-kDa ligand (McPherron et al., '97; Thomas et al., 2000; Ríos et al., 2004; Matsakas and Diel, 2005). Therefore, the negative relationship between MM and myostatin expression in NP-winter, which is missing in LP, can also be a result of posttranslational modifications depending on season, i.e. photoperiod. However, these implications have to be further elucidated in future studies. Nevertheless, our data suggest that myostatin is seasonally regulated and contributes to low MM and hence low lean and BM during seasonal acclimatization in the Djungarian hamster, *Phodopus sungorus*.

LITERATURE CITED

Adam CL, Mercer JG. 2004. Appetite regulation and seasonality: implications for obesity. Proc Nutr Soc 63:413–419.

Axelrod J. 1974. The pineal gland: a neurochemical transducer. Science 184:1341–1348.

Bartness TJ, Wade GN. 1985. Photoperiodic control of seasonal body weight cycles in hamsters. Neurosci Biobehav Rev 9:599–612.

Biewener AA. 1991. Musculoskeletal design in relation to body size. J Biomech 24:19–29.

Bullough WS. 1962. The control of mitotic activity in adult mammalian tissues. Biol Rev 37:307–342.

Bullough WS. 1965. Mitotic and functional homeostasis: a speculative review. Cancer Res 25:1683–1727.

Chomczynski P, Sacchi N. 1987. Single-step method of RNA isolation by acid guanidinium thiocyanate-phenol-chloroform extraction. Anal Biochem 162: 156–159.

Dark J, Zucker I. 1984. Gonadal and photoperiodic control of seasonal body weight changes in male voles. Am J Physiol 247:84–88.

Elkasrawy MN, Hamrick MW. 2010. Myostatin (GDF-8) as a key factor linking muscle mass and bone structure. J Musculoskelet Neuronal Interact 10:56–63.

Figala J, Hoffmann K, Goldau G. 1973. Zur Jahresperiodik beim Dsungarischen Zwerghamster *Phodopus sungorus* PALLAS. Oecologia (Berlin) 12:89–118.

Flint WE. 1966. Die Zwerghamster der paläarktischen Fauna. In: editors. Die neue Brehm Bücherei. Wittenberg Lutherstadt: A. Ziemsen Verlag.

Goldman BD, Darrow JM. 1983. The pineal gland and mammalian photoperiodism. Neuroendocrinology 37:386–396.

Heldmaier G. 1989. Seasonal acclimatization of energy requirements in mammals: Functional significance of body weight control, hypothermia, torpor and hibernation. In: Wieser W, Gnaiger E, editors. Energy transformations in cells and organisms. Stuttgart, New York: Thieme Verlag. p 130–139.

Heldmaier G, Klingenspor M. 2003. Role of photoperiod during seasonal acclimatization in winter-active small mammals. In: Heldmaier G, Werner D, editors. Enviromental signal Processing and adaptation. Berlin, Heidelberg, New York: Springer. p 251–273.

Heldmaier G, Lynch GR. 1986. Pineal involvement in the thermoregulation and acclimatization. Pineal Res Reviews 4:97–139.

Heldmaier G, Steinlechner S. 1981a. Seasonal control of energy requirements for thermoregulation in the Djungarian hamster (*Phodopus sungorus*) living in natural photoperiod. J Comp Physiol 142:429–437.

Heldmaier G, Steinlechner S. 1981b. Seasonal pattern and energetics of short daily torpor in the Djungarian hamster *Phodopus sungorus*. Oecologia (Berlin) 48:265–270.

Heldmaier G, Steinlechner S, Ruf T, Wiesinger H, Klingenspor M. 1989. Photoperiod and thermoregulation in vertebrates: body temperature rhythms and thermogenic acclimation. J Biol Rhythms 4:251–265.

Hoffmann K. 1973. The influence of photoperiod and melatonin on testis size, body weight, and pelage color in the Djungarian hamster (*Phodopus sungorus*). J Comp Physiol 85:267–282.

Hoffmann K. 1978. Effect of short photoperiod on puberty, growth, and molt in the Djungarian hamster (*Phodopus sungorus*). J Reprod Fertil 54:29–35.

Hoffmann K. 1981. Photoperiodism in vertebrates. In: Aschoff J, editor. Handbook of behavioral neurobiology, Vol 4, Plenum, New York: Biological Rhythms. p 449–473.

Hoffmann K. 1982. The critical photoperiod in the Djungarian hamster *Phodopus sungorus*. In: Aschoff J, Daan S, Groos G, editors. Vertebrate circadian systems. Berlin, Heidelberg, New York: Springer. p 297–304.

Klingenspor M, Niggemann H, Heldmaier G. 2000. Modulation of leptin sensitivity by short photoperiod acclimation in the Djungarian hamster, *Phodopus sungorus*. J Comp Physiol B 170:37–43.

Lee SJ. 2004. Regulation of muscle mass by myostatin. Annu Rev Cell Dev Biol 20:61–86.

Lee SJ, McPherron AC. 1999. Myostatin and the control of skeletal muscle mass. Curr Opin Genet Dev 9:604–607.

Lee SJ, McPherron AC. 2001. Regulation of myostatin activity and muscle growth. Proc Natl Acad Sci USA 98:9306–9311.

Matsakas A, Diel P. 2005. The growth factor myostatin, a key regulator in skeletal muscle growth and homeostasis. Int J Sports Med 26:83–89.

Mauer MM, Bartness TJ. 1994. Body fat regulation after partial lipectomy in Siberian hamsters is photoperiod dependent and fat pad specific. Am J Physiol 266:870–878.

McPherron AC, Lawler AM, Lee SJ. 1997. Regulation of skeletal muscle mass in mice by a new TGF-beta superfamily member. Nature 387:83–90.

Mercer JG, Tups A. 2003. Neuropeptides and anticipatory changes in behaviour and physiology: seasonal body weight regulation in the Siberian hamster. Eur J Pharmacol 480:43–50.

Moffatt-Blue CS, Sury JJ, Young KA. 2006. Short photoperiod-induced ovarian regression is mediated by apoptosis in Siberian hamsters (*Phodopus sungorus*). Reproduction 131:771–782.

Rios R, Fernández-Nocelos S, Carneiro I, Arce VM, Devesa J. 2004. Differential response to exogenous and endogenous myostatin in myoblasts suggests that myostatin acts as an autocrine factor in vivo. Endocrinology 145:2795–2803.

Steinlechner S, Heldmaier G. 1982. Role of photoperiod and melatonin in seasonal acclimatization of the Djungarian hamster, *Phodopus sungorus*. Int J Biometeorol 26:329–337.

Steinlechner S, Heldmaier G, Becker H. 1983. The seasonal cycle of body weight in the Djungarian hamster: photoperiod control and the influence of starvation and melatonin. Oecologia 60: 401–405.

Steinlechner S, Puchalski W. 2002. Mechanisms of seasonal control of reproduction in small mammals. In: Heldmaier G, Werner D, editors. Enviromental signal processing and adaption. Heidelberg: Springer. p 233–250.

Stieglitz A, Spiegelhalter F, Klante G, Heldmaier G. 1995. Urinary 6-sulphatoxymelatonin excretion reflects pineal melatonin secretion in the Djungarian hamster (*Phodopus sungorus*). J Pineal Res 18: 69–76.

Thomas M, Langley B, Berry C, Sharma M, Kirk S, Bass J, Kambadur R. 2000. Myostatin, a negative regulator of muscle growth, functions by inhibiting myoblast proliferation. J Biol Chem 275:40235–40243.

Wade GN, Bartness TJ. 1984. Effects of photoperiod and gonadectomy on food intake, body weight and body composition in Siberian hamsters. Am J Physiol 246:26–30.

Wiesinger H. 1989. Kälteakklimation beim Djungarischen Zwerghamster, *Phodopus sungorus*. Dissertation, Philipps Universität Marburg.

Journal of Neuroendocrinology, 2006, Vol. 18, 413–425 doi:10.1111/j.1365-2826.2006.01431.x

PC1/3 and PC2 Gene Expression and Post-Translational Endoproteolytic Pro-Opiomelanocortin Processing is Regulated by Photoperiod in the Seasonal Siberian Hamster (*Phodopus sungorus*)

M. Helwig,*† R. M. H. Khorooshi,‡ A. Tups,† P. Barrett,* Z. A. Archer,* C. Exner,† J. Rozman,† L. J. Braulke,† J. G. Mercer* and M. Klingenspor†

*Molecular Endocrinology Group, Division of Obesity and Metabolic Health, Rowett Research Institute, Aberdeen Centre for Energy Regulation and Obesity (ACERO), Aberdeen, UK.

†Department of Animal Physiology, Biology Faculty, Philipps University Marburg, Marburg, Germany.

‡Medical Biotechnology Centre, University of Southern Denmark, Odense, Denmark.

Key words: seasonal body weight regulation, proteolytic processing, photoperiod, prohormone convertases, POMC.

Abstract

A remarkable feature of the seasonal adaptation displayed by the Siberian hamster (*Phodopus sungorus*) is the ability to decrease food intake and body weight (by up to 40%) in response to shortening photoperiod. The regulating neuroendocrine systems involved in this adaptation and their neuroanatomical and molecular bases are poorly understood. We investigated the effect of photoperiod on the expression of prohormone convertases 1 (PC1/3) and 2 (PC2) and the endoproteolytic processing of the neuropeptide precursor pro-opiomelanocortin (POMC) within key energy balance regulating centres of the hypothalamus. We compared mRNA levels and protein distribution of PC1/3, PC2, POMC, adrenocorticotrophic hormone (ACTH), α-melanocyte-stimulating hormone (MSH), β-endorphin and orexin-A in selected hypothalamic areas of long day (LD, 16 : 8 h light : dark), short day (SD, 8 : 16 h light : dark) and natural-day (ND, photoperiod depending on time of the year) acclimated Siberian hamsters. The gene expression of PC2 was significantly higher within the arcuate nucleus (ARC, $P < 0.01$) in SD and in ND (versus LD), and is reflected in the day length profile between October and April in the latter. PC1/3 gene expression in the ARC and lateral hypothalamus was higher in ND but not in SD compared to the respective LD controls. The immunoreactivity of PC1/3 cleaved neuropeptide ACTH in the ARC and PC1/3-colocalised orexin-A in the latyeral hypothalamus were not affected by photoperiod changes. However, increased levels of PC2 mRNA and protein were associated with higher abundance of the mature neuropeptides α-MSH and β-endorphin ($P < 0.01$) in SD. This study provides a possible explanation for previous paradoxical findings showing lower food intake in SD associated with decreased POMC mRNA levels. Our results suggest that a major part of neuroendocrine body weight control in seasonal adaptation may be effected by post-translational processing mediated by the prohormone convertases PC1/3 and PC2, in addition to regulation of gene expression of neuropeptide precursors.

Seasonal animals such as the Siberian hamster (*Phodopus sungorus*) exhibit remarkable physiological and metabolic adaptations in response to the seasonally changing environment. These adaptations include changes in coat insulation and colour, reproductive activity, food intake and body weight (1). The drive to reduce food intake in shortening winter photoperiod persists even if food is provided *ad lib* demonstrating the importance of this regulatory energy balance mechanism. A key neuronal centre that regulates these physiological responses is the hypothalamus, an area of the central nervous system (CNS) that integrates photoperiodic and peripheral inputs in a complex network of interacting orexigenic and anorexigenic neuropeptides (2, 3). The Siberian hamster processes information on changing photoperiod through the pineal hormone, melatonin, and about internal energy stores via peripherally released hormones such

Correspondence to: Michael Helwig, Animal Physiology, Department of Biology, Philipps-University, Karl-von-Frisch-Str. 8, 35032 Marburg, Germany (e-mail: helwigmi@staff.uni-marburg.de).

as leptin and ghrelin, to generate appropriate responses in terms of energy balance regulation (4–6). The voluntary decrease in food intake and body weight in short day (SD) presumably reflects the increased activity of anorexigenic components of this neuroendocrine system. One of the neuropeptides that would meet this criterion is alpha-melanocyte-stimulating hormone (α-MSH) (7, 8), a product of the 30–32 kDa molecule pro-opiomelanocortin (POMC), which exerts an inhibitory control on food intake and energy storage through its action in the CNS at the melanocortin 3 and 4 receptors (9). Unexpectedly, previous studies demonstrated decreased gene expression of the precursor POMC in SD which could in principal result in lower concentrations of α-MSH during winter (10–12). However, most neuropeptide precursors such as POMC have to undergo post-translational processing by proteolytic cleavage before their products acquire biological activity. The post-translational process is accomplished by highly specific cleavage enzymes (prohormone convertases) and is therefore an essential step not only as a part of the protein biosynthetic process, but also as a regulatory step in neuropeptide synthesis. In mammals, prohormone convertases 1/3 (PC1/3) and 2 (PC2), which are members of the subtilisin-like proprotein convertases, have been identified to be responsible for the proteolytic processing of neuropeptides and peptide hormones in neuronal endocrine tissue (13).

Both PC1/3 and PC2 are expressed in neuroendocrine tissues such as hypothalamic neurones and cleave prohormones at paired basic residues. The biosynthesis of several major orexigenic and anorexigenic peptides derived from precursors within this neuroendocrine network is reliant on the post-translational activity of these enzymes. Neuropeptides such as neuropeptide-Y (NPY) (14), and cocaine- and amphetamine-regulated transcript (CART) (15), which are involved in the regulation of energy homeostasis and feeding, are subject to enzymatic processing by PC1/3 and PC2. Consequently, this system must be considered an extensive control mechanism in neuropeptide maturation. Interestingly, PC2 has been shown to be mainly involved in the production of the anorexigenic peptides, α-MSH and CART, whereas PC1/3 is responsible for the generation of potent orexigenic NPY in the hypothalamus (16–18).

The cleavage-specificity of PC1/3 and PC2 in POMC processing was reported by cell transfection experiments. It has been demonstrated that PC1/3 cleaves POMC into large intermediate molecules, such as adrenocorticotrophic hormone (ACTH) and β-lipotrophin, whereas PC2 subsequently cleaves ACTH and β-lipotrophin into α-MSH and β-endorphin, respectively (Fig. 1) (19, 20). Thus, coordinated cleavage activity of both prohormone convertases is necessary to process neuropeptide precursors such as POMC into specific neuropeptides. Because PC1/3 and PC2 are essential for the post-translational processing of various neuropeptide precursors, it is likely that changes in gene expression and biosynthesis have fundamental effects on the maturation of neuropeptides and hence energy homeostasis.

We hypothesised that POMC processing is photoperiodically regulated by differential expression of PC1/3 and PC2. It is likely that decreasing body weight in SD acclimated hamsters is associated with higher levels of anorexigenic neuropeptides

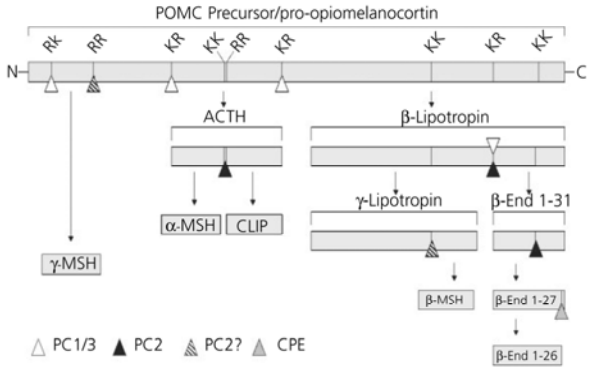

FIG. 1. Diagrammatic representation of post-translational endoproteolytic pro-opiomelanocortin (POMC) processing by prohormone convertases 1/3 (PC1/3) and 2 (PC2) and carboxypeptidase E (CPE). Cleavage sites are marked by paired basic amino acids R (Lysine) and K (Arginine). Sites believed but not confirmed as being processed by PC2 are indicated by hatched triangles. ACTH, Adrenocorticotrophic hormone; CLIP, corticotrophin-like intermediate peptide.

such as α-MSH despite down-regulated gene expression of POMC. We suggest that differential endoproteolytic activity of prohormone convertases in SD and long day (LD) is responsible for photoperiod-regulated biosynthesis of smaller POMC-derived neuropeptides. To test this, gene expression of PC1/3 and PC2 was investigated in hamsters exposed to ambient photoperiod in winter (October to April) to profile long-term effects. In addition, we measured mRNA expression levels of PC1/3 and PC2 following transfer of Siberian hamsters back into LD, after 14 weeks in artificial SD photoperiod. This experimental setup provided a better assessment of the temporal responsiveness of photoperiod-induced regulation of gene expression. Neuroanatomical protein distribution and differential expression of PC1/3, PC2, POMC, ACTH, α-MSH, and β-endorphin in SD and LD acclimated hamsters were investigated by immunohistochemistry. In a second approach, we used dual-fluorescence immunohistochemistry to colocalise the prohormone convertases with POMC and the derived neuropeptides to evaluate the ratio of proteolytic activity of PC1/3 and PC2 in SD and LD, respectively.

Previous reports have indicated neuroanatomical localisation of PC1/3 mRNA in the lateral hypothalamus (LH) (21), an important region of energy balance regulation (22) containing various potential targets for PC1/3 cleavage. As a consequence, we also focused on a neuropeptide precursor candidate for post-translational modification within this region. Although POMC is not expressed in this region, several pro-forms of different neuropeptides have been localised in the LH including pro-dynorphin (23), pro-melanin-concentrating hormone (24) and pro-orexin (25). All of these molecules are precursors of anabolic neuropeptides that exert opposing effects to those derived from POMC in the arcuate nucleus (ARC) (26). Pro-orexin was selected for investigation because we previously observed PC1/3 mRNA localised in prepro-orexin mRNA expressing neurones in the LH, which suggested a functional relationship of these neuroendocrine components. These recent observations at the mRNA level were extended to the protein level using immunohistochemical methods.

Materials and methods

Animals and experimental procedures

All described procedures were performed in accordance with German animal welfare regulation, or were licensed under the UK Home Office Animals (Scientific Procedures) Act, 1986, and had local ethical approval.

Siberian hamsters (*P. sungorus*) were drawn from breeding colonies established in the Biology Faculty in Marburg (Germany) and at the Rowett Research Institute in Aberdeen (Scotland). All animals were housed individually and had *ad lib* access to food (Marburg: Standard breeding chow diet, 7014, Altromin, Lage, Germany; Aberdeen: Labsure pelleted diet, Special Diet Services, Witham, UK) and water. Body weights were assessed weekly. Photoperiods referred to in this article are defined as LD (long day, 16 : 8 h light : dark), SD (short day, 8 : 16 h light : dark) and ND (natural day, with day length depending on time of the year).

Experiment 1

Siberian hamsters (n = 72, Marburg colony) were born and reared in ND at 23 °C. At the age of 4–6 months, they were divided into two groups. One group (n = 36, matched for sexes) was transferred to LD whereas the other (n = 36, matched for sexes) was maintained in ND and exposed to the progressive change in natural day length from October until April. At intervals of 40 days (October, November, January, February, March, April), hamsters from the LD and ND group (three males, three females per group) were killed with CO_2 and decapitated. Brains were immediately dissected, frozen on dry ice and stored at − 80 °C until required. The day length in ND photoperiod was calculated using the Sunrise/Sunset Calculator software (National Oceanic and Atmospheric Administration, Washington, DC, USA) based on the geographical location of the breeding facility in Marburg (8°46′17, 7′/50°48′17, 5′).

Experiment 2

Male Siberian hamsters (n = 32, Aberdeen colony) were housed individually at 22 °C. Hamsters used in this experiment were born and reared in LD. When they were 4–6 months old, half the animals (n = 16) were transferred to SD. After 14 weeks (week 0), a group of LD and SD hamsters (n = 4/group) were killed by cervical dislocation. All the remaining SD hamsters were transferred back to LD photoperiod. LD controls and hamsters transferred back from SD to LD (n = 4 per group) were then killed at intervals of 2 weeks (week 2, 4 and 6; 27). Brains were immediately dissected, frozen on dry ice and stored at −80 °C until required.

In situ *hybridisation*

Messenger RNA levels for PC1/3 and PC2 were quantified by *in situ* hybridisation in 15-μm coronal sections. Sections were collected throughout the extent of the hypothalamus onto two sets of 12 slides with six or seven sections mounted on each slide. Accordingly, slides spanned the lateral hypothalamic region approximating from −1.5 mm to −3.2 mm and the arcuate nucleus from −1.8 mm to −3.7 mm relative to Bregma, according to the atlas of the golden hamster brain (27). Two slides (one per set) from each animal were hybridised with a Siberian hamster specific PC1/3 or PC2 riboprobe cloned from cDNA, using techniques described in detail elsewhere (28). A control was performed by hybridising sections with equal length sense riboprobes of PC1/3 and PC2 resulting in no signal. Riboprobes complementary to partial fragments of PC1/3 and PC2 gene were generated from cloned Siberian hamster brain cDNA. The amplification of the PC1/3 (248 bp, GenBank AY625692) and PC2 (232 bp GenBank AY625693) fragments was performed by PCR using the primers: 5′-ATGGGGGTCGTCAAGGAG-ATAACT-3′ and 5′-GATGCCAGCAGCAGCCAGAGGTG-3′ (rat PC1/3, GenBank M76705) and 5′-GCGGCCGGGCTTCTCTTCT-3′ and 5′-GCT-GCCGCTTGTGATGTAGG-3′ (rat PC2, GenBank M76706), respectively. Both DNA fragments were ligated into pGEM-T-easy (Promega, Madison, WI, USA), transformed into *Escherichia coli* DH5α and sequenced. Sequence alignment of the species-specific fragments cloned from *P. sungorus* revealed a 96.4% (PC1/3) and 97% (PC2) identity to rat prohormone convertases at the nucleotide level. Sections were fixed, acetylated, and hybridised overnight at 58 °C using ^{35}S-labelled antisense riboprobes (1–1.5 × 10^7 d.p.m./ml). Slides were treated with RNase A to remove unhybridised probe and then desalted with a final high stringency wash in 0.1 × saline-sodium citrate (SSC) at 60 °C for 30 min. Hybridised slides were apposed with Kodak BioMax MR film (Kodak, Rochester, NY, USA) and, where appropriate, were coated with LM-1 film emulsion (Amersham, Bucks, UK). The levels of hypothalamic mRNAs were analysed and quantified by computerised densitometry (Image Pro-Plus software, Version 5.5.1; Media Cybernetics, Wokingham, Berkshire, UK) of *in situ* hybridisation autoradiograms. This determined the intensity and area of the hybridisation signal on the basis of set parameters; the integrated intensity was then computed using standard curves generated from ^{14}C autoradiographic microscales (Amersham). Image analysis was performed on representative sections, by an observer blind to the respective treatment groups, on four or five comparable sections spanning the ARC and three sections spanning the lateral hypothalamus. Micropictures of emulsion autoradiography sections were taken by bright field microscopy using an Olympus BX-50 microscope (Olympus Microscopes Ltd, Middlesex, UK) with attached digital camera system (Hitachi HV-C20, Hitachi Europe Ltd, Maidenhead, UK).

Dual immunostaining

Male Siberian Hamsters (n = 24, Aberdeen colony) were kept under conditions described above (Experiment 2). Half of them (n = 12) were transferred to SD. After 14 weeks in LD or SD, hamsters were anaesthetised with sodium pentobarbital and perfused with 4% paraformaldehyde (PFA) in 0.1 M phosphate-buffered saline (PBS, pH 7.4). Brains were dissected and transferred into a 4% PFA-PBS solution (8 h, 4 °C), followed by cryoprotection in 30% sucrose–0.1 M PBS (48 h, 4 °C), and were deep frozen in isopentane over dry ice (1 min). Coronal sections (35 μm) of the brain, corresponding to −1.5 to −3.7 mm relative to Bregma (27), were processed on a cryostat. Free-floating sections were treated with blocking solution (BS) containing 3% bovine serum albumin (BSA) in 0.5% Triton X-100–0.1 M PBS (0.5% PBS-T) for 1 h to block nonspecific reactions. Then, sections of LD (n = 3) and SD (n = 3) hamster brains were incubated with polyclonal rabbit anti-orexin-A (dilution 1 : 200, H-003–30, Phoenix Pharmaceuticals Inc., Belmont, CA, USA), anti-POMC (dilution 1 : 100, H-029–30, Phoenix), or anti-β-endorphin (dilution 1 : 100, H-022–33, Phoenix) in BS overnight (4 °C). Following washes in 0.25% PBS-T, sections were incubated for 2 h with unconjugated goat anti-rabbit Fab-fragment antibody (111-007-003, Jackson ImmunoResearch, West Grove, PA, USA) diluted 1 : 60 in BS at room temperature (RT). Sections were rinsed briefly in 0.25% PBS-T and incubated with Cy3 (Ex_{max} 554 nm, Em_{max} 566 nm) conjugated donkey anti-goat secondary antibody in BS (dilution 1 : 250, 705-165-147, Jackson) for 2 h at RT, rinsed again in 0.25% PBS-T and incubated with the second polyclonal rabbit anti-PC1/3 primary antibody (dilution 1 : 400, AB1260, Chemicon Inc., Temecula, CA, USA) or anti-PC2 (dilution 1 : 400, AB1262, Chemicon), in BS overnight at 4 °C. Sections were incubated with Alexa 488 dye (Ex_{max} 492 nm, Em_{max} 520 nm) conjugated goat anti-rabbit secondary antibody (dilution 1 : 250, Molecular Probes, Eugene, OR, USA) in BS for 2 h at RT. Colocalisation for α-MSH was performed with polyclonal sheep anti-α-MSH antibody (dilution 1 : 15.000, Chemicon) in BS overnight at 4 °C. In this case, different host species in which the applied primary antibodies were raised made an intermediate step of Fab-fragment incubation obsolete. α-MSH was visualised by incubation with Fluorescein (Ex_{max} 494 nm, Em_{max} 520 nm) conjugated donkey anti-sheep secondary antibody (dilution 1 : 100, AP184F, Chemicon) in BS for 2 h at RT. Incubation with the second primary antibodies and secondary antibody matched the steps described above. Sections were then rinsed in PBS, mounted on gelatin-coated slides, air-dried, dehydrated in graded alcohol, cleared in xylene and coverslipped with Enthelan (Merck Biosciences, Darmstadt, Germany). Sections were examined under a conventional Leica DMR epifluorescent microscope (Leica Microsystems, Wetzlar, Germany). Cell bodies were counted in two distinct hypothalamic regions, the lateral hypothalamus and the arcuate nucleus approximating from −1.5 mm to −3.2 mm (LH) and −1.8 mm to −3.7 mm (ARC) relative to Bregma, according to the atlas of the golden hamster brain (27). Immunoreactive (ir) cells in three (ARC) or four (LH) comparable sections of each individual animal were counted without knowledge of the experimental treatment. Total ir-cell number for each individual animal from the respective regions was calculated followed by the assessment of mean values for each experimental group. Images were taken by a digital camera system mounted on the microscope. Merging of images was performed by colour channel overlay using image processing software (Adobe Photoshop version 7.0; Adobe Systems Inc., San Jose, CA, USA). The anatomical localisation of neuropeptides within the brain of Siberian

hamsters was annotated according to the atlas of the golden hamster brain (27).

Controls

For controls, each of the primary antibodies was preincubated with its complementary peptide (α-MSH, 043-01, Phoenix; β-endorphin, 022-33, Phoenix; orexin-A, 003-30, Phoenix; POMC, 029-30, Phoenix; PC 1/3, AB5011, Abcam; PC2, AB5012, Abcam), prior to application. Incubation with preadsorbed primary antibodies resulted in no staining. Additional negative controls were performed by incubation of sections lacking primary antisera. Labelling of the primary antibodies by incubation with interchanged secondary antibodies showed an identical staining pattern.

Single immunostaining

Female Siberian hamsters (n = 20, Marburg colony) at 7 months of age were divided into two groups of 10. One group was kept in LD, whereas the other was transferred to SD. After 14 weeks, hamsters were killed in a CO_2 atmosphere and decapitated. Brains were excised, fixed in 4% PFA (48 h, 4 °C), and cryoprotected in 20% sucrose in 0.1 M PBS for 24 h at 4 °C. Brains were deep frozen in isopentane over dry ice (1 min) and stored in −80 °C until required. Coronal sections were cut on a cryostat at 30 µm. Endogenous peroxidase activity was inhibited in sections using 80% PBS, 10% methanol and 10% H_2O_2 for 15 min at RT. Free-floating sections were rinsed in PBS and 0.5% PBS-T. Following preincubation in a blocking solution containing 0.5% PBS-T and 3% BSA, sections were incubated with primary polyclonal rabbit anti-ACTH (Phoenix; H-001-21) antibody diluted 1 : 350 in BS overnight at 4 °C. Following washing in 0.5% PBS-T, sections were then incubated with peroxidase-conjugated goat anti-rabbit antibody (Jackson Immunoresearch, 111-035-144) diluted 1 : 500 in BS for 1 h at RT. Using Vector SG substrate kit for peroxidase (SK-4700, Vector Laboratories, Burlingame, CA, USA), the colour reaction resulted in dark-grey/blue immunostaining. Sections were then rinsed in PBS, mounted on gelatin-coated slides, air-dried, dehydrated in graded alcohol, cleared in xylene and coverslipped with Enthelan (Merck). Immunoreactive cell bodies were counted as for the dual-immunostaining protocol, using a Zeiss Axioskop (Carl Zeiss, Jena, Germany) microscope (objective, ×20). Images were taken by a mounted digital camera. Quantification and illustration of PC1/3, PC2, POMC, α-MSH, β-endorphin and orexin-A immunohistochemistry was performed on sections obtained from the dual-staining experiment described above. Micrographs showing the neuroanatomical distribution were colour inverted to greyscale mode using image editing software for enhanced visibility.

Controls

The specificity of primary antibody was tested by adding an excess of ACTH- (Phoenix; 001-21) peptide to the primary antibody for 3 h at RT before application to sections, or by omission of the primary antibody. Brain sections incubated either with preadsorbed primary antiserum or in the absence of primary antibodies did not exhibit any ACTH-ir (data not shown).

Statistical analysis

Data were analysed by two-way analysis of variance (ANOVA) followed by the Student–Newman–Keuls multiple comparison test, where appropriate (for *in situ* experiments), and one-way ANOVA (for immunohistochemistry data) using a statistical software package (SigmaStat, Jandel Corp, Richmond, VA, USA). Data from *in situ* hybridisation experiments are presented as means ± SEM; Data for immunohistochemistry experiments are presented as percentage values of LD control ± SEM. $P < 0.05$ was considered statistically significant.

Results

Effect of seasonal changing photoperiod on body weight

The body weight trajectory of ND animals was inversely related to the seasonal change in ambient photoperiod (Fig. 2). Beginning with an average body weight of 32.3 ± 3.4 g in October, ND body weight decreased by 17.3% to a minimum of 26.7 ± 2.1 g in January, followed by a weight gain of 53.9% to a body weight of 41.1 ± 3.9 g in April Control group animals kept in constant LD photoperiod (16 : 8 h light : dark) maintained an average body weight of 38.3 ± 3.6 g throughout the 6 months of the experiment. As a result, mean body weights of ND and LD animals differed by 12 g in January ($P < 0.01$), and were also significantly different in November ($P < 0.05$).

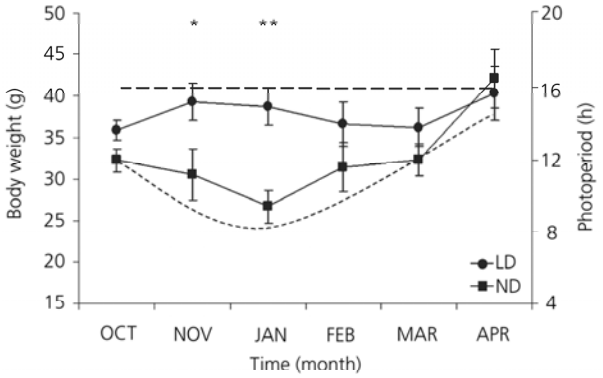

FIG. 2. Body weight of Siberian hamsters kept in constant long day (LD) (16 : 8 h light : dark; dashed line) or dynamic natural-day (ND) photoperiod (day length depending on ambient light during winter; dotted line) over 6 months from October until April (means ± SEM, n = 6 per time point). Photoperiod ranged from a minimum of 8.07 h light in January to a maximum of 14.19 h light in April. **P < 0.01; *P < 0.05, ND versus LD.

Effect of natural photoperiod on gene expression of PC1/3 and PC2

PC1/3 and PC2 mRNA were detected in various areas of the hamster hypothalamus with region-specific intensity differences (Fig. 3). Gene expression of both PC1/3 and PC2 was observed in ARC, paraventricular nucleus (PVN) and ventromedial nucleus (VMH), although gene expression in the PVN and VMH was close to the limit of detection and consequently was not quantified. In addition, PC1/3 mRNA was observed in the LH. Autoradiographs of PC1/3 and PC2 in the ARC revealed similar expression patterns to previously observed POMC mRNA distribution in this area (10). In addition, high concentrations of PC2 mRNA were observed in a small group of neurones within the dorsal medial posterior part of the arcuate nucleus (dmpARC).

Gene expression of PC1/3 within the ARC (Fig. 4A) and LH (Fig. 4B) revealed a significant overall effect of photoperiod ($P < 0.05$ for both regions) with higher levels of mRNA in ND (versus LD controls). However, PC1/3 mRNA levels in the ARC and LH were not correlated with the profile of changing photoperiod in ND; there were no effects of time (month) and no time × photoperiod interaction. In the LH (Fig. 4B), the apparent reflection of ND photoperiod in trends to increased levels of PC1/3 mRNA from October until January followed by a decline to February were not statistically significant.

Gene expression of PC2 in the ARC (Fig. 4C) and the dmpARC (Fig. 4D) also revealed strong effects of photoperiod with higher levels of mRNA in ND ($P < 0.001$ for both

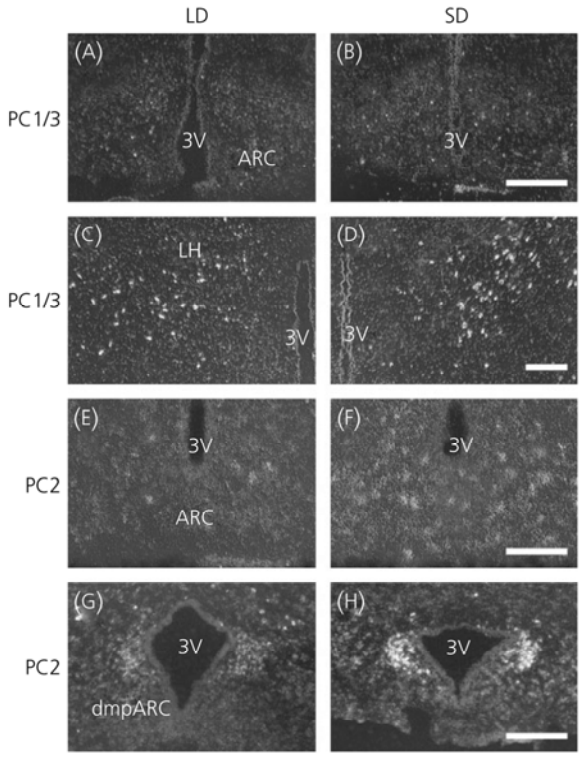

FIG. 3. Representative dark-field micrographs of autoradiographs showing gene expression of prohormone convertases 1/3 (PC1/3) and 2 (PC2) in quantified areas of the hypothalamus in long day (LD) and short day (SD) animals. Scale bars = 80 μm (A–B, E–H) and 100 μm (C–D).

regions). In addition, a seasonal pattern of PC2 gene expression in the ARC (Fig. 4C, quantified area excluding the dmpARC) was observed in ND hamsters (two-way ANOVA: $P < 0.01$ for effect of time; $P < 0.05$ for time × photoperiod interaction) with maximal mRNA levels observed in January (multiple comparison: $P < 0.05$). Although a similar temporal gene expression profile was apparent for gene expression of PC2 in the dmpARC (and for PC1/3 in LH), this could not be consolidated statistically (Fig. 4D).

Effect of transfer of hamsters from SD to LD on body weight

Body weights of the Siberian hamsters used in these experiments have been documented previously (29). Fourteen weeks in SD resulted in a 27% reduction in body weight, compared to LD controls. Transfer back to LD had little effect on body weight for the first 2 weeks but, thereafter, body weight increased significantly ($P < 0.001$) and achieved a level similar to that of LD controls by 6 weeks.

Effect of transfer of hamsters from SD to LD on gene expression of PC1/3 and PC2

Gene expression of PC1/3 in the ARC and LH did not change significantly after 14 weeks in SD (Fig. 4E,F, week 0). PC1/3 mRNA levels in the ARC and LH were unaffected by transfer from SD back to LD photoperiod (week 2, week 4, week 6) and were similar to those of LD controls. There were no effects of photoperiod or time, and no interaction. Neuroanatomical distribution patterns of PC1/3 mRNA analysed by emulsion autoradiography in the ARC (Fig. 3A–B) and LH (Fig. 3C–D) of SD and LD (week 0) also showed no apparent differences.

Photoperiod had no overall effect on PC2 gene expression in the ARC (Fig. 4G) or dmpARC (Fig. 4H) but PC2 gene expression revealed a significant effect of time ($P < 0.001$ for both regions), and a time × photoperiod interaction ($P < 0.001$ for both regions). Significantly higher levels of PC2 mRNA were found in the ARC ($P < 0.05$) and dmpARC ($P < 0.05$) of SD animals compared to LD controls after 14 weeks in SD photoperiod (week 0). This observation was corroborated by emulsion autoradiographs showing a higher content of silver grains with PC2 probes within the ARC (Fig. 3E–F) and dmpARC (Fig. 3G–H) of SD hamsters at time point week 0. Following the transfer from SD back to LD photoperiod, gene expression of PC2 in the ARC decreased to a nadir at week 4. A significant down regulation of gene expression was observed after transfer from SD back to LD at all three time points (week 2, week 4, week 6; $P < 0.05$, versus week 0 SD, respectively). Between 4 and 6 weeks after transfer back to LD, mRNA levels of PC2 increased significantly ($P < 0.05$). In the dmpARC, gene expression of PC2 was decreased after 2 weeks and remained significantly lower until 6 weeks (week 2, week 4, week 6; $P < 0.05$, versus week 0 SD, respectively) after transfer back to LD.

Effect of photoperiod on protein expression of PC1/3, PC2, POMC, ACTH, α-MSH, β-endorphin and orexin-A

Immunoreactive cells and fibres for PC1/3, PC2, POMC, ACTH, α-MSH, β-endorphin and orexin-A were observed in different hypothalamic areas of the Siberian hamster brain. Immunolocalised distribution patterns of PC1/3 and PC2 protein matched the mRNA pattern, except for a lack of PC2-ir in the dmpARC. Unlike the strong signal detected for PC2 mRNA in this region, little immunoreactivity for its protein could be observed (data not shown).

In the ARC, there was no effect of photoperiod on the number of counted PC1/3-ir cells (Fig. 5A,B, a-b); hamsters kept in LD had 167 ± 15 ir-cells and those in SD 153 ± 11 ir-cells within the investigated region of the ARC. However immunohistochemical staining of PC2 in the ARC showed 125% more ir-cells in SD (88 ± 19 ir-cells), leading to a significant difference ($P < 0.01$) compared to those counted in LD controls (39 ± 6 ir-cells) (Fig. 5A,B, c-d). POMC-ir in LD (178 ± 22 ir-cells) and SD (156 ± 10 ir-cells) revealed no significant difference in ir-cell number (Fig. 5A,B, e-f). ACTH-ir (LD, 105 ± 14; SD, 81 ± 9 ir-cells) as well as α-MSH-ir (LD, 47 ± 11; SD, 54 ± 13 ir-cells) levels in the ARC were also unaffected by photoperiod (Fig. 5A,B, g–h,k–l). By contrast, the density of α-MSH-ir fibres appeared greater in SD, but was not quantifiable (Fig. 5A,B, k–l). The neuroanatomical distribution pattern of β-endorphin-ir was similar to that of α-MSH-ir, but was mainly concentrated in cell bodies. Counting of β-endorphin-ir cells revealed 76%

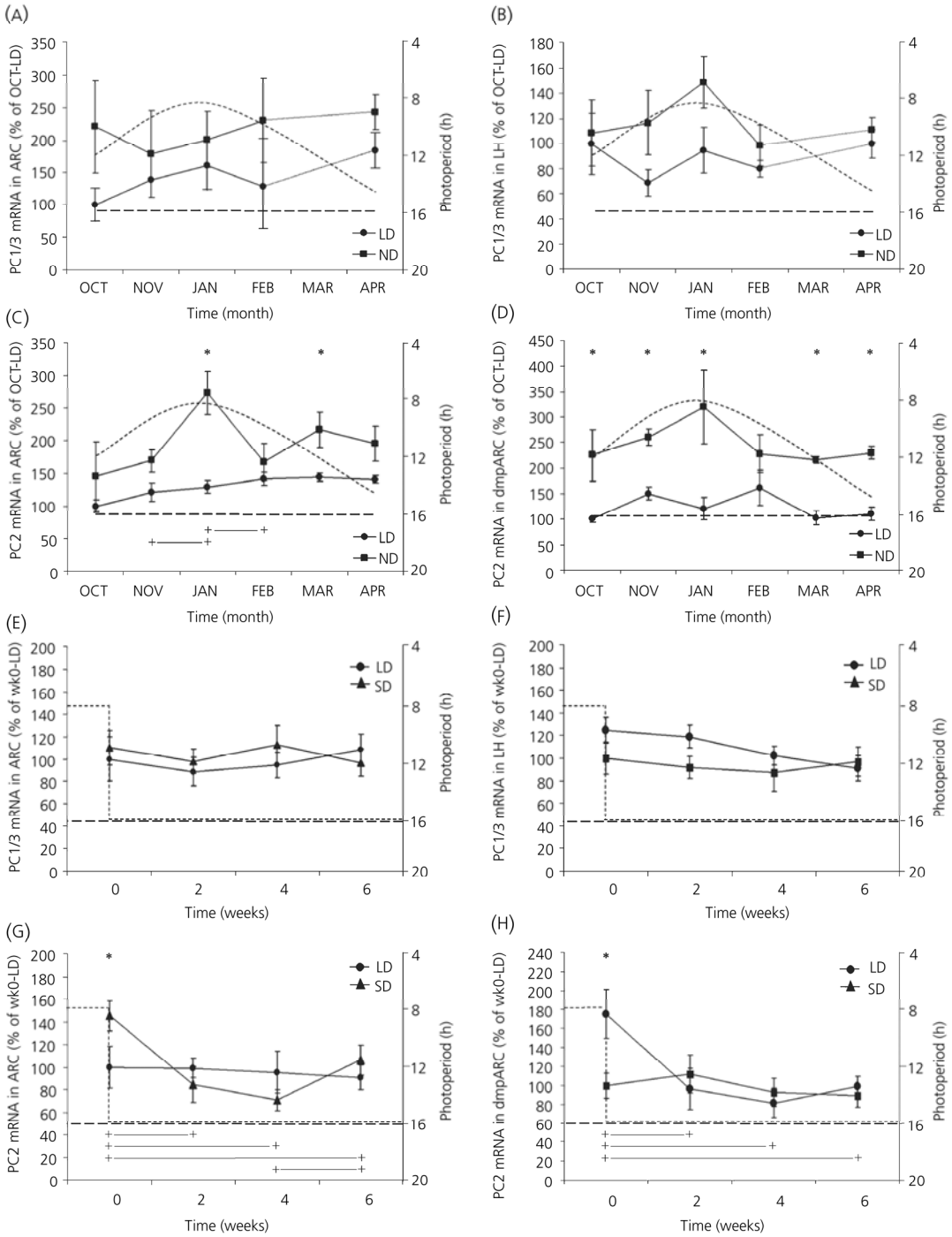

FIG. 4. Gene expression of prohormone convertases 1/3 (PC1/3) and 2 (PC2) in selected areas of the Siberian hamster hypothalamus. (A–D) Effect of changing photoperiod during winter on expression of PC1/3 (A, ARC; B, LH) and PC2 (C, ARC; D, dmpARC) genes. mRNA levels are expressed as mean percentages of LD controls in October (± SEM, n = 6 per time point). (E–H) PC1/3 (E, ARC; F, LH) and PC2 (G, ARC; H, dmpARC) gene expression after switch from SD (week 0) back to LD (week 2, week 4, week 6) photoperiod. mRNA levels are expressed as mean percentages of LD controls at week 0 (± SEM, n = 4 per group). LD is indicated by dashed lines, whereas dotted curves mark ND (A–D) or SD (E–H). Significances ($P < 0.05$) are marked by asterisks (*) for same time points but different photoperiods and crosses (+) for the same photoperiod (ND or SD, respectively) but at different time points.

 Journal of Neuroendocrinology, **18**, 413–425

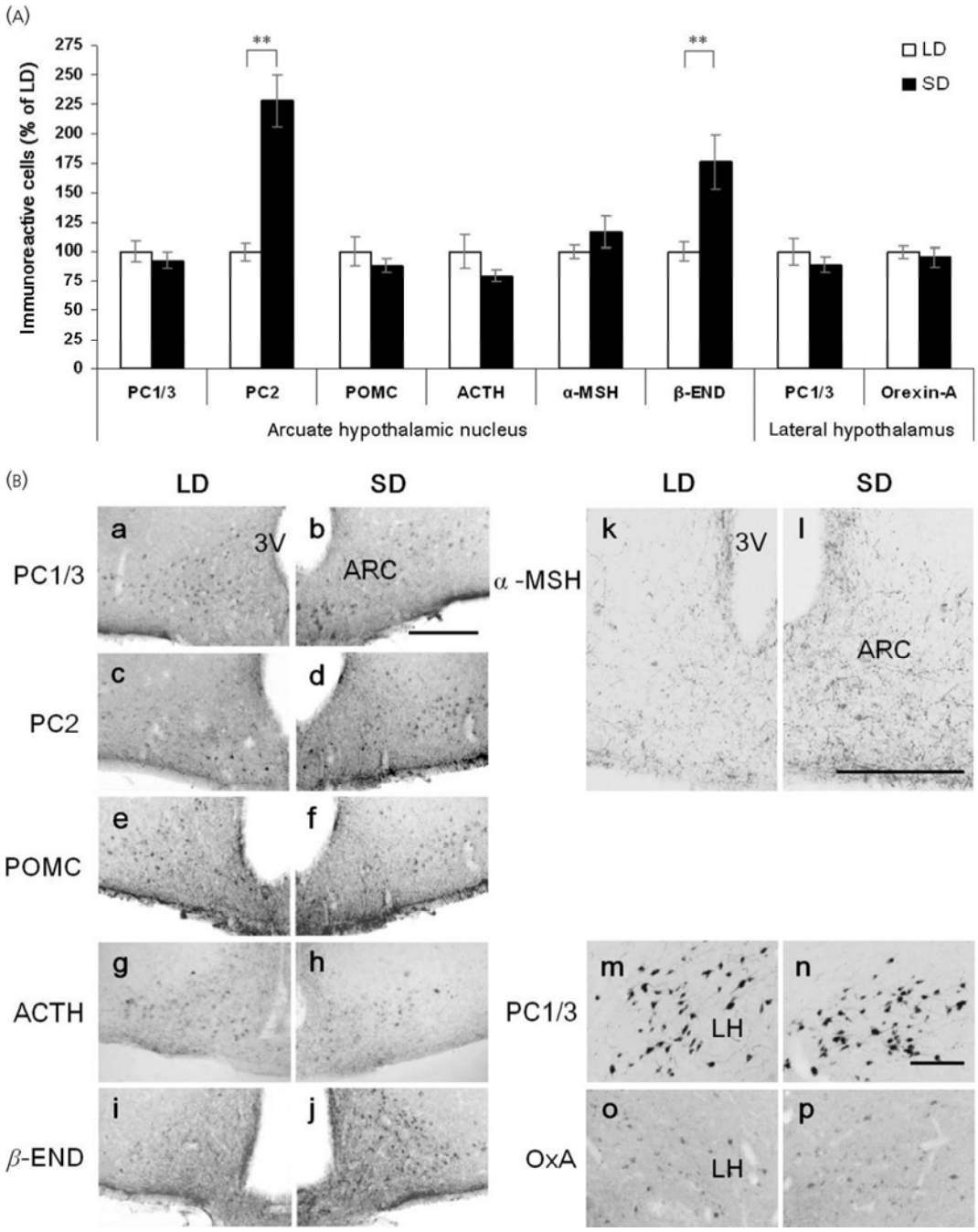

FIG. 5. (A) Quantitative analysis of immunoreactive (-ir) cells in selected areas of the Siberian hamster hypothalamus. Data are number of ir-cells expressed as percentage of long day (LD) controls (**$P < 0.01$, $n = 3$ per group). (B) Representative photomicrographs showing neuroanatomical distribution of immunoreactive cells in comparable hypothalamic areas of LD and short day (SD) animals. Colour inverted images of immunofluorescence stained sections (a–f, i–p) or peroxidase/substrate stained sections (g–h). 3V, Third ventricle; ARC, arcuate nucleus; LH, lateral hypothalamus. Scale bars = 100 μm (a–l) and 180 μm (m–p).

($P < 0.01$) more neurones in SD (74 ± 18 ir-cells) compared to LD (42 ± 9 ir-cells) (Fig. 5A,B, i–j). Quantification of PC1/3-ir (LD, 119 ± 16; SD, 104 ± 13 ir-cells) and orexin-A-ir (LD, 105 ± 14; SD, 97 ± 11 ir-cells) within the LH did not reveal differences between SD and LD controls (Fig. 5A,B, m–p).

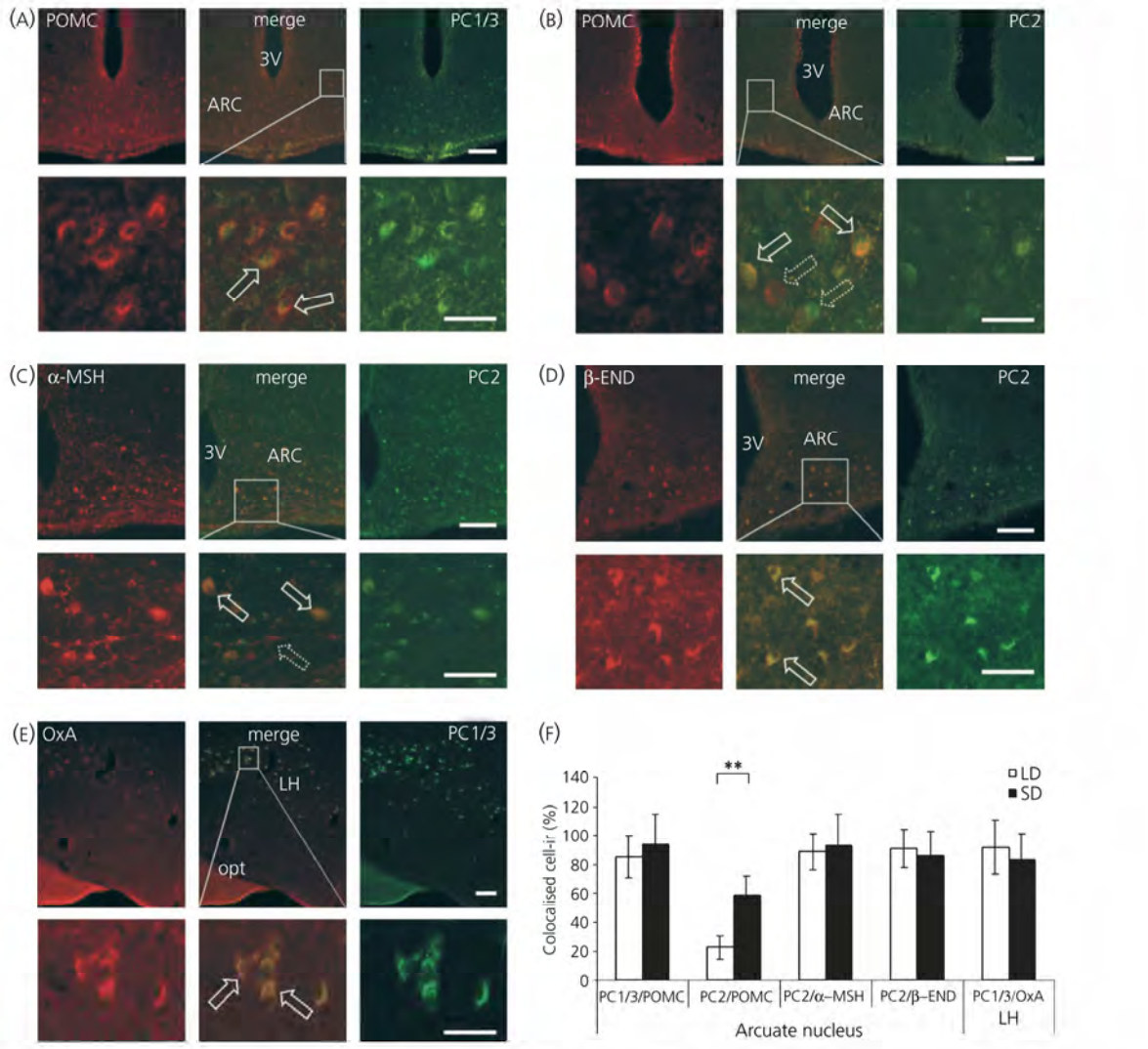

FIG. 6. (A–D) Photomicrographs showing immunofluorescence double staining of prohormone convertase 1/3 (PC1/3)-immunoreactivity (-ir) or prohormone convertase 2 (PC2)-ir with pro-opiomelanocortin (POMC)-ir and its derived neuropeptides in the arcuate nucleus and (E) PC1/3-ir and orexin-A-ir double staining in the lateral hypothalamus. Images derive from SD hamsters. For each panel, the upper row shows low magnification images and the lower row high magnification images of selected (boxed) areas. Merged images (centre) demonstrate colocalisation of immunoreactive products. Colocalisation is indicated by solid arrows, single cell-ir by dashed arrows. (F) Quantitative colocalisation analysis of prohormone convertase-ir (PC1/3 or PC2) and neuropeptide-ir. Values are expressed as mean percentages (± SEM) of counted POMC-ir, α-MSH-ir, β-endorphin-ir and orexin-A-ir cells in long day (LD) and short day (SD) (n = 3 per group). 3V, Third ventricle; ARC, arcuate nucleus; LH, lateral hypothalamus; opt, optical tract. Scale bars, low magnification images = 100 μm; high magnification images = 40 μm.

Effect of photoperiod on colocalisation of PC1/3 and PC2 with POMC, α-MSH, β-endorphin and orexin-A immunoreactivity

Dual fluorescence immunohistochemistry in the ARC showed no significant differences between the proportion of POMC-ir cells colocalised with PC1/3-ir cells in SD and LD. In both LD (87.5 ± 21%) and SD (94.1 ± 14.7%), nearly all POMC-ir cells were also PC1/3-ir positive (Fig. 6A,F). By contrast, the overall level of PC2-ir colocalisation with POMC-ir was lower and revealed significantly ($P < 0.01$) more POMC-ir cells which also contained PC2-ir in SD (59.14 ± 12.9%) than in LD (22.9 ± 8%) (Fig. 6B,F). Colocalisation of PC2-ir cells with α-MSH and β-endorphin immunoreactivity (Fig. 6C,D) revealed a nearly complete match of these POMC derived neuropeptides and the cleavage mediating prohormone convertase in SD and LD (Fig. 6F; α-MSH, LD, 89.1 ± 12.6%; SD, 93.2 ± 21.5%; β-endorphin, LD, 90.9 ± 13.5%; SD, 86.4 ± 16.3%). In the LH, there was no effect of photoperiod on the colocalisation of orexin-A-ir and PC1/3-ir (Fig. 6E,F); the neuropeptide product of prepro-orexin was localised with the majority of PC1/3-ir cells in this area in both LD (92 ± 18.4%) and SD (83.2 ± 18.7%).

Discussion

Seasonal body weight in mammals is regulated by a complex interaction of neuropeptides in a hypothalamic network of neurones that integrates environmental photoperiod inputs. Most of these energy balance-regulating neuropeptides are derived from larger biologically inactive precursors and have to undergo post-translational processing by endoproteolytic cleavage. The present study presents evidence substantiating the hypothesis that an important part of the photoperiod-driven regulation of POMC product biosynthesis is mediated by post-translational processing through PC1/3 and PC2, and thus provides valuable information over and above the control of precursor gene expression at a transcriptional level.

Neuroanatomical distribution patterns of PC1/3 and PC2 transcripts in the hamster hypothalamus match with previously described localisations in other rodent species such as rats and mice (21, 30). Hamsters kept in ND and SD displayed typical physiological adaptations to shortening or short photoperiod, including change of coat colour, reduction of reproductive tissue, reduced food intake and body weight loss. These photoperiod-induced physiological changes were not accompanied by temporal change in PC1/3 mRNA levels. Gene expression of PC1/3 in ARC and LH was higher overall in ND (versus LD) but this effect was not observed after 14 weeks in SD (versus LD) artificial photoperiod, suggesting some impact of prior photoperiodic history. At present, there is no clear explanation for this unexpected difference between ND and SD because gene expression of PC1/3 in summer ND (May to September) was not measured. Furthermore, short-term change of photoperiod induced by transfer from SD to LD was also without discernible effect on gene expression of PC1/3 in ARC and LH, suggesting that, on a transcriptional level, PC1/3 is not directly regulated by photoperiodic inputs. However, previous observations have demonstrated a regulatory effect of the adipose tissue hormone, leptin, on gene expression of PC1/3 in LH and ARC because reduced PC1/3 mRNA levels observed in obese *ob*/*ob* mice were up-regulated in response to leptin injection (31). Although PC1/3 gene expression appears to be sensitive to leptin in this natural knockout model, contrary to expectation, in Siberian hamsters, PC1/3 gene expression appears to be independent of seasonal modulation of leptin, despite the effect of photoperiod on this hormone (32). This suggests that the adipose tissue signal may be responsible for the maintenance of basal PC1/3 gene expression level.

By contrast to PC1/3, gene expression of PC2 in the ARC and dmpARC broadly paralleled the profile of changing ambient ND photoperiod in winter resulting in elevated mRNA when photoperiod was shortest. This photoperiod dependency was substantiated by up-regulated PC2 gene expression in hamsters kept in SD for 14 weeks. After transfer from SD to LD, mRNA levels of PC2 decreased rapidly and, within 2 weeks, levels were similar to those in LD. This acute regulatory change in PC2 gene expression preceded body weight loss and is therefore unlikely to be a secondary effect of metabolic and physiological changes. The photoperiod-driven gene expression profile suggests that PC2 may be an important part of a molecular neuroendocrine mechanism that is closely related to the integration of photoperiod information and the mediation of seasonal responses. Previous studies demonstrated a photoperiod-dependent differential gene expression of the neuropeptide precursor POMC in the ARC with lower mRNA levels in SD (11, 33). Initially, this observation appears paradoxical because down-regulation of POMC would most likely result in lower levels of its derived neuropeptide, α-MSH, whereas photoperiod-induced changes in metabolism and physiology such as reduced food intake and body weight loss would appear to require a higher concentration of the anorexic peptide, α-MSH. Artificial square-wave photoperiod transformation did not affect gene expression of PC1/3 and, consequently, cleavage activity of PC1/3 most likely results in unaltered levels of larger POMC derivates such as ACTH and β-lipotrophin, which are generated by PC1/3 cleavage. By contrast, increased gene expression of PC2 in SD is likely to increase proteolytic activity of PC2 at specific cleavage sites resulting in higher levels of smaller peptides such as α-MSH, β-MSH, γ-MSH, β-endorphin and corticotrophin- like intermediate peptide.

Despite reported decreased gene expression of POMC in SD, protein distribution in neurones of the ARC remained unaltered by photoperiod, suggesting that gene expression may not be the primary regulator of POMC product biosynthesis. Gene expression of PC1/3 in SD (versus LD) animals was also unaffected by photoperiod and was reflected in similar levels of PC1/3 protein in SD and LD acclimated hamsters. The regulation of PC2 transcript by photoperiod in the ARC was also reflected at a translational level because there was more PC2 protein detected in SD than LD animals. Similar levels of PC1/3 and POMC protein in SD and LD are reflected in unaltered ACTH-ir, with ACTH peptide known to be a direct result of POMC cleavage by PC1/3 (34). Although inhibitory properties of ACTH on food intake (35) would presume an accumulation of this peptide in SD animals, our results imply a minor role in regulation of seasonal body weight. By contrast, increased PC2 protein in SD animals was accompanied by higher levels of α-MSH-ir fibres and β-endorphin-ir cells, in line with previous studies demonstrating that α-MSH production varies directly in accordance with the expression of PC2 (36). Similar observations were reported for the maturation of β-endorphin (37). Interestingly, the fate of β-endorphin after its cleavage from β-lipotrophin is more extensive than that of α-MSH, and the implications of the observed immunoreactive protein levels are worthy of further consideration. The initially generated β-endorphin$_{1-31}$ is further processed to β-endorphin$_{1-27}$ and β-endorphin$_{1-26}$ (Fig. 1), which are considered to be opiate receptor antagonists opposing the effects of β-endorphin$_{1-31}$ (38). Whereas proteolytic processing of β-endorphin$_{1-27}$ is solely mediated by PC2 activity (39) and removal of the terminal basic residue of β-endorphin$_{1-27}$ by carboxypeptidase's E yields β-endorphin$_{1-26}$ (40), the cleavage of β-lipotrophin to β-endorphin$_{1-31}$ by PC2 is contentious. *In vivo* studies scrutinising β-endorphin$_{1-31}$ levels by radioimmunoassay in PC2-deficient mouse hypothalamus reported increased β-endorphin$_{1-31}$ levels despite PC2 inactivity, suggesting that β-endorphin$_{1-31}$ is likely to be a PC2 substrate rather than a direct product (18). In contrast, *in vitro* studies performed on AtT-20 anterior pituitary cells overexpressing

PC2 demonstrated enhanced conversion of β-lipotrophin to β-endorphin$_{1-31}$ (41). Another experiment performed *in vivo* in the hypothalamus of mice lacking functional PC2 found the processing of β-lipotrophin to β-endorphin$_{1-31}$ diminished by two-thirds. This result suggests that a minor part of the proteolytic conversion from β-lipotrophin to β-endorphin$_{1-31}$ could be mediated by a supplementary processing of the β-lipotrophin substrate by PC1/3 (42). The polyclonal antibody against β-endorphin used in the present study reacts with epitopes of all three β-endorphin forms (1-31, 1-27, 1-26) and hence displays immunoreactivity of total β-endorphin. However, in the hypothalamus, β-endorphin$_{1-31}$ constitutes more than 60% of the total β-endorphin-ir, in contrast to less than 30% β-endorphin$_{1\text{-}27\ +\ 1\text{-}26}$-like immunoreactivity (43). Our results corroborate these findings because PC2 up-regulation in SD results in higher concentrations of total β-endorphin. Current opinions on the physiological function of β-endorphin are conflicting; pharmacological studies generally indicate a short-term stimulatory effect of opioids on food intake (44, 45), but longer term regulation of energy balance has not been reported (46, 47), although β-END$^{-/-}$ mice (48) are characterised by an obese phenotype. This latter finding may support our observation of increased β-endorphin protein levels in states of reduced feeding behaviour and negative energy balance in SD, and the time scale over which these changes are manifested. These characteristics are consistent with our results because seasonal regulation of energy balance is a long-term process rather than an acute induced inhibition of food intake. An opposing and antagonistic effect of the processed β-endorphin$_{1-27}$, evidently a cleavage product mediated exclusively by PC2 activity (39), on opioid receptors could be an interesting target for further experiments attempting to explain this observation. By contrast to immunoreactivity of β-endorphin, which is more confined to the cell body, α-MSH-ir was widely distributed throughout fibres and boutons of neurones in the ARC. Thus, the biological relevance of quantification of relative α-MSH protein content by counting of ir-neurones is questionable. Appraisal of SD and LD α-MSH-ir distribution patterns revealed more intense staining of α-MSH-ir fibres in SD and hence higher levels of protein in SD. This observation is supported by the fact that the concentrations of α-MSH and β-endorphin are closely correlated, in agreement with their production in equimolar amounts as products of the same precursor (49).

Therefore, it is unlikely that less α-MSH than β-endorphin is processed and the immunoreactivity patterns observed in the present study could reflect different rates of transport and routes of intracellular trafficking within the neuronal network. Visually apparent increased levels of α-MSH could be appropriate to the state of negative energy balance in SD (7, 50). Combined with increased expression of β-endorphin in SD, these findings suggest a complementary interaction between the melanocortin, α-MSH, and the opioid, β-endorphin, on seasonal regulation of energy homeostasis, rather than opposing effects.

Colocalisation of PC1/3-ir with POMC-ir in ARC showed almost complete coexpression. This observation implies that cleavage of POMC by PC1/3 is a fundamental process that provides the same relative amounts of PC1/3-cleaved POMC-derived peptides independent of changing photoperiod in SD. We substantiated this hypothesis by demonstrating levels of ACTH-ir that were nearly equal in SD and LD. Even though we did not scrutinise the proteolytic processing fate of β-lipotrophin, the intermediate precursor of β-endorphin, similar results would be expected because β-lipotrophin is cleaved by PC1/3 in a similar manner to ACTH. α-MSH and β-endorphin were almost completely colocalised with PC2 in SD and LD reflecting their derivation from larger intermediate POMC fragments by proteolytic PC2 processing. As a result of higher protein concentrations of PC2 in SD (versus LD), more α-MSH-ir and β-endorphin-ir was processed and could be observed in animals that were exposed to short photoperiod.

The precise involvement of the hypocretins, orexins A and B, in feeding behaviour remains uncertain. Whereas early studies demonstrated an orexigenic effect (51), more recent observations suggest a more complex influence of both neuropeptides on energy balance. In particular, the role of orexin-B remains controversial with only a weak effect on food intake (52). By contrast, the orexin-A-induced hyperphagia and effects (increase) on metabolic rate are more robust (53). However, the exact mechanism by which orexin-A exerts its orexigenic action is not fully elucidated. Orexin-A and orexin-B are highly specifically localised in the LH and are generated by proteolytic processing of the precursor peptide prepro-orexin (54), whose gene expression in the LH was previously colocalised with mRNA encoding for PC1/3 (31). To date, the exact post-translational enzymatic mechanism by which prepro-orexin cleavage is mediated is unknown and there is no evidence from studies performed *in vivo* of direct PC1/3 involvement. Immunohistochemical colocalisation of PC1/3-ir and orexin-A-ir in the present study suggests a close relationship between these two neuroendocrine components at a protein level. Interestingly, virtually all orexin-positive neurones in the LH also express dynorphin (55), whose precursor molecule pro-dynorphin has been reported to be processed by PC1/3 in studies performed *in vitro* (56). Hence pro-dynorphin could be another possible target of PC1/3 activity within the orexin-ir positive neurones of the LH. Current evidence indicates that gene expression of prepro-orexin, such as that of PC1/3 in LH, is unaffected by photoperiod (10, 11). Our observations of equivalent levels of PC1/3-ir and orexin-A-ir are consistent with these published studies in SD and LD. In addition, we recently demonstrated that photoperiod had no effect on the second prepro-orexin derived neuropeptide, orexin-B, because no differences of orexin-B-ir were found in LH of SD and LD acclimated hamsters (57). Combined, these observations suggest that PC1/3 does not play a major role in the seasonal regulation of post translational neuropeptide maturation processes in the LH and hence in seasonal energy balance.

Interestingly, despite distinct gene expression of PC2 in dmpARC, immunoreactive protein was not observed and consequently the function of PC2 mRNA within these neurones remains unclear. This phenomenon could reflect rapid protein denaturation in this nucleus or the ability of neuronal cells to transport mRNA and perform protein biosynthesis in remote locations away from cell bodies (58, 59). Thus, PC2 mRNA could be transported to, and protein

synthesis located in, regions and areas within the hypothalamus other than its origin in the dmpARC. Post-translational modification of proPC2 to PC2 represents another possible explanation for the failure to detect PC2-ir (60). However, because of the polyclonal structure of the PC antibodies, a cross reaction with epitope sequences of the proforms should be possible. Neuronal projections from the dmpARC to other nuclei and the integration of dmpARC neurones in the hypothalamic neuroendocrine network remain to be established. There is growing evidence that the dmpARC is a functionally important component of the neuroendocrine network that regulates energy balance during seasonal adaptation; previous studies have identified a number of photoperiod regulated genes in this area (29, 61, 62). One of the identified neuropeptides within this subdivision of the ARC is the precursor proVGF, which is cleaved by PC1/3 and PC2 into biological active energy balance regulating peptides (63, 64). By contrast to VGF, where gene expression is increased in the dmpARC in SD but decreased in the ARC, gene expression of PC2 was up-regulated in both hypothalamic areas in SD. Interestingly, VGF-ir in the ARC is, like PC2-ir, also characterised by the apparent absence of protein in the dmpARC despite abundant mRNA expressed in this subnucleus (P. Barrett, unpublished data). Therefore PC2 might be transported away from its site of synthesis in the dmpARC very quickly to perform subsequent post-translational processing of proVGF at a different location of the CNS. ProVGF mRNA in the dmpARC suggests a possible target of post-translational PC2 activity as mRNA levels of proVGF are also significantly increased in SD hamsters and respond promptly, like gene expression of PC2, following photoperiod manipulation.

Thus, our results demonstrate that decreasing photoperiod up-regulates PC2 gene expression and PC2 protein, whereas gene expression and protein of PC1/3 are unaffected by SD. We hypothesise that this intensifies proteolytic processing of POMC intermediate derivatives (ACTH and β-lipotrophin), and is the reason for higher concentrations of POMC-derived α-MSH and β-endorphin in short photoperiod despite apparently paradoxical findings showing down-regulated POMC gene expression in SD. By contrast, unaltered PC1/3 gene expression and protein in LH and ARC suggests that regulation by photoperiod is not accomplished via proteolytic processing at PC1/3 specific sites. Thus, regulation of proteolytic processing activity by photoperiod via coordinated expression of PC1/3 and PC2 at transcriptional and translational levels is critical for the maturation of neuropeptide precursors.

Interestingly, the proteolytic enzymes, PC1/3 and PC2 not only mediate post-translational modifications, but are also targets of post-translational modification. First, both enzymes are initially synthesised as inactive precursor molecules, and propeptide cleavage is therefore necessary to activate the enzymes. Second, interaction with small associated neuroendocrine proteins such as proSAAS with PC1/3 (65) and dimerisation of 7B2 with PC2 (66) leads to an inhibition of their enzymatic activities, making these proteins important factors in the intracellular endocrine pathway. In particular, the dependency of PC2 activity on the presence of 7B2 is highly complex because the neuroendocrine protein 7B2 has also been implicated in the activation of the zymogene proPC2 *in vivo* (67). This initially paradoxical observation reflects the complex dimension of interactions between small associated neuroendocrine proteins and the regulation of proteolytic capacity of prohormone convertases. Because the influence of these proteins on the proteolytic activity is evidently most distinct, future studies should focus on these factors to elucidate the exact mechanisms by which photoperiodic regulation of propeptide synthesis is mediated.

The photoperiod-driven regulatory mechanism on a post-translational level observed in the present study could be an additional universal control point for other energy balance related neuropeptide precursors such as proNPY, proTRH and CART. In addition, we provide further evidence for the dmpARC as an area with distinct photoperiod influenced neuroendocrine activity, suggesting that this subdivision of hypothalamic arcuate neurones is an important integral part of the seasonal energy balance regulation network.

Acknowledgements

This collaborative study was funded by the Scottish Executive Environment and Rural Affairs Department (to J. G. Mercer) and EC FP6 funding ('DIABESITY' contract no. LSHM-CT-2003-503041 to J. G. Mercer), Deutsche Forschungsgemeinschaft (German Research Foundation KL973/5; to M. Klingenspor), the National Genome Research Network (NGFN 01GS0483; to M. Klingenspor) and the Danish Research Agency (to R. M. H. Khorooshi). M. Helwig was recipient of a fellowship funded by the European Commission to attend the ObeS[e]chool European Union Marie Curie Training Site at the Rowett Research Institute.

Accepted 3 March 2006

References

1 Mercer JG. Regulation of appetite and body weight in seasonal mammals. *Comp Biochem Physiol* 1998; **119:** 295–303.
2 Morgan PJ, Ross AW, Mercer JG, Barrett P. Photoperiodic programming of body weight through the neuroendocrine hypothalamus. *J Endocrinol* 2003; **177:** 27–34.
3 Schwartz MW, Woods SC, Porte D Jr, Seeley RJ, Baskin DG. Central nervous system control of food intake. *Nature* 2000; **404:** 661–671.
4 Mercer JG, Tups A. Neuropeptides and anticipatory changes in behaviour and physiology: seasonal body weight regulation in the Siberian hamster. *Eur J Pharmacol* 2003; **480:** 43–50.
5 Klingenspor M, Dickopp A, Heldmaier G, Klaus S. Short photoperiod reduces leptin gene expression in white and brown adipose tissue of Djungarian hamsters. *FEBS Lett* 1996; **399:** 290–294.
6 Tups A, Helwig M, Khorooshi RM, Archer ZA, Klingenspor M, Mercer JG. Circulating ghrelin levels and central ghrelin receptor expression are elevated in response to food deprivation in a seasonal mammal (*Phodopus sungorus*). *J Neuroendocrinol* 2004; **16:** 922–928.
7 Fan W, Boston B, Kesterson R, Hruby V, Cone R. Role of melanocortinergic neurons in feeding and the agouti obesity syndrome. *Nature* 1997; **385:** 165–168.
8 McMinn JE, Wilkinson CW, Havel PJ, Woods SC, Schwartz MW. Effect of intracerebroventricular alpha-MSH on food intake, adiposity, c-Fos induction, and neuropeptide expression. *Am J Physiol Regul Integr Comp Physiol* 2000; **279:** R695–R703.
9 Cone RD. The central melanocortin system and energy homeostasis. *Trends Endocrinol Metab* 1999; **10:** 211–216.
10 Mercer JG, Moar KM, Ross AW, Hoggard N, Morgan PJ. Photoperiod regulates arcuate nucleus POMC, AGRP, and leptin receptor mRNA in the Siberian hamster hypothalamus. *Am J Physiol Regul Integr Comp Physiol* 2000; **278:** R271–R281.

11 Reddy AB, Cronin AS, Ford H, Ebling FJ. Seasonal regulation of food intake and body weight in the male Siberian hamster. Studies of hypothalamic orexin (hypocretin), neuropeptide Y (NPY) and pro-opiomelanocortin (POMC). *Eur J Neurosci* 1999; **11:** 3255–3264.

12 Atcha Z, Cagampang FR, Stirland JA, Morris ID, Brooks AN, Ebling FJ, Klingenspor M, Loudon AS. Leptin acts on metabolism in a photoperiod-dependent manner, but has no effect on reproductive function in the seasonally breeding Siberian hamster (*Phodopus sungorus*). *Endocrinology* 2000; **141:** 4128–4135.

13 Tanaka S. Comparative aspects of intracellular proteolytic processing of peptide hormone precursors: studies of proopiomelanocortin processing. *Zool Sci* 2003; **20:** 1183–1198.

14 Paquet L, Zhou A, Chang EY, Mains RE. Peptide biosynthetic processing. distinguishing prohormone convertases PC1 and PC2. *Mol Cell Endocrinol* 1996; **120:** 161–168.

15 Dey A, Xhu X, Carroll R, Turck CW, Stein J, Steiner DF. Biological processing of the cocaine and amphetamine-regulated transcript precursors by prohormone convertases, PC2 and PC1/3. *J Biol Chem* 2003; **278:** 15007–15014.

16 Miller R, Toneff T, Vishnuvardhan D, Beinfeld M, Hook VY. Selective roles for the PC2 processing enzyme in the regulation of peptide neurotransmitter levels in brain and peripheral neuroendocrine tissues of PC2 deficient mice. *Neuropeptides* 2003; **37:** 140–148.

17 Laurent V, Jaubert-Miazza L, Desjardins R, Day R, Lindberg I. Biosynthesis of proopiomelanocortin-derived peptides in prohormone convertase 2 and 7B2 null mice. *Endocrinology* 2004; **145:** 519–528.

18 Miller R, Aaron W, Toneff T, Vishnuvardhan D, Beinfeld MC, Hook VY. Obliteration of alpha-melanocyte-stimulating hormone derived from POMC in pituitary and brains of PC2-deficient mice. *J Neurochem* 2003; **86:** 556–563.

19 Benjannet S, Rondeau N, Day R, Chretien M, Seidah NG. PC1 and PC2 are proprotein convertases capable of cleaving proopiomelanocortin at distinct pairs of basic residues. *Proc Natl Acad Sci USA* 1991; **88:** 3564–3568.

20 Thomas L, Leduc R, Thorne BA, Smeekens SP, Steiner DF, Thomas G. Kex2-like endoproteases PC2 and PC3 accurately cleave a model prohormone in mammalian cells: evidence for a common core of neuroendocrine processing enzymes. *Proc Acad Sci USA* 1991; **88:** 5297–5301.

21 Schafer MKH, Day R, Cullinan WE, Chrétien M, Seidah NG, Watson SJ. Gene expression of prohormone an proprotein convertases in the rat CNS. A comparative in situ hybridisation analysis. *J Neurosci* 1993; **13:** 1258–1279.

22 Brobeck JR. Mechanism of the development of obesity in animals with hypothalamic lesions. *Physiol Rev* 1946; **26:** 541–559.

23 Watson SJ, Khachaturian H, Taylor L, Fischli W, Goldstein A, Akil H. Pro-dynorphin peptides are found in the same neurons throughout rat brain: immunocytochemical study. *Proc Natl Acad Sci USA* 1983; **80:** 891–894.

24 Zamir N, Skofitsch G, Bannon MJ, Jacobowitz DM. Melanin-concentrating hormone: unique peptide neuronal system in the rat brain and pituitary gland. *Proc Natl Acad Sci USA* 1986; **83:** 1528–1531.

25 de Lecea L, Kilduff TS, Peyron C, Gao X, Foye PE, Danielson PE, Fukuhara C, Battenberg EL, Gautvik VT, Bartlett FS, 2nd Frankel WN, van den Pol AN, Bloom FE, Gautvik KM, Sutcliffe JG. The hypocretins: hypothalamus-specific peptides with neuroexcitatory activity. *Proc Natl Acad Sci USA* 1998; **95:** 322–327.

26 Klingenspor M, Niggemann H, Heldmaier G. Modulation of leptin sensitivity by short photoperiod acclimation in the Djungarian hamster, *Phodopus sungorus*. *J Comp Physiol [B]* 2000; **170:** 37–43.

27 Morin LP, Wood RI. *A Sterotaxic Atlas of the Golden Hamster Brain*. San Diego, CA: Academic Press, 2001.

28 Simmens DM, Arriza JL, Swanson LW. A complete protocol for *in situ* hybridisation of messenger RNAs in brain and other tissues with radiolabeled single-stranded RNA probes. *J Histotechnol* 1989; **12:** 169–181.

29 Ross AW, Bell LM, Littlewood PA, Mercer JG, Barrett P, Morgan PJ. Temporal changes in gene expression in the arcuate nucleus precede seasonal responses in adiposity and reproduction. *Endocrinology* 2005; **146:** 1940–1947.

30 Seidah NG, Marcinkiewicz M, Benjannet S, Gaspar L, Beaubien G, Mattei MG, Lazure C, Mbikay M, Chretien M. Cloning and primary sequence of a mouse candidate prohormone convertase PC1 homologous to PC2, Furin, and Kex2: distinct chromosomal localization and messenger RNA distribution in brain and pituitary compared to. *Pc2, Mol Endocrinol* 1991; **5:** 111–122.

31 Nilaweera KN, Barrett P, Mercer JG, Morgan PJ. Precursor-protein convertase 1 gene expression in the mouse hypothalamus. differential regulation by ob gene mutation, energy deficit and administration of leptin, and co expression with prepro-orexin. *Neuroscience* 2003; **119:** 713–720.

32 Williams G, Cai XJ, Elliott JC, Harrold JA. Anabolic neuropeptides. *Physiol Behav* 2004; **81:** 211–222.

33 Mercer JG, Moar KM, Ross AW, Morgan PJ. Regulation of leptin receptor, POMC, and AGRP gene expression by photoperiod in the hypothalamic nucleus of the male Siberian hamster (*Phodopus sungorus*). *Appetite* 2000; **34:** 109–111.

34 Friedman TC, Loh YP, Birch NP. In vitro processing of proopiomelanocortin by recombinant PC1 (SPC3). *Endocrinology* 1994; **135:** 854–862.

35 Al-Barazanji KA, Miller JE, Rice SQ, Arch JR, Chambers JK. C-terminal fragments of ACTH stimulate feeding in fasted rats. *Horm Metab Res* 2001; **33:** 440–445.

36 Kato H, Kuwako K, Suzuki M, Tanaka S. Gene expression patterns of pro-opiomelanocortin-processing enzymes PC1 and PC2 during postnatal development of rat corticotrophs. *J Histochem Cytochem* 2004; **52:** 943–957.

37 Marcinikewicz M, Day R, Seidah NG, Chretien M. Ontogeny of the prohormone convertases PC1 and PC2 in the mouse hypophysis and their colocalization with corticotropin and alpha-melanotropin. *Proc Natl Acad Sci USA* 1993; **90:** 4922–4926.

38 Hammonds RG Jr, Nicolas P, Li CH. beta-endorphin-(1-27) is an antagonist of beta-endorphin analgesia. *Proc Natl Acad Sci USA* 1984; **81:** 1389–1390.

39 Zhou A, Bloomquist BT, Mains RE. The prohormone convertases PC1 and PC2 mediate distinct endoproteolytic cleavages in a strict temporal order during proopiomelanocortin biosynthetic processing. *J Biol Chem* 1993; **268:** 1763–1769.

40 Fricker LD. Carboxypeptidase E. *Annu Rev Physiol* 1988; **50:** 309–321.

41 Zhou A, Mains RE. Endoproteolytic processing of proopiomelanocortin and prohormone convertases 1 and 2 in neuroendocrine cells overexpressing prohormone convertases 1 or 2. *J Biol Chem* 1994; **269:** 17440–17447.

42 Allen RG, Peng B, Pellegrino MJ, Miller ED, Grandy DK, Lundblad JR, Washburn CL, Pintar JE. Altered processing of pro-orphanin FQ/nociceptin and pro-opiomelanocortin-derived peptides in the brains of mice expressing defective prohormone convertase 2. *J Neurosci* 2001; **21:** 5864–5870.

43 Millington WR, Smith DL. The posttranslational processing of beta-endorphin in human hypothalamus. *J Neurochem* 1991; **57:** 775–781.

44 Glass MJ, Billington CJ, Levine AS. Opioids and food intake: distributed functional neuronal pathways? *Neuropeptides* 1999; **33:** 360–368.

45 Kalra SP, Horvath TL. Neuroendocrine interactions between galanin, opioids, and neuropeptide Y in the control of reproduction and appetite. *Ann NY Acad Sci* 1998; **863:** 236–240.

46 de Zwaan M, Mitchell JE. Opiate antagonists and eating behaviour in humans: a review. *J Clin Pharmacol* 1992; **32:** 1060–1072.

47 Levine AS, Billington CJ. Opioids. Are they regulators of feeding? *Ann NY Acad Sci* 1989; **575:** 209–219.

48 Appleyard SM, Hayward M, Young JI, Butler AA, Cone RD, Rubinstein M, Low MJ. A role of endogenous opioids beta-endorphin in energy homeostasis. *Endocrinology* 2003; **144:** 1753–1760.

49 Bertagna X. Proopiomelanocortin-derived peptides. *Endocrinol Metab Clin North Am* 1994; **23:** 467–485.

50 Brown KS, Gentry RM, Rowland NE. Central injection in rats of alpha-melanocyte stimulating hormone analog: effects on food intake and brain Fos. *Regul Pept* 1998; **78:** 89–94.

51 Sakurai T, Amemiya A, Ishii M, Matsuzaki I, Chemelli RM, Tanaka H, Williams SC, Richarson JA, Kozlowski GP, Wilson S, Arch JR, Buckingham RE, Haynes AC, Carr SA, Annan RS, McNulty DE, Liu WS, Terrett JA, Elshourbagy NA, Bergsma DJ, Yanagisawa M. Orexins and orexin receptors: a family of hypothalamic neuropeptides and G protein-coupled receptors that regulate feeding behavior. *Cell* 1998; **92:** 696.

52 Edwards CM, Abusnana S, Sunter D, Murphy KG, Ghatei MA, Bloom SR. The effect of the orexins on food intake. comparison with neuropeptide Y, melanin-concentrating hormone and galanin. *J Endocrinol* 1999; **160:** R7–R12.
53 Haynes AC, Jackson B, Overend P, Buckingham RE, Wilson S, Tadayyon M, Arch JR. Effects of single and chronic intracerebroventricular administration of the orexins on feeding in the rat. *Peptides* 1999; **20:** 1099–1105.
54 Sakurai T, Moriguchi T, Furuya K, Kajiwara K, Nakamura T, Yanagisawa M, Goto K. Structure and function of human prepro-orexin gene. *J Biol Chem* 1999; **274:** 17771–17776.
55 Chou TC, Lee CE, Lu J, Elmquist JK, Hara J, Willie JT, Beuckmann CT, Chemelli RM, Sakurai T, Yanagisawa M, Saper CB, Scammell TE. Orexin (hypocretin) neurons contain dynorphin. *J Neurosci* 2001; **21:** RC168.
56 Dupuy A, Lindberg I, Zhou Y, Akil H, Lazure C, Chretien M, Seidah NG, Day R. Processing of prodynorphin by the prohormone convertase PC1 results in high molecular weight intermediate forms. Cleavage at a single arginine residue. *FEBS Lett* 1994; **337:** 60–65.
57 Khorooshi RM, Klingenspor M. Neuronal distribution of melanin-concentrating hormone, cocaine- and amphetamine-regulated transcript and orexin-B in the brain of the Djungarian hamster (*Phodopus sungorus*). *J Chem Neuroanatom* 2005; **29:** 137–148.
58 Lee SK, Hollenbeck PJ. Organization and translation of mRNA in sympathetic axons. *J Cell Sci* 2003; **116:** 4467–4478.
59 Koenig E, Giuditta A. Protein-synthesizing machinery in the axon compartment. *Neuroscience* 1999; **89:** 5–15.
60 Braks JA, Van Horssen AM, Martens GJ. Dissociation of the complex between the neuroendocrine chaperone 7B2 and prohormone convertase PC2 is not associated with proPC2 maturation. *Eur J Biochem* 1996; **238:** 505–510.
61 Barrett P, Ross AW, Balik A, Littlewood PA, Mercer JG, Moar KM, Sallmen T, Kaslin J, Panula P, Schuhler S, Ebling FJ, Ubeaud C, Morgan PJ. Photoperiodic regulation of histamine H3 receptor and VGF messenger ribonucleic acid in the arcuate nucleus of the Siberian hamster. *Endocrinology* 2005; **146:** 1930–1939.
62 Ross AW, Webster CA, Mercer JG, Moar KM, Ebling FJ, Schuhler S, Barrett P, Morgan PJ. Photoperiod regulation of hypothalamic retinoid signalling: association of retinoid X receptor gamma with body weight. *Endocrinology* 2004; **145:** 13–20.
63 Trani E, Giorgio A, Canu N, Amadoro G, Rinaldi AM, Halban PA, Ferri GL, Possenti R, Schinina ME, Levi A. Isolation and characterization of VGF peptides in rat brain. Role of PC1/3 and PC2 in the maturation of VGF precursor. *J Neurochem* 2002; **81:** 565–574.
64 Hahm S, Mizuno TM, Wu TJ, Wisor JP, Priest CA, Kozak CA, Boozer CN, Peng B, McEvoy RC, Good P, Kelley KA, Takahashi JS, Pintar JE, Roberts JL, Mobbs CV, Salton SR. Target deletion of the VGF gene indicates that the encoded secretory peptide precursor plays a novel role in the regulation of energy balance. *Neuron* 1999; **23:** 537–548.
65 Fricker LD, McKinzie AA, Sun J, Curran E, Qian Y, Yan L, Patterson SD, Courchesne PL, Richards B, Levin N, Mzhavia N, Devi LA, Douglass J. Identification and characterization of proSAAS, a granin-like neuroendocrine peptide precursor that inhibits prohormone processing. *J Neurosci* 2000; **20:** 639–648.
66 Mbikay M, Seidah NG, Chretien M. Neuroendocrine secretory protein 7B2: structure, expression and functions. *Biochem J* 2001; **357:** 329–342.
67 Westphal CH, Muller L, Zhou A, Zhu X, Bonner-Weir S, Schambelan M, Steiner DF, Lindberg I, Leder P. The neuroendocrine protein 7B2 is required for peptide hormone processing in vivo and provides a novel mechanism for pituitary Cushing's disease. *Cell* 1999; **96:** 689–700.

J Comp Physiol B (2008) 178:167–177
DOI 10.1007/s00360-007-0208-x

ORIGINAL PAPER

3-Iodothyronamine: a novel hormone controlling the balance between glucose and lipid utilisation

L. J. Braulke · M. Klingenspor · A. DeBarber · S. C. Tobias · D. K. Grandy · T. S. Scanlan · G. Heldmaier

Received: 25 April 2007 / Revised: 22 August 2007 / Accepted: 22 August 2007 / Published online: 3 October 2007

Abstract 3-Iodothyronamine is considered as a derivate of thyroid hormone as a result of enzymatic deiodination and decarboxylation. The physiological role of thyronamine (T1AM) is not known. The aim of this study was to analyze the metabolic response to T1AM in the Djungarian hamster *Phodopus sungorus*. We measured the influence of T1AM (50 mg/kg) on metabolic rate (VO_2), body temperature (T_b) and respiratory quotient (RQ) in this species and in BL/6 mice. T1AM treated hamsters as well as the mice showed a rapid decrease in VO_2 and T_b, accompanied by a reduction of RQ from normal values of about ~0.9 to ~0.70 for several hours. This indicates that carbohydrate utilisation is blocked by the injection of T1AM and that metabolic pathways are rerouted from carbohydrate to lipid utilisation in response to T1AM. This assumption was further supported by the observation that the treatment of T1AM caused ketonuria and a significant loss of body fat. Our results indicate that T1AM has the potential to control the balance between glucose and lipid utilisation in vivo.

Keywords Thyroid hormone · Torpor · Hypometabolism · Hypothermia · RQ · Glucose utilisation · Lipid metabolism

Abbreviations

2-DG	2-Deoxy-D-glucose
BM	Body mass
DEXA	Dual energy X-ray absorption
DMSO	Dimethyl sulfoxide
FM	Fat mass
LM	Lean mass
LP	Long photoperiod
MA	Mercaptoacetate
MP	Methyl palmoxirate
RQ	Respiratory quotient
SP	Short photoperiod
T1AM	3-Iodothyronamine
T_a	Ambient temperature
T_b	Body temperature
TH	Thyroid hormone
VO_2	Metabolic rate (volume oxygen consumed)

Communicated by H.V. Carey.

L. J. Braulke (✉) · M. Klingenspor · G. Heldmaier
Department of Biology, Philipps-University Marburg,
Karl von Frisch Str.8, 35032 Marburg, Germany
e-mail: braulkel@staff.uni-marburg.de

A. DeBarber · D. K. Grandy · T. S. Scanlan
Department of Physiology and Pharmacology,
Oregon Health & Science University, Portland, OR, USA

S. C. Tobias · T. S. Scanlan
Department of Pharmaceutical Chemistry,
University of California-San Francisco,
San Francisco, CA, USA

Introduction

In endotherms a major portion of energy expenses is required to maintain a constant and high body temperature. This is especially true for small mammals, which are exposed to a great risk of cooling because of the unfavourable surface to volume ratio. Limitations in fuel availability therefore pose a great challenge for the maintenance of high body temperature. In times where thermogenic costs are high and food availability and/or quality is low, e.g., in winter months, some small mammals reduce their high-energy requirements by entering a hypometabolic and hypothermic state called torpor. These torpid states can last

for hours like in spontaneous daily torpor (shallow, daily torpor) or for several days and weeks (multiday torpor bouts) during hibernation.

The Djungarian hamster *Phodopus sungorus*, a small rodent of 25–45 g, which mainly occurs in the Siberian steppe shows seasonal acclimation cued by short photoperiod (SP < 12 h Hoffmann 1981), which includes reductions of food intake (Wade and Bartness 1984) and body mass (Heldmaier and Steinlechner 1981), a reduction of the reproductive organs, a change in fur color from the brown summer state to snow-white winter acclimatized condition (Figala et al. 1973), an increase in fur density (Heldmaier and Steinlechner 1981; Heldmaier et al. 1989) and the incidence of torpor (Heldmaier and Steinlechner 1981; Heldmaier et al. 1989; Ruf et al. 1991). Under ad libitum feeding conditions the occurrence of torpor is restricted to short photoperiod (SP) acclimated hamsters and does not occur in long photoperiod (SP) conditions.

Animals displaying shallow daily torpor show a dramatic drop of T_b and VO_2 during the diurnal resting phase. Metabolic rate is lowered by ~70% of the basal metabolic rate (Heldmaier and Ruf 1992; Heldmaier et al. 2004) and is accompanied with a reduction in heart rate and ventilation (Zosky 2002; Elvert and Heldmaier 2005). During prolonged torpor bouts glucose stores are exhausted, which is supported by the fact that animals undergoing torpor become hypoglycemic (Heldmaier et al. 1999; Dark et al. 1999) and lipid fuelled metabolism takes over (Heldmaier et al. 1999). This switch to lipid utilisation can then be observed by a decrease in respiratory quotient (RQ).

Food intake plays an important role for the incidence of torpor, since limitations in food intake may enhance the frequency and depth of torpor in *Phodopus sungorus* (Ruf et al., 1993) or even initiate daily torpor as observed in *Peromyscus* (Tannenbaum and Pivorun 1987). Fasting induced torpor by food restriction was also displayed in mice, which usually do not show spontaneous daily torpor (Hudson and Scott 1979; Swoap et al. 2006). Even though SP acclimatized hamsters fed ad libitum enter torpor spontaneously it seems most likely that fuel availability mediates or influences the occurrence of torpor. This is why manipulations of pathways involved in the regulation of food uptake and cellular energy supply have been used to induce hypometabolic and hypothermic states (Paul et al. 2005; Gluck et al. 2006).

3-Iodothyronamine (T1AM), a recently discovered naturally occurring thyroid hormone (TH) derivative induces hypothermia in mice and may therefore offer new perspectives on the initiation of hypometabolic states (Scanlan et al. 2004). T1AM is proposed to be derived from thyroxine (T4) presumably as a result of enzymatic deiodination and decarboxylation. In vivo it has been detected in brains from rats and guinea pigs and also in extracts from brain, heart, liver and blood from adult C57BL/6J mice. In vitro T1AM is a potent agonist of the G protein-coupled trace amine-associated receptor TAAR1 (Grandy 2007). The physiological role of T1AM is not known. Injection of synthetic T1AM into C57BL/6J mice caused a profound hypothermia, bradycardia and reduced cardiac output in this species, effects that are opposite those of TH, such as increased VO_2, T_b and cardiac performance (Scanlan et al. 2004; Chiellini et al. 2007).

In this study we tested whether T1AM is capable of inducing a hypometabolic state in *Phodopus sungorus* and whether this compares to the hypometabolic response during spontaneous daily torpor. Hamsters were either acclimated to long photoperiod where no spontaneous daily torpor can be observed, or they were acclimated to short photoperiod until they showed maximum frequency of spontaneous daily torpor. If only the latter would become torpid in response to T1AM it would suggest a seasonal role of this hormone in torpor induction. If hamsters from both acclimation states become torpid one interpretation is that T1AM is capable of causing hypometabolic responses irrespective of seasonal preparation for daily torpor.

Animals, material and methods

Animals

80 Djungarian hamsters (*Phodopus sungorus*) were bred and raised in the laboratory of the University of Marburg under long photoperiod conditions (LP; LD 16:8; light on: 0400 h, light off: 2,000 h) and a constant ambient temperature (T_a) of 24 ± 1°C. At the age of 3 months 40 hamsters were put into short photoperiod conditions (SP; LD 8:16; light on: 0800 h, light off: 1,600 h) and a constant T_a of 24 ± 1°C for 14 weeks to achieve maximal adaptation to winter, the other 40 remained in long photoperiod (LP) to keep the summer state.

10 Adult male mice (*Mus musculus*) aged about 7–10 weeks, with the genetic background C57BL/6, obtained from Charles River Laboratories (Sandhofer Weg 7, 97633 Sulzfeld) were kept at a constant ambient temperature (T_a) of 24 ± 1°C and LD 12:12 (light on: 0600 h, light off: 1,800 h).

All animals were housed individually in makrolon-cages type II (16 cm × 21 cm × 13 cm) with wood shavings and were constantly fed with water and food (hamster: ALTROMIN 7014; mice: ALTROMIN 1314) ad libitum. Body mass was measured up to five times a week. Body temperature and metabolic rate were measured continuously for 1 day prior to the injection of T1AM and for 2 days following the injection of T1AM. For all injections T1AM (T1AM, 50 mg/kg, 100 µl) was dissolved in 60%

J Comp Physiol B (2008) 178:167–177

dimethyl sulfoxide (DMSO) and 40% physiological saline (pH 7.4). At this time we do not know whether this dosage causes physiological or pharmacological responses. Only vehicle (60% DMSO and 40% saline, pH 7.4, 100 µl) was used as control injection. Injections were given i.p. between 12:00 an 13:00. All experiments were done in accordance with approved guidelines for the use and care of animals by the German animal welfare law (Deutsches Tierschutzgesetz).

Telemetric recording of T_b

For the measurement of body temperature (T_b) animals were implanted intraperitoneally with calibrated temperature transmitters (Mini-Mitter, Model X, Sunriver, Oregon, USA, accuracy 0.1°C) under ketamine hydrochloride anaesthesia (Ketavet, Pharmacia Upjohn GmbH, Erlangen, Germany, 50 mg × kg^{-1}) and 1–2% Isoflurane (Forene, Abbott, Wiesbaden, Germany). The detection of the transmitter signals was accomplished by a radio receiver and processed by a microcomputer system (Heldmaier and Ruf 1992).

Metabolic rate measurement

During metabolic rate measurements animals were kept individually in makrolon-cages type II inside a climate chamber with a constant T_a of 24°C and constant light cycle of either LP (LD 16:8) or SP (LD 8:16). Air flow was adjusted to about 45 l × h^{-1} and continuously monitored by mass flow meters (FM 360, Tylan, München, Germany). O_2-consumption and CO_2-production were measured by a one-channel O_2 analyser (S3AII, Ametek, Sunnyvale USA) and a CO_2 two-channel analyser (UNOR 6N, Maihak AG, Hamburg, Germany) each with a 0.001 Δ Vol% resolution. Sample air from the cages was compared with reference air from the climate chamber. Air was dried by an electric freeze trap (M&C Cooler, EPC, Ratingen, Germany). A magnetic valve system controlled by a computer allowed a measurement of up to three cages simultaneously. One of the three cages was used for automated continuous zero readjustments. Metabolic rate was calculated according to the equation: $\dot{V}O_2$ [ml O_2 h^{-1}] = Δ Vol% O_2 × Flow [l h^{-1}] × 10. The RQ was calculated from the volume of CO_2 produced per volume O_2 consumed.

Urine sampling and ketone analysis

Urine samples were collected by the use of special metabolic cages (Ø18 cm × height 12 cm) integrated in an automated setup (Stieglitz et al. 1995). Each metabolic cage contained a small plastic house (Ø6 cm × 10 cm) for retirement and animals received food and water ad libitum. Urine was separated from feces and other solids by a funnel system and was automatically sampled in 4 h intervals. Urine was centrifuged for 5 Min at 2,500*g* at 25°C and frozen at −80°C for further analysis. Ketone bodies in the urine were measured by Ketostix Reagent Strips (Bayer HealthCare, Mishawaka, USA), which is a semiquantitative method measuring the concentration of acetoacetic acid in 6 steps (0, 5, 15, 40, 80, 160 mg^{-dl}) based on a colour reaction from buff-pink to maroon when acetoacetic acid reacts with nitroprusside. For statistical analysis the semiquantitative results were converted into rank orders ranging from 0 to 5 (0 = 0 mg^{-dl}, 1 = 5 mg^{-dl}, 2 = 15 mg^{-dl}, 3 = 40 mg^{-dl}, 4 = 80 mg^{-dl}, 5 = 160 mg^{-dl}).

Liquid chromatography tandem mass spectrometry

Hamster brain was weighed and homogenized in 10 ml cold 1 M HCl. The homogenate was centrifuged for 20 min at 14,000 rpm in a cold room, the supernatant was transferred to falcon tubes and 10 µM T1AM-d_4 was added (to 100 pmol/sample). The pH was adjusted to 10–11 with 40% KOH followed by the addition of 1 ml of 1 M CHES buffer. Ethyl acetate was used to extract the aqueous layer five times. Anhydrous sodium sulfate was added to the combined ethyl acetate layers, filtered and concentrated. A modified procedure with improved extraction efficiency was used for isolation of T1AM from plasma (200 µl) that involved spiking with 10 µM T1AM-d_4 (to 2.5 pmol/sample), followed by solid-phase extraction using Bond Elut Certify cartridges (Varian). The residue obtained in both cases was re-dissolved in 70 µl methanol:water (45:55) at 0.1 M HCl for analysis. T_1AM and T_1AM-d_4 were detected using a triple-quadrupole Thermo TSQ Quantum Discovery mass spectrometer equipped with an electro-spray ionization source. The ionization interface was operated using the following settings: sheath and aux gas flow rates, 45 and 20, respectively; source voltage, 3.0 kV; tube lens voltage, 180 V; capillary voltage, 35 V; and capillary temperature, 325°C. The mass spectrometry method was optimized for sensitivity and selectivity using infusion experiments to examine analyte ionization and fragmentation. A syringe pump was used to provide a constant stream of T_1AM and T_1AM-d_4 into the LC flow using a T-connection. A full scan mass spectrum in the positive mode demonstrated abundant molecular ions $[M + H]^+$ at *m/z* 356 and 360, corresponding to T_1AM and T_1AM-d_4, respectively. Each readily fragmented by tandem MS to give product ions as previously described (Scanlan et al. 2004). An instrument method was created to monitor the transitions from *m/z* 356 → 212 and *m/z* 356 → 339 for T1AM, and *m/z* 360 → 216 and *m/z* 360 → 343 for T1AM-d_4. Scan event settings were Q2 collision gas 1.0 mTorr, collision energy 12, scan width 1.2 *m/z*, scan time 0.5 s, Q1 peak width 0.7 and Q3 peak

width 0.9. An isocratic LC separation was developed to separate T1AM for other components using a 200× 2.1 mm, 5 µm Hypurity Advance C_{18} column (Thermo Hypersil, Waltham, MA). The 0.4 ml/min mobile phase consisted of methanol:water (45:55) with 0.01% trifluoroacetic acid. Injection volumes were 10–20 µl. The autosampler needle was copiously flushed and washed with methanol/0.1% acetic acid between injections to ensure no sample carry-over. The first 1.6 min of the LC run were diverted to waste. T_1AM and T1AM-d_4 demonstrated acceptable peak shape with retention times of around 5 min.

Experiment 1: Thermal and metabolic response to T1AM

To investigate the metabolic response to T1AM, $\dot{V}O_2$, T_b and RQ of adult C57BL/6J mice, adult SP and LP hamsters were monitored for 24 h after which animals were either injected with T1AM or with carrier only and then followed for another 24 h (BL/6-T1AM, $n = 5$; BL/6-carrier, $n = 5$; SP-T1AM, $n = 6$; SP-carrier, $n = 7$; LP-T1AM, $n = 7$; LP-carrier, $n = 7$).

Experiment 2: T1AM and ketonuria

To verify the influence of T1AM on the carbohydrate metabolism, Djungarian hamsters were kept in the metabolic cages for 4 days and urine samples were gathered. After the second day without treatment hamsters were either injected with T1AM or with carrier only (SP-T1AM, $n = 6$; LP-T1AM, $n = 6$; SP-carrier, $n = 6$; LP-carrier, $n = 6$). All urine samples were weighed and ketone content was measured as described above.

Experiment 3: T1AM effects on body weight and body composition

To detect an influence of T1AM on body weight LP and SP hamsters were weighed daily 10 days before and 15 days after treatment with T1AM or carrier injection (SP-T1AM, $n = 6$; LP-T1AM, $n = 6$; SP-carrier, $n = 6$; LP-carrier, $n = 6$). To test the influence of T1AM on body composition, such as lean mass (LM g^{-1}) and fat mass (FM g^{-1}), hamsters were analysed one day before and one day after treatment (SP-T1AM, $n = 6$; LP-T1AM, $n = 6$; SP-carrier, $n = 6$; LP-carrier, $n = 6$) via a dual energy X-ray absorption (DEXA) scanner (PIXIMUS2 scanner, software version 1.46.007, GE Medical Systems, Madison, WI, USA).

Experiment 4: Detection of T1AM in hamster tissue

To determine that T1AM is present in *Phodopus sungorus* in vivo, SP and LP control hamsters were sacrificed for brain and serum collection. To determine whether T1AM injection elevates the serum T1AM levels as compared to carrier injection SP and LP hamsters were sacrificed 3 h after injection. Crude biogenic amine brain and serum extracts were prepared as described above which then were analysed by liquid chromatography tandem mass spectroscopy (LC/MS) using tetradeuterated T1AM (T_1AM-d_4) as an internal standard.

Results

Experiment 1: Thermal and metabolic response to T1AM

Figure 1 shows the time course of metabolic rate (Fig. 1a), body temperature (Fig. 1b) and RQ (Fig. 1c) of SP and LP hamsters before and after treatment with T1AM. Before drug treatment both winter- and summer-acclimatized hamsters show normometabolic and normothermic values of about 2.5 ml h^{-1} g^{-1} and 36°C and a typical RQ of 0.9 as described in Heldmaier (1975) for an ambient temperature of 24°C. Furthermore $\dot{V}O_2$, T_b and RQ showed ultradian variation typical for these animals (Heldmaier et al. 1999). After injection of T1AM metabolic rate, body temperature and RQ of the hamsters decreased within minutes. Another obvious reaction was the loss of ultradian variations of these parameters in all treated animals (Fig. 1). All hamsters showed a similar time course of these responses. Within 3 h metabolic rate and body temperature reached minimal values whereas minimal RQ is obtained after about 4.5 h post injection. Normometabolic and normothermic states together with normal ultradian variations are recovered after 6 h in SP hamsters and 12 h in LP (Fig. 1a, b). The reduced RQ was maintained longer than the hypometabolic and hypothermic states. Five hours post injection the RQ of the SP hamsters rises again but even after 24 h initial values are not reached. The return to higher values in mean RQ of the LP hamsters proceeds even slower. The final values at the end of measurement, 24 h post injection are RQ = 0.87 for SP hamsters and RQ = 0.74 for the LP hamsters (Fig. 1c).

C57BL/6 mice also showed a hypometabolic and hypothermic response to T1AM injection with a profound depression of the RQ. The hypothermic response is equivalent to previous observations in mice by Scanlan et al. (2004). The magnitude of $\dot{V}O_2$ and T_b reduction was more pronounced in mice than in hamsters (Fig. 2a, b). However both species reach the same minima of RQ at about 0.7 and this minimum is reached in mice within 1.5 h as compared to LP hamsters, which require 4.5 h (Fig. 2c). Carrier injections failed to induce any of the reactions caused by T1AM in all experimental animals (Fig. 3).

J Comp Physiol B (2008) 178:167–177

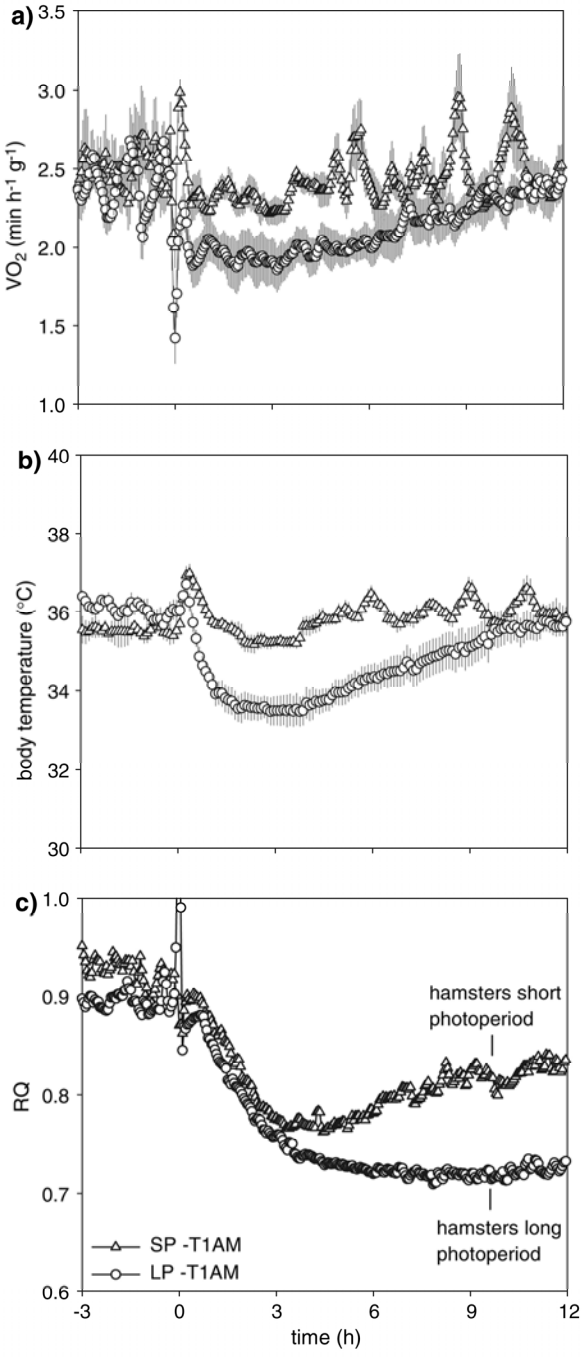

Fig. 1 Effects of T1AM, injected i.p. (hour 0), on mean (±SE) metabolic rate (VO_2), body temperature (T_b) and respiratory quotient (RQ) in winter and summer acclimatized Djungarian hamsters maintained at 24°C. **a** T1AM lead to a loss of the typical ultradian variations and significantly decreased VO_2 up to 4 h in SP hamsters and up to 12 h in LP hamsters. **b** Effect of T1AM on T_b resembles that on VO_2, T_b was reduced significantly for up to 4 h in SP hamsters and up to 12 h in LP hamsters and ultradian variations were lost for the same time. **c** Postinjection RQ dropped significantly in SP and LP hamsters. Reduced levels of RQ were maintained for more than 12 h in SP and LP hamsters, but SP hamsters regain normal values earlier than LP hamsters

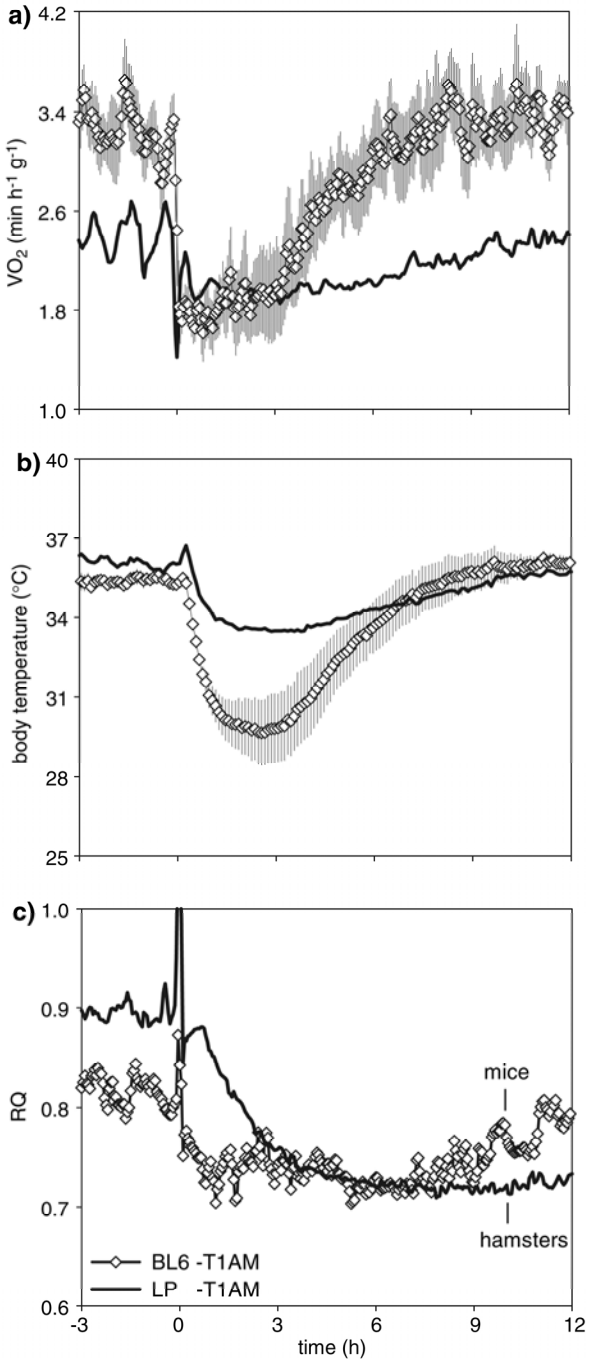

Fig. 2 Effects of T1AM, injected i.p. (hour 0), on mean (±SE) metabolic rate (VO_2), body temperature (T_b) and respiratory quotient (RQ) in C57BL/6 mice (*open diamond*) compared to LP hamsters [*solid line* (repeat of mean values in Fig. 1)] maintained at 24°C. **a**, **b** The decrease in VO_2 and T_b due to T1AM injection is greater in mice than in hamsters. **c** The minimal values of RQ~0.7 postinjection in mice are reached 3 h earlier compared to hamsters

In response to T1AM SP hamsters reduce their metabolic rate from 2.49 ± 0.08 ml h^{-1} g^{-1} to a minimal value of 2.23 ± 0.07 ml h^{-1} g^{-1}, LP hamsters from 2.38 ± 0.07

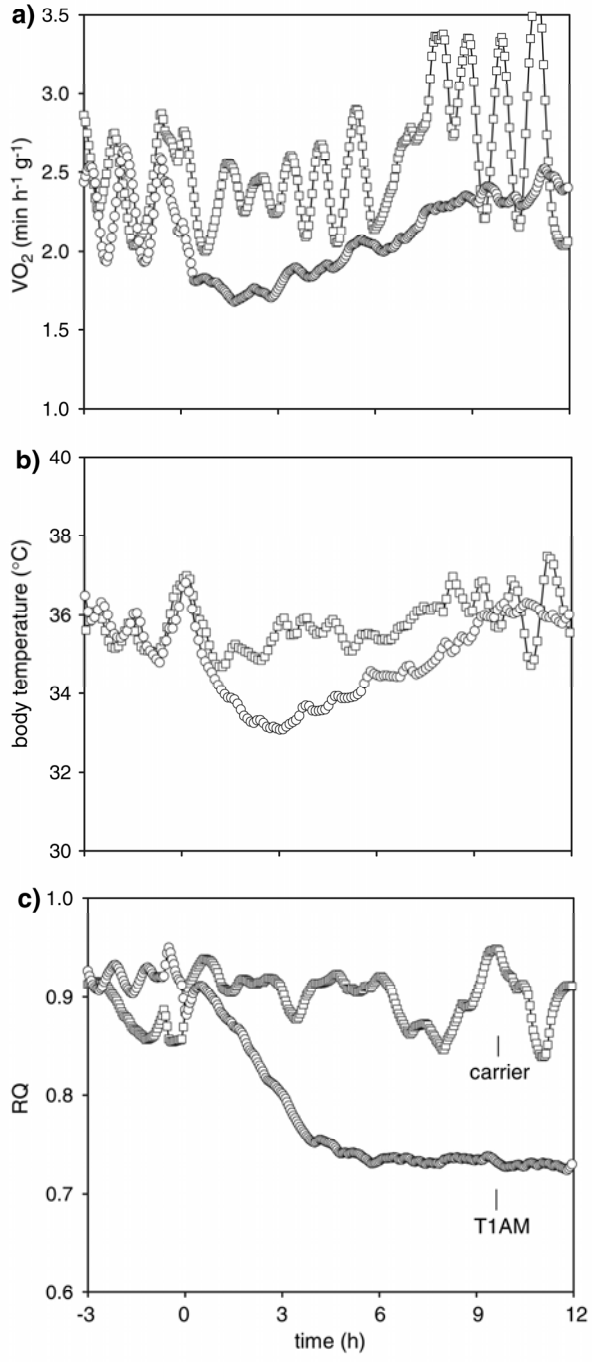

Fig. 3 Comparison of VO_2 (**a**), T_b (**b**) and RQ (**c**) of one LP hamster, once after carrier injection and 2 weeks later after T1AM treatment (i.p.: hour = 0). Carrier injection had neither effects on VO_2, T_b and RQ nor on ultradian rhythmicity

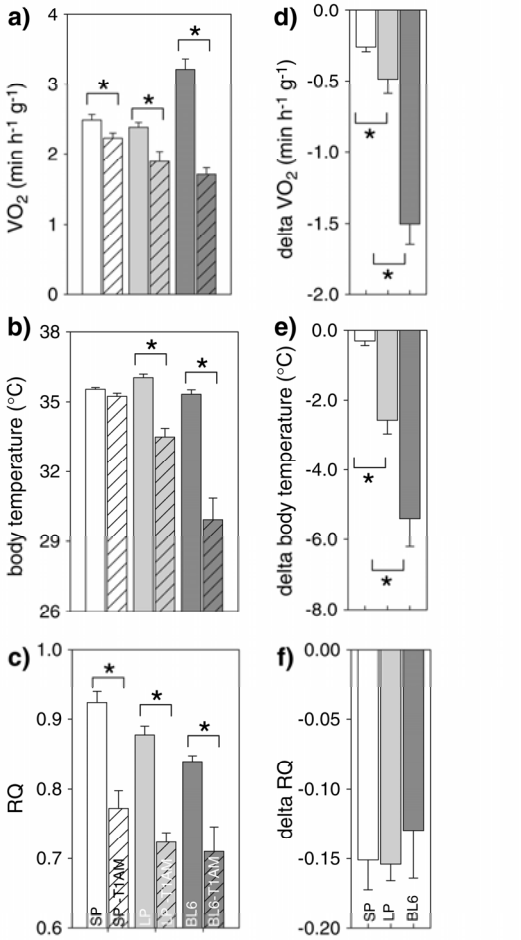

Fig. 4 **a–c** Three hour means (±SE) of VO_2, T_b and RQ before (*plain bars*) and after (*striped bars*) T1AM injection of SP- (*white bars*) and LP- (*grey bars*) acclimatized hamsters and of C57BL/6 mice (*dark grey bars*). The treatment caused a significant decrease in all parameters ($P < 0.05$), except for the T_b of the SP hamsters. **d–f** Mean difference (±SE) between the individual three hour means of VO_2, T_b and RQ before and after treatment. The decrease of VO_2 and T_b is significantly greater in LP than in SP hamsters and even higher in mice, whereas the RQ is lowered for the same amount

to 1.90 ± 0.14 ml $h^{-1} g^{-1}$ and mice from 3.21 ± 0.15 to 1.71 ± 0.09 ml $h^{-1} g^{-1}$ (Fig. 4a). Lowest T_b of 35.2 ± 0.1°C was obtained in SP hamsters, 33.5 ± 0.4°C in LP hamsters and 29.9 ± 0.9°C in mice (Fig. 4b). $VO_{2\ min}$ and $T_{b\ min}$ were lower in mice than in their controls treated with vehicle (not illustrated) or than in hamsters of both acclimation states injected with T1AM ($P < 0.05$, for each). LP hamsters reached lower $VO_{2\ min}$ and $T_{b\ min}$ than SP hamsters. Minimal values of RQ of 0.77 ± 0.025 are reached in SP hamsters, 0.72 ± 0.013 for LP hamsters and 0.71 ± 0.034 in mice (Fig. 4c). The amplitude of VO_2 and T_b reduction differs significantly between LP hamsters and SP hamsters and mice (*t*-test; $P < 0.05$; Fig. 4d, e) but the reduction in RQ is the same for all experimental animals (*t*-test; $P > 0{,}05$; Fig. 4f).

Figure 5 shows delta VO_2 of individual hamsters and mice as related to body mass. The amplitude of the response to T1AM was significantly correlated with body

J Comp Physiol B (2008) 178:167–177

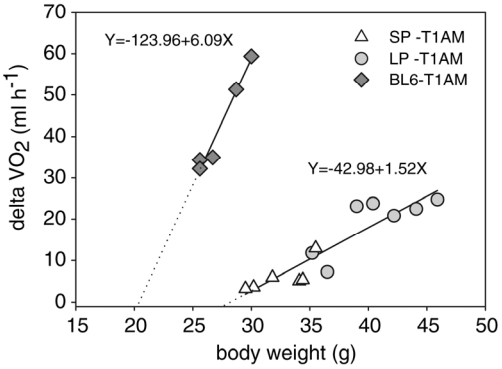

Fig. 5 Relation between the decrease of VO_2 (delta VO_2) after T1AM treatment and the body weight of injected SP (*open triangle*) and LP (*open circle*) hamsters and C57BL/6 mice (*open diamond*). Each data point corresponds to one individual. The magnitude of delta VO_2 in hamsters and mice significantly correlates with body weight (hamsters: $r = 0.923$; $P < 0.05$; mice: $r = 0.983$; $P < 0.05$)

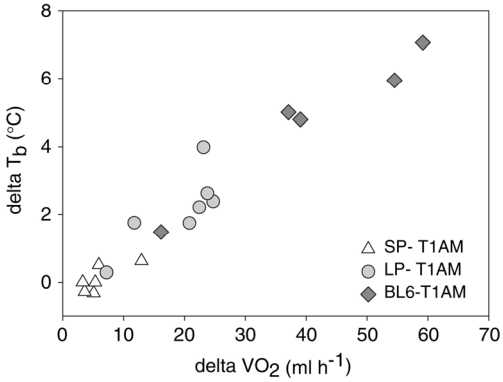

Fig. 6 Relation between the decrease of VO_2 (delta VO_2) and the decrease of T_b (delta T_b) after T1AM treatment of SP (*open triangle*) and LP (*open cirlce*) hamsters and C57BL/6 mice (*open diamond*). Each data point corresponds to one individual. The magnitude of delta VO_2 significantly correlates with the loss of body temperature ($r = 0.926$; $P < 0.05$)

mass (Pearson correlation; hamsters: $r = 0.923$; $P < 0.05$; mice: $r = 0.983$; $P < 0.05$). The largest hamster with a body weight of 45.9 g showed a depression of metabolic rate by 24.7 ml h^{-1}, whereas the smallest hamster with 29.5 g body mass decreased its metabolic rate only by about 3.3 ml h^{-1}. This range in body mass reflects seasonal acclimation in Djungarian hamsters, concluding that short photoperiod acclimated hamsters showed only a weak response to T1AM and long photoperiod acclimated hamsters showed a pronounced response to T1AM. Regression analysis of the data suggests that this difference is due to the difference in body mass but not the state of acclimation. The positive correlation between delta VO_2 and body mass differs between mice and hamsters.

The time course of body temperature reduction highly resembles the metabolic depression due to T1AM treatment (Figs. 1a, b, 2a, b). These parameters correlate significantly within the magnitude of reaction as shown in Fig. 6, in which delta T_b is plotted against delta VO_2 of each treated animal (Pearson correlation; $r = 0.926$; $P < 0.01$). This relation is independent of species and acclimatisation of the hamsters.

To investigate whether T1AM affected the rate of heat loss and therefore caused hypothermia we calculated thermal conductance before and after injection. Thermal conductance did not increase after treatment with T1AM, indicating no major changes in peripheral circulation or other pathways of heat loss.

Experiment 2: T1AM and ketonuria

Treatment with T1AM caused ketonuria in both acclimatization groups. The measured ketone content in urine was transformed into ranks ranging from 0 to 5. Mean values of these ranks are diagrammed in Fig. 7. Eight hours post injection one of 6 SP hamsters and 3 of 6 LP hamsters were tested positive for ketonuria. As time proceeds the number of animals becoming ketonuric as well as the quantity of urine ketones rises in both T1AM treated groups. Highest values of ketone bodies are reached after 16 h in LP and after 20 h in SP. The ketonuric response to T1AM is not different within the two acclimatizations (Two way RM ANOVA; $P > 0.05$). After 28 h ketonuria is lost again. Carrier treated hamsters showed no ketonuria at any point of the experiment (Two way RM ANOVA; $P > 0.05$; Fig. 7).

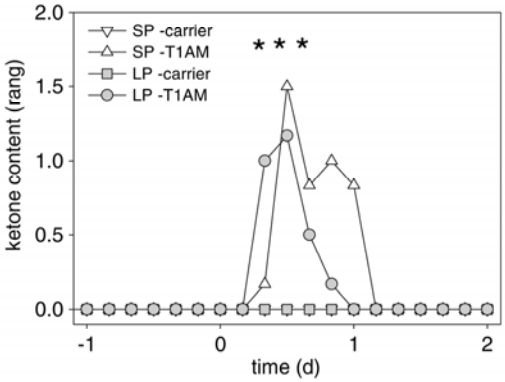

Fig. 7 Effects of T1AM, injected i.p. (day 0), on urine ketone content of SP (*white symbols*) and LP (*grey symbols*) hamsters in comparison to animals injected with carrier solution. T1AM leads to the development of ketonuria* as well in SP (*open triangle*) as in LP (*open circle*) hamsters. Control hamsters did not show ketonuria at any time. *$P < 0.05$ compared with values of day 0

Experiment 3: T1AM effects on body weight and body composition

One day after T1AM application body mass decreased significantly as compared to values before treatment and carrier injections. Body mass is lowered by about 1.3 g in SP hamsters and about 1.5 g in LP hamsters and then gradually increases again. This effect of T1AM on body mass is maintained for 4 days in LP and for 6 days SP hamsters (Two way RM ANOVA; $P = < 0.001$; Fig. 8). T1AM treated hamsters from LP and SP showed the same changes in body weight and body composition (Two Way ANOVA; $P > 0.05$) measured by DEXA analysis and therefore the results from both acclimation states were pooled (Fig. 9). T1AM caused a decrease in fat mass of 0.5 ± 0.1 g compared to carrier injections with 0.1 ± 0.1 g (Mann–Whitney Rank Sum Test; $P = 0.009$; Fig. 9) whereas the loss of lean mass is not significantly different within T1AM and carrier injected hamsters (Mann–Whitney Rank Sum Test; $P = 0.121$; Fig. 10). Hamsters showed a greater loss of body mass in carrier and T1AM injected animals within the DEXA analysis (Figs. 8, 9). The additional loss is due to the anaesthesia which is required for the DEXA measurement. Nevertheless the weight loss of 1.7 ± 0.3 g of T1AM treated animals is significantly higher than the loss of 0.6 ± 0.2 g in carrier injected hamsters (Mann–Whitney Rank Sum Test; $P = 0.011$; Fig. 9). Body weight loss also occurred in mice after T1AM injection. One day after T1AM treatment a significant loss of 2.0 ± 0.3 g (Paired *T*-Test; $P = <0.001$) was measured whereas the carrier treated mice showed no weight loss (Paired *T*-Test; $P = 0.813$).

Experiment 4: Detection of T1AM in hamster tissue

To determine that T1AM is present as a TH metabolite in *Phodopus sungorus*, crude biogenic amine brain and serum extracts were prepared. The extracts were analysed by liquid chromatography tandem mass spectrometry as described previously (Scanlan et al. 2004; Chiellini et al. 2007) using synthetic tetradeuterated T1AM (T1AM-d_4) as an internal standard (Miyakawa and Scanlan 2006). Figure 10 shows the chromatograms of serum and brain extracts from *control hamsters*. Significant T1AM levels were detected in all extracts, demonstrating that T1AM is an endogenous compound in *Phodopus sungorus*, as was shown previously for mouse, rat and guinea pig (Scanlan et al. 2004). Table 1 shows the T1AM levels in hamster serum 3 h after injection. In T1AM injected hamsters the blood levels are about tenfold above the T1AM levels in carrier injected controls. The hamsters acclimated to different photoperiods show similar levels of T1AM in carrier injected controls as well as in response to T1AM injection.

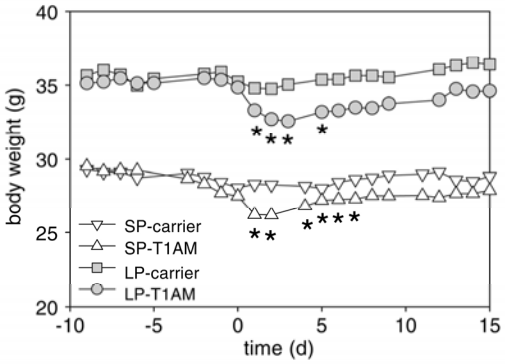

Fig. 8 Effects of T1AM, injected i.p. (day 0), on mean body weight of SP (*white symbols*) and LP (*grey symbols*) hamsters in comparison to animals injected with carrier solution. T1AM induced weight loss* as well in SP (*open triangle*) as in LP (*open cirlce*) hamsters. *$P < 0{,}05$ compared with values of day 0

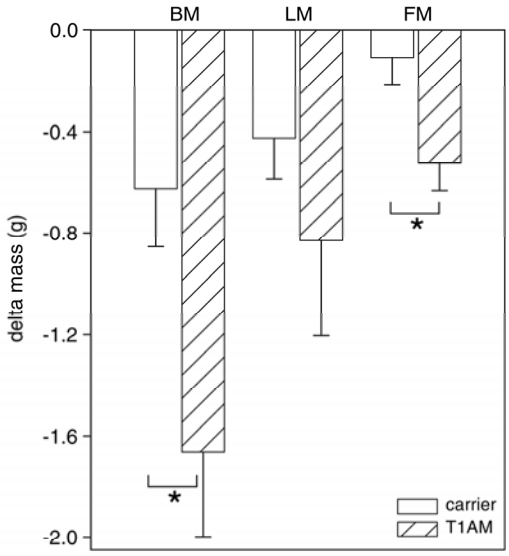

Fig. 9 Effects of T1AM on mean (±SE) body compositions one day after treatment in hamsters. The significant* loss of body mass (*BM*) due to T1AM injection results from a decrease in lean mass (*LM*) and fat mass (*FM*). Compared with carrier injection the decrease in fat mass* but not in lean mass is significant. *$P < 0{,}05$ compared with carrier injection

Discussion

T1AM induced hypometabolism and hypothermia in *Phodopus sungorus* and mice for several hours. In every animal it was accompanied by a reduction of RQ which implies a rapid change in metabolic fuel utilisation from predominantly carbohydrates (RQ∼0.9) before treatment to mainly lipids after treatment (RQ∼0.7). The assumption that predominantly lipids are used as primary fuel in response to

J Comp Physiol B (2008) 178:167–177

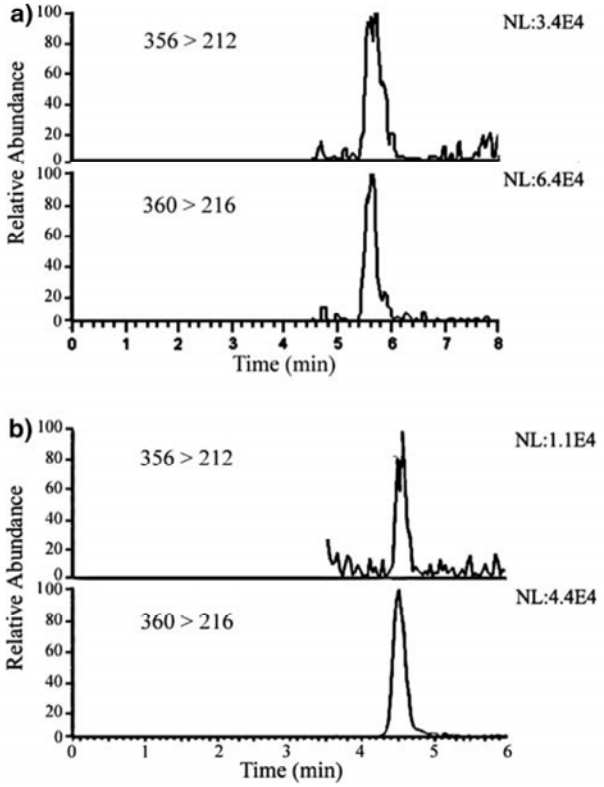

Fig. 10 T1AM (3-iodothyronamine) detected in hamster serum and brain extracts by LC-tandem mass spectrometry (*LC/MS*). Shown are hamster serum (**a**) and brain (**b**) extracts monitored for T1AM along with T1AM-d_4 internal standard. Upper extracted ion chromatograms demonstrate detection of T1AM (*m/z* 356 > 212). Lower chromatograms demonstrate detection of deuterated T1AM-d_4 (*m/z* 360 > 216) spiked into plasma or brain homogenate

Table 1 T1AM levels in Djungarian hamster serum 3 hours following T1AM or carrier injection

Injection	Photoperiod	T1AM (nM)	P
Carrier-IP (n = 5)	SP (LD 8:16)	5.86 ± 1.7069	
Carrier-IP (n = 4)	LP (LD 16:8)	5.95 ± 2.7912	* P = 0.003
T1AM-IP (n = 6)	SP (LD 8:16)	55.58 ± 10.9497	* P = 0.038
T1AM-IP (n = 6)	LP (LD 16:8)	58.90 ± 32.3368	

T1AM injection leads to a tenfold increase in T1AM serum levels compared to carrier injection. Acclimatization has no effect on T1AM levels

T1AM treatment was confirmed by the development of ketonuria 8 h post injection (Fig. 7). In contrast carrier injected animals showed neither a metabolic depression nor a reduction in RQ. Furthermore the significant loss of body fat mass (Fig. 9) indicates that body lipids are mobilized and utilized in response to T1AM. These results, the rapid decrease of the RQ from ~0.9 to ~0.7, the development of ketonuria together with the loss of body fat indicate that the utilisation of carbohydrates is suppressed in response to T1AM and energy requirements are largely covered by lipid utilisation, i.e. metabolic pathways are rerouted from carbohydrate to lipid metabolism.

Limitations of energy fuels, like lipoprivation and especially glucose deprivation, are considered to be important cues for torpor initiation. Injection with 2-deoxy-D-glucose (2-DG) for example, a nonmetabolizable glucose analogue that disrupts glycolysis (Wick et al. 1957), induces a hypothermic state in SP and LP acclimatized Siberian hamsters (Dark et al. 1994, 1996; Stamper et al. 1999). Methyl palmoxirate (MP), an inhibitor of fatty acid utilisation caused torpid responses in *Syrian hamsters*, whereas 2-DG did not (Schneider et al. 1993). Fatty acid deprivation via mercaptoacetate (MA) lead to hypothermia only in SP Siberian hamsters and the marsupial hibernator *Cercartetus nanus* (Stamper et al., 1999; Westman and Geiser, 2004) and in *Peromyscus* glucoprivation and lipoprivation resulting from 2-DG and MA treatments were inadequate to instigate torpor at all (Stamper and Dark 1997). These divergent responses of the different natural torpidators leave it questionable whether these artificial induced hypometabolic states are similar to natural spontaneous torpor.

The question remains whether T1AM can be considered as hormonal cue for torpor initiation, via its inhibitory effects on glucose metabolism. In response to T1AM the metabolic reduction occurs faster and the return to normometabolic conditions much slower than observed in a typical torpor bout. Furthermore the amplitude of metabolic reduction and the extend of hypothermia developed by T1AM treatment is much less pronounced as compared to torpid hamsters. Also the rapid and extremely long lasting reduction in RQ does not recapitulate the small changes in RQ during torpor (see Heldmaier et al. 1999). The metabolic depression via T1AM was more pronounced in mice as compared to hamsters (Figs. 2, 4) and the effect was greater in LP hamsters as compared to SP hamsters (Figs. 1, 4). This result differs from our initial expectation since SP acclimatized Djungarian hamsters can spontaneously enter torpor with a depressed metabolic rate and a profound hypothermia even when fed ad libitum, whereas mice require severe starvation for the induction of torpor. Therefore one would expect that Djungarian hamsters would show a greater response to T1AM as observed in mice. Also the greater response of LP acclimatized hamsters as compared to SP acclimatized hamsters contradicts their inclination for torpor. However we do not know at this time whether the tenfold changes in T1AM level in our study can be considered as physiological or pharmacological. Still our results suggest that although T1AM can cause

a significant depression of metabolic rate, by interfering with carbohydrate utilisation in both species, this is most likely not the major stimulus responsible for inducing spontaneous daily torpor.

The time course of the metabolic depression and hypothermia provoked by T1AM occur in parallel but the reduction in body temperature is slightly delayed relative to the reduction in metabolic rate (Fig. 1a, b). Figure 6 demonstrates that the amount of metabolic reduction and the extent of hypothermia are highly correlated, showing that the greater the metabolic depression due to T1AM treatment the more pronounced the hypothermia. The provoked hypothermia can therefore be considered as a result of reduced metabolic rate. The reduced RQ, and therefore the diminished carbohydrate metabolism, is maintained even after the recovery of metabolic rate and return to normothermia (Fig. 1). This indicates that T1AM treated hamsters required several hours to replace the lack of glucose utilisation and to readjust their metabolic machinery to the exclusive use of lipids for the coverage of their normal energy requirements.

Even though it appears that SP hamsters show a smaller response to T1AM as compared to LP hamsters it remains unclear whether this is related to the acclimatization state or whether this is a consequence of lowered body mass in SP hamsters (Fig. 5). The correlation between delta $\dot{V}O_2$ and body mass was also observed in mice, yet with a steeper slope and a lower *x*-axis intercept. In both species the regression curves extrapolate at zero delta $\dot{V}O_2$ to values typical for lean mass of these species with 20.35 g for mice and of 28.24 g for hamsters. The lean mass of C57BL/6 mice with a mean body weight of 28.23 g is 21.7 g (http://www.phenome.jax.org/phenome). For Phodopus sungorus with a mean body mass of 36.83 g lean mass was 29.3 g. This concludes that the amplitude of the metabolic effect of T1AM does not only depend on body mass, but rather on fat content or secondary factors correlating with body fat content.

In summary, our observations conclude that T1AM is an endogenous hormone that can depress metabolism via a rapid interruption of carbohydrate utilisation followed by a compensatory rise in lipid utilisation.

References

Chiellini G, Frascarelli S, Ghelardoni S, Carnicelli V, Tobias SC, DeBarber A, Brogioni S, Ronca-Testoni S, Cerbai E, Grandy DK, Scanlan TS, Zucchi R (2007) Cardiac effects of 3-iodothyronamine: a new aminergic system modulating cardiac function. FASEB J (in press)

Dark J, Miller DR, Zucker I (1994) Reduced glucose availability induces torpor in Siberian hamsters. Am J Physiol 267(2 Pt 2):R496–R501

Dark J, Lewis DA, Zucker I (1999) Hypoglycemia and torpor in Siberian hamsters. Am J Physiol 276(3 Pt 2):R776–R781

Dark J, Miller DR, Licht P, Zucker I (1996) Glucoprivation counteracts effects of testosterone on daily torpor in Siberian hamsters. Am J Physiol 270(2 Pt 2):R398–R403

Elvert R, Heldmaier G (2005) Cardiorespiratory and metabolic reactions during entrance into torpor in dormice, *Glis glis*. J Exp Biol 208(Pt 7):1373–1383

Figala J, Hoffmann K, Goldau G (1973) Zur Jahresperiodik beim Dsungarischen Zwerghamster *Phodopus sungorus* PALLAS. Oecologia (Berlin) 12:89–118

Gluck EF, Stephens N, Swoap SJ (2006) Peripheral ghrelin deepens torpor bouts in mice through the arcuate nucleus neuropeptide Y signaling pathway. Am J Physiol Regul Integr Comp Physiol 291(5):R1303–R1309

Grandy DK (2007) Trace amine-associated receptor 1-family archetype or iconoclast? J Pharmacol Ther (in press)

Heldmaier G (1975) Metabolic and thermoregulatory response to heat and cold in the Djungarian Hamster, *Phodopus sungorus*. J Comp Physiol 102:115–122

Heldmaier G, Ruf T (1992) Body temperature and metabolic rate during natural hypothermia in endotherms. J Comp Physiol [B] 162(8):696–706

Heldmaier G, Steinlechner S (1981) Seasonal pattern and energetics of short daily torpor in the Djungarian hamster *Phodopus sungorus*. Oecologia (Berl) 48:265–270

Heldmaier G, Steinlechner S, Ruf T, Wiesinger H, Klingenspor M (1989) Photoperiod and thermoregulation in vertebrates: body temperature rhythms and thermogenic acclimation. J Biol Rhythms 4(2):251–265

Heldmaier G, Klingenspor M, Werneyer M, Lampi BJ, Brooks SP, Storey KB (1999) Metabolic adjustments during daily torpor in the Djungarian hamster. Am J Physiol 276(5 Pt 1):E896–E906

Heldmaier G, Ortmann S, Elvert R (2004) Natural hypometabolism during hibernation and daily torpor in mammals. Respir Physiol Neurobiol 12:141(3):317–329

Hoffmann K (1981) Photoperiodism in vertebrates. In: Aschoff J (ed) Handbook of behavioral neurobiology, biological rhythms, vol 4. Plenum, New York, pp 449–473

Hudson JW, Scott IM (1979) Daily torpor in the laboratory mouse, *Mus musculus* var. albino. Physiol Zool 52:205–218

Miyakawa M, Scanlan TS (2006) Synthesis of [^{125}I]-, [^{2}H]-, and [^{3}H]-labeled 3-iodothyronamine (T_1AM). Synth Comm 36:891–902

Paul MJ, Freeman DA, Park JH, Dark J (2005) Neuropeptide Y induces torpor-like hypothermia in Siberian hamsters. Brain Res 7:1055(1–2):83–92

Ruf TP, Klingenspor M, Preis H, Heldmaier G (1991) Daily torpor in the Djungarian hamster (*Phodopus sungorus*): interactions with food intake, activity, and social behaviour. J Comp Physiol B 160:609–615

Ruf T, Stieglitz A, Steinlechner S, Blank JL, Heldmaier G (1993) Cold exposure and food restriction facilitate physiological responses to short photoperiod in Djungarian hamsters (*Phodopus sungorus*). J Exp Zool 1:267(2):104–112

Scanlan TS, Suchland KL, Hart ME, Chiellini G, Huang Y, Kruzich PJ, Frascarelli S, Crossley DA, Bunzow JR, Ronca-Testoni S, Lin ET, Hatton D, Zucchi R, Grandy DK (2004) 3-Iodothyronamine is an endogenous and rapid-acting derivative of thyroid hormone. Nat Med 10(6):638–642

Schneider JE, Friedenson DG, Hall AJ, Wade GN (1993) Glucoprivation induces anestrus and lipoprivation may induce hibernation in *Syrian hamsters*. Am J Physiol 264:R573–R577

Stamper JL, Dark J (1997) Metabolic fuel availability influences thermoregulation in deer mice (*Peromyscus maniculatus*). Physiol Behav 61(4):521–524

Stamper JL, Dark J, Zucker I (1999) Photoperiod modulates torpor and food intake in Siberian hamsters challenged with metabolic inhibitors. Physiol Behav 66(1):113–118

Stieglitz A, Spiegelhalter F, Klante G, Heldmaier G (1995) Urinary 6-sulphatoxymelatonin excretion reflects pineal melatonin secretion in the Djungarian hamster (*Phodopus sungorus*). J Pineal Res 18(2):69–76

Swoap SJ, Gutilla MJ, Liles LC, Smith RO, Weinshenker D (2006) The full expression of fasting-induced torpor requires beta 3-adrenergic receptor signaling. J Neurosci 4:26(1):241–245

Tannenbaum MG, Pivorun EB (1987) Differential effects of food restriction on the induction of daily torpor in *Peromyscus maniculatus* and *Peromyscus leucopus*. J Therm Biol 12:159–162

Wade GN, Bartness TJ (1984) Effects of photoperiod and gonadectomy on food intake, body weight and body composition in Siberian hamsters. Am J Physiol 246:R26–R30

Westman W, Geiser F (2004) The effect of metabolic fuel availability on thermoregulation and torpor in a marsupial hibernator. J Comp Physiol [B] 174(1):49–57

Wick AN, Drury DR, Nakada HI, Wolfe JB (1957) Localization of the primary metabolic block produced by 2-deoxyglucose. J Biol Chem 224(2):963–969

Zosky GR (2002) The parasympathetic nervous system: its role during torpor in the fat-tailed dunnart (*Sminthopsis crassicaudata*). J Comp Physiol [B] 172(8):677–684

Cryobiology 60 (2010) 198–203

Contents lists available at ScienceDirect

Cryobiology

journal homepage: www.elsevier.com/locate/ycryo

Torpor and ultradian rhythms require an intact signalling of the sympathetic nervous system ☆

Luzie J. Braulke *, Gerhard Heldmaier

Department of Biology, Philipps-University Marburg, Karl von Frisch Str. 8, 35032 Marburg, Germany

ARTICLE INFO

Article history:
Received 24 June 2009
Accepted 5 November 2009
Available online 12 November 2009

Keywords:
Phodopus sungorus
Torpor
Hypometabolism
Hypothermia
Ultradian rhythm
Sympathetic nervous system
Parasympathetic nervous system
6-Hydroxydopamine
Atropine

ABSTRACT

During entrance into torpor heart and respiration rates are greatly reduced in parallel with the reduction of metabolic rate, suggesting an involvement of parasympathetic control. We compared the effect of parasympathetic inhibition with the effect of sympathetic inhibition on spontaneous torpor behaviour in the Djungarian hamster. Hamsters were acclimated to short photoperiod and displayed their standard torpor pattern as observed from T_b records. Parasympathetic inhibition was achieved by a subcutaneous implant of 21-day release pellets with Atropine and the sympathetic noradrenergic pathway was inhibited with a single injection of 6-Hydroxydopamine. Atropine treatment did not affect the occurrence and quality of spontaneous daily torpor at all. However, the reversible sympathetic inhibition by 6-Hydroxydopamine injection resulted in a complete disappearance of torpor for about 6 days. These results conclude that the onset of daily torpor requires an intact noradrenergic signalling of the sympathetic nervous system. We further observed that parasympathetic as well as sympathetic blockade resulted in an immediate abolishment of ultradian rhythms of body temperature. This suggests that the expression of ultradian oscillations in body temperature require a continued interaction of sympathetic and parasympathetic activity.

Introduction

Shallow daily torpor and hibernation are characterized by a dramatic drop of metabolic rate (VO_2) and body temperature (T_b). The reduction in metabolic rate is accompanied by a reduction in heart rate (HR) and ventilation of similar extent [7,29,42]. The decline in HR and ventilation occurs prior to the decrease in body temperature, indicating that these vital functions are actively depressed prior to the development of hypothermia [7,27,40]. The depression in heart rate and ventilation, the maintenance of ventilatory tachycardia, as well as the occurrence of skipped beats and regular asystoles suggest a dominating parasympathetic influence during torpor entrance [24,26,29,36,41]. Once animals had started to enter torpor a vagal inhibition by the administration of Atropine abolishes typical skipped beats, asystoles and ventilatory tachycardia and elevates overall heart rate [24,39,42]. Similar results were achieved by vagotomy [27] and application of lidocaine hydrochloride [11].

These signs for a dominating parasympathetic activity are paralleled by signs for a downregulation of the peripheral sympathetic activity during torpor as has been shown by the reduction of plasma catecholamines and plasma dopamine-β-hydroxylase activity in prehibernating animals, such as *Citellus tridecemlineatus* and *Eliomys quercinus* [1,5]. In summary, these observations suggested that entrance into the torpid state is caused or controlled by a dominating influence of parasympathetic activity, whereas sympathetic influences are reduced. However, it has been shown recently that mutant mice lacking dopamine-β-hydroxylase do not become torpid following fasting and cold exposure, and this ability could be restored by the injection of β3-adrenergic agents [37,38].

Short day (SP) acclimated Djungarian hamster do not need any load of their energy balance for the induction of torpor but show spontaneous daily torpor when fed ad libitum even at thermoneutrality [14,17]. Therefore we attempted to analyse the effect of vagal or sympathetic blockade on the spontaneous torpor behaviour in Djungarian hamsters. Vagal inhibition was produced by s.c. implants delivering Atropine for 21 days. Sympathetic blockade was produced by chemical sympathectomy with 6-Hydroxydopamine (6-OHDA). 6-OHDA is an isomer of norepinephrine, which acts as a false neurotransmitter and reversibly destroys catecholaminergic neurons with a high degree of selectivity [22].

Animals, material and methods

Animals

Djungarian hamsters (*Phodopus sungorus*) were bred and raised at Marburg University under long photoperiod conditions (LP; LD

☆ This project was supported by the Deutsche Forschungsgemeinschaft (DFG).
* Corresponding author.
E-mail address: braulkel@staff.uni-marburg.de (L.J. Braulke).

0011-2240/$ - see front matter © 2009 Elsevier Inc. All rights reserved.
doi:10.1016/j.cryobiol.2009.11.001

16:8; light on: 0400 h, light off: 2000 h) and a constant ambient temperature (T_a) of 24 ± 1 °C. Hamsters were housed individually in makrolon-cages type II (16 cm × 21 cm × 13 cm) with wood shavings and were constantly supplied with water and food (ALTROMIN 7014) ad libitum. At the age of three months hamsters were transferred into short photoperiod conditions (SP; LD 8:16; light on: 0800 h, light off: 1600 h) and a constant T_a of 15 ± 1 °C to induce winter-acclimatization.

Telemetric recording of T_b

For the measurement of torpor behaviour body temperature (T_b) of the animals was recorded continuously. Hamsters were implanted intraperitoneally with calibrated temperature transmitters (Minimitter, Model X, Sunriver, OR, USA, accuracy 0.1 °C) under ketamine hydrochloride anaesthesia (Ketavet, Pharmacia Upjohn GmbH, Erlangen, Germany, 50 mg kg^{-1}) and 1–2% Isoflurane (Forene, Abbott, Wiesbaden, Germany). The detection of the transmitter signals was accomplished by a radio receiver and processed by a microcomputer system [15]. T_b records were started after 8 weeks in SP and drug treatments were applied after 14 weeks in SP. To determine torpor duration per day the time spent at body temperatures below 32 °C was calculated, averaged for each group and expressed in minutes per day. Ultradian rhythm was analysed by autocorrelation, Chi-square periodogram analysis and sine wave fitting.

Inhibition of the parasympathetic nervous system

Atropine (Sigma (Fluka), Deisenhofen, Germany) was administered via implantation of a 21-day release pellet (Innovative Research of America, Sarasota, FL) which contains a biodegradable matrix that continuously releases the active product. Pellets containing Atropine- (0.25 mg) or Placebo-pellets containing the vehicle were injected subcutaneously on the lateral side of the neck with a 10-gauge trochar (Innovative Research of America). The pellet dose of 0.25 mg reflects the total amount of net active product released over the indicated period of time which corresponds to ca. 0.48 mg/kg per day. After application hamsters were returned to their cages and body temperature recording was continued (Atropine, $n = 6$; Placebo, $n = 6$).

Inhibition of the sympathetic nervous system

6-Hydroxydopamine (6-OHDA; Sigma (Fluka), Deisenhofen, Germany) was administered once by intraperitoneal injection. 6-OHDA (200 mg/kg) was dissolved in 0.9% physiological saline

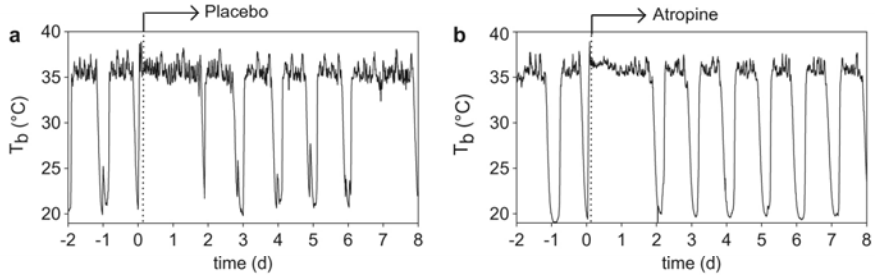

Fig. 1. Trajectory of body temperature (T_b) 2 days before and 8 days after implantation (dashed line) of Placebo- (a) or Atropine-pellet (b) of *Phodopus sungorus*. Beside the day of implantation Atropine did not have any influence on torpor occurrence.

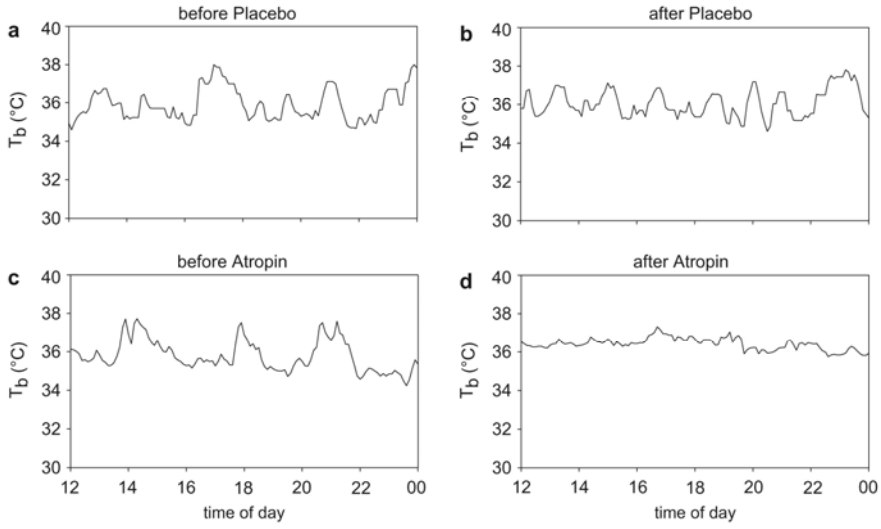

Fig. 2. Twelve-hour trajectory of body temperature (T_b) 2 days before (a and c) and directly after implantation of Placebo- (b) or Atropine-pellet (d). Compared to T_b before treatment or control treatment, Atropine reduced typical ultradian rhythm of T_b of *Phodopus sungorus*.

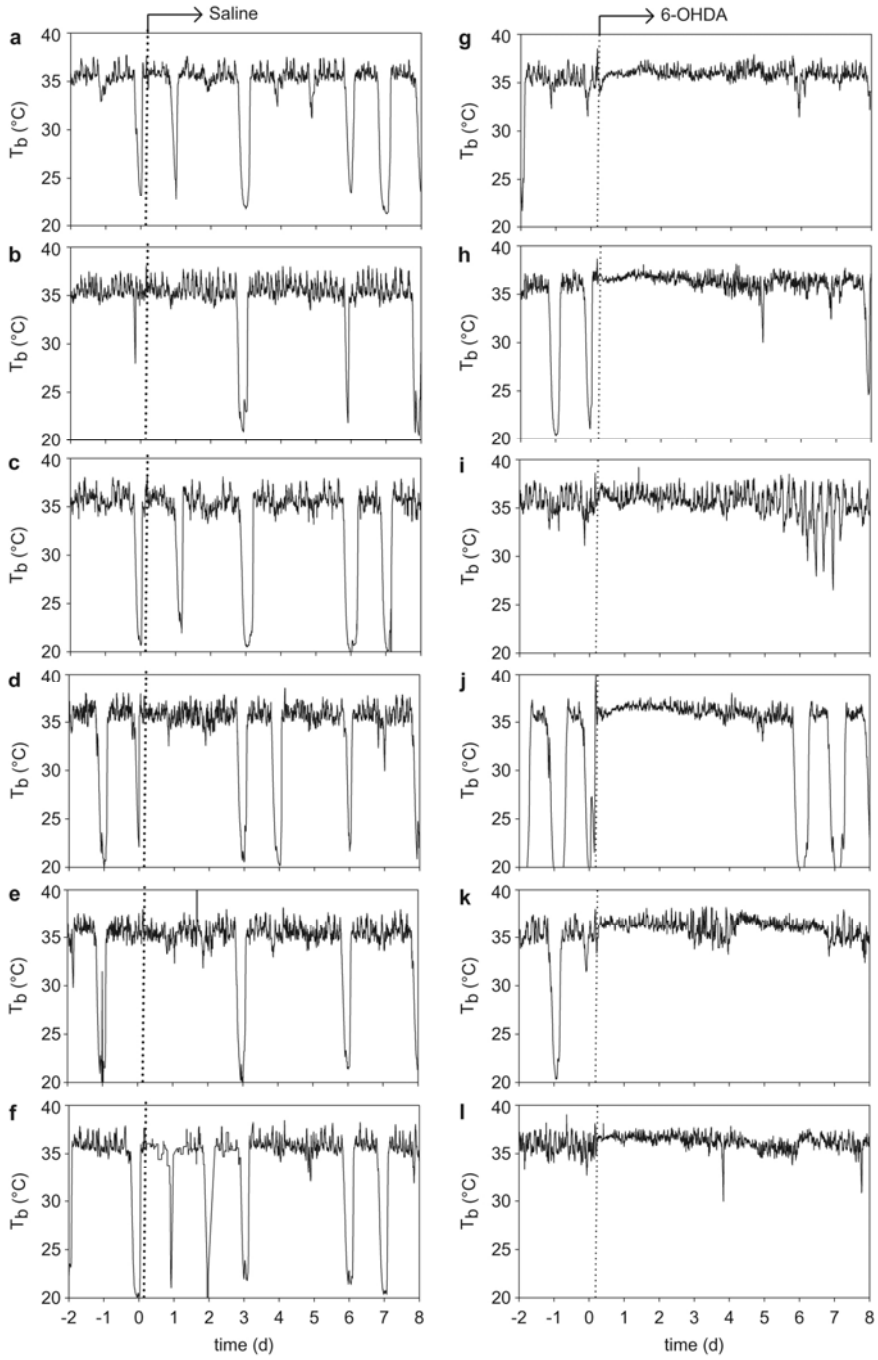

Fig. 3. Trajectory of individual body temperature (T_b) 2 days before and 8 days after injection (dotted line) of saline (a–f) or 6-OHDA (g–l). In contrast to control treatment torpor occurrence was abolished for at least 4 days in response to 6-OHDA injection.

(pH 7.4) and applied in a final volume of 100 µl. Physiological saline (0.9% saline, pH 7.4, 100 µl) was used as control injection. After application hamsters were returned to their cages and body temperature recording was continued (6-OHDA, $n = 6$; saline, $n = 6$).

A third control group was left untreated and received neither i.p. injections nor s.c. implants (untreated, $n = 6$).

All experiments were done in accordance with approved guidelines for the use and care of animals by the German animal welfare law (Deutsches Tierschutzgesetz).

Results

Untreated hamsters displayed their normal torpor pattern with a torpor bout occurring every second or third day (on average 1.62 times per 3 days). Minimal body temperatures during torpor ranged from 18 to 29 °C and torpor duration from 30 to 672 min per bout. During normothermia hamsters showed an ultradian rhythm of body temperature with a period length of 2.88 ± 0.25 h. This ultradian rhythm was not visible in the torpid state.

Inhibition of the parasympathetic nervous system

Fig. 1 shows the time course of body temperature of two individual hamsters for 10 days, 2 days before and 8 days after implantation of Placebo- or Atropine-pellet. Both, Placebo and Atropine implanted hamsters continued to display their normal pattern of torpor behaviour except for the first day following the implantation, where torpor was omitted in both groups. However parasympathetic inhibition disturbed ultradian rhythm of body temperature (Fig. 2). Prior to Atropine treatment hamsters showed an ultradian rhythm of body temperature with an average period length of 2.80 ± 0.45 h. In five out of six hamsters their ultradian oscillations of body temperature were immediately abolished in response to Atropine treatment. In one hamster this effect was delayed for about 9 h. In all Atropine treated hamsters the ultradian rhythm was restored to its former condition within about 24 h. Placebo-pellets had no effect on ultradian rhythm of body temperature (Fig. 2).

Inhibition of the sympathetic nervous system

Chemical sympathectomy with 6-OHDA immediately suppressed the occurrence of torpor about a week (Fig. 3g–l). The complete suppression of torpor by 6-OHDA is also seen in mean values of torpor duration (Fig. 4). Before treatments the hamsters entered torpor for 309.5 ± 18.4 min. After administration of the 6-OHDA the torpor duration dropped to zero. On average hamsters returned to their normal torpor pattern 7.2 ± 0.97 days after the injection of 6-OHDA. A few individuals regained this ability in a transient manner by slowly enhancing depth and duration of individual torpor bouts (Figs. 3 and 4).

Neither the Atropine treated group nor the both control groups showed significant alterations in torpor behaviour and therefore values of torpor duration of these animals do not differ from those of the untreated hamsters (Fig. 4).

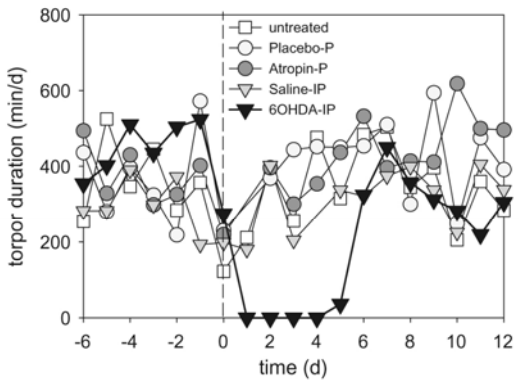

Fig. 4. Comparison of torpor behaviour (torpor duration) of *Phodopus sungorus* untreated ($n = 6$) or after treatment with either saline IP ($n = 6$), 6-OHDA IP ($n = 6$), s.c. Placebo-pellet ($n = 6$), s.c. Atropine-pellet ($n = 6$).

The inhibition of the sympathetic activity by 6-OHDA also disturbed the ultradian rhythm of body temperature (Fig. 5). Untreated hamsters showed an ultradian rhythm of body temperature with an average period length of 2.97 ± 0.24 h. In response to 6-OHDA injection these oscillations were immediately abolished in all treated animals, comparable to the response to vagal blockade (see Fig. 2). Reestablishment of ultradian rhythm was achieved within 2–6 days.

Discussion

After blockade of the sympathetic nervous system by 6-OHDA the display of torpor was eliminated for about a week, implying that the expression of spontaneous daily torpor is dependant on intact sympathetic signalling. Blockade of sympathetic nervous system is based on a destruction of terminal sympathetic vesicles. This destruction is reversible and the sympathetic varicosities restore their norepinephrine content within days or weeks. The duration of this recovery process is highly variable and depends upon the initial dosage, and may differ between different organs and species, e.g. after injection of 100 mg/kg 6-OHDA in mice 25% recovery of norepinephrine content of the heart was observed after 7 days [21]. After injection of 170 mg/kg 6-OHDA in rat 25% restoration was detected within 24 h [3]. We could not analyse the constitution of the sympathetic varicosities because we continued to observe the behaviour of the hamsters. However, the duration of torpor inhibition for about a week in response to 6-OHDA was within the time frame of sympathetic recovery observed in other species [22].

A direct link between torpor behaviour and sympathetic signalling is supported by findings of Swoap et al. [37,38]. They demonstrated that dopamine-hydroxylase knock-out ($Dbh^{-/-}$) mice, which lack the ability to produce the sympathetic transmitters, norepinephrine (NE) and epinephrine, are not able to display fasting induced torpor. This disability for torpor in these knock-out mice can be reversed by administration of β3-adrenergic receptor specific agonist CL 316243.

Inhibition of the parasympathetic nervous system by Atropine did not prevent the display of torpor in winter acclimatized Djungarian hamsters. Following Atropine treatment all animals continued to undergo torpor in the same frequency as observed before treatment and also torpor quality was not altered by vagal blockade, since torpor duration and depth were not influenced by this treatment. Former observations suggested dominating parasympathetic activity during torpor. During torpor entrance heart rate and ventilation are largely depressed, ventilatory tachycardia is maintained and skipped beats and regular asystoles occur and this can be reversed by vagal blockade [24,26,27,29,37,39,42]. Nevertheless, even though vagal actions are involved in the transient period of entrance into torpor an inhibition of vagal signalling by Atropine had no effect on torpor behaviour.

Previous studies have shown that sympathetic activity is predominant during arousal from torpor, inducing the increase of overall heart rate and breathing frequency [7,25,29]. Furthermore regional heterothermy was shown in hamsters arousing from hibernation. The thoracic and head regions warm faster than the abdominal and hind limb regions and this is controlled by a sympathetic adrenergic regulation of blood flow and volume [32]. Also the increased lipid utilization for the energetically expensive arousal from torpor [4,14] demonstrates an increased involvement of the sympathetic signalling during arousal, since lipolysis by adipocytes is triggered primarily by norepinephrine release from sympathetic nerve terminals. During the arousal process about 50% of heat is generated by non shivering thermogenesis largely originating from BAT [8,12,13,19,20,23]. This process is mediated via the

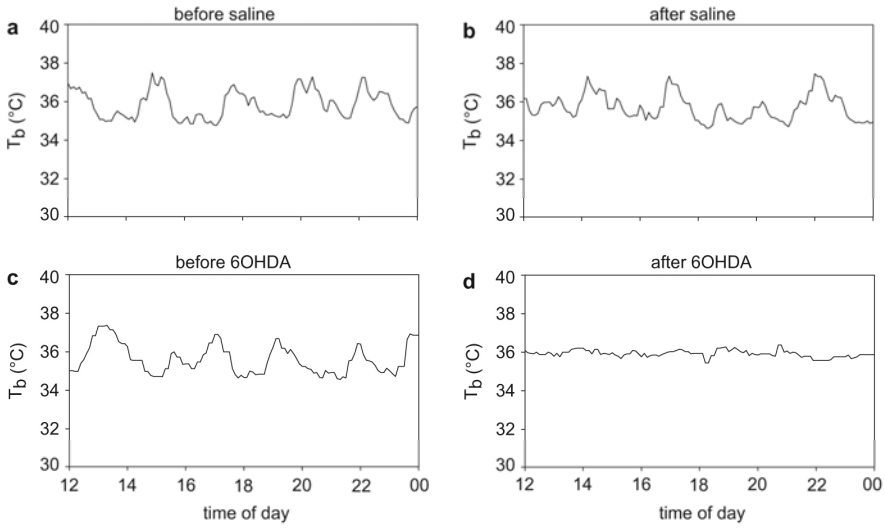

Fig. 5. Twelve-hour trajectory of body temperature (T_b) 2 days before (a and c) and directly after injection of saline (b) or 6-OHDA (d). Compared to T_b before treatment or control treatment, 6-OHDA reduced typical ultradian rhythm of T_b of *Phodopus sungorus*.

adrenergic activation of the brown adipocytes [10,13,34] and shows that sympathetic activation is essential for arousal from a torpid state.

Recent findings in dormice have shown that prior to the entrance into hibernation there is a peak in metabolic rate, ventilation and heart rate for about 30 min and this stage is terminated by a sudden decrease in MR and other physiological functions [7]. Literature data from other species, such as from the Gould's long-eared bat, the eastern pygmy possum, the golden-mantled ground squirrel and the alpine marmot, frequently show similar peaks of metabolic rate anticipating the entrance into torpor [16,30,31,35]. This high metabolic rate, heart rate and ventilation indicate high sympathetic activity prior to the entrance into the torpid state. We suggest that sympathetic blockade by 6-OHDA prevented this preparatory surge of metabolic activities and may be the reason why torpor was suppressed.

Given that 6-OHDA is unable to cross the blood–brain barrier [2] we may conclude that the loss of torpor occurrence is caused by the degeneration of *peripheral* sympathetic nerve terminals.

In this study, we furthermore observed an immediate abolishment of ultradian rhythm of body temperature in all animals after treatment with either Atropine or 6-OHDA. This finding concludes a major involvement of both, cholinergic as well as adrenergic signalling, in the regulation of ultradian oscillation of T_b. Interestingly the inhibitory effect of Atropine on ultradian rhythm of body temperature is much shorter than the release time of Atropine from the pellet, suggesting that the primary control of ultradian rhythm by parasympathetic tone can be compensated for by other, secondary mechanisms. The latter may also be suggested for the inhibitory effect of 6-OHDA on ultradian rhythms, because they were restored within about 2 days following injection of 6-OHDA whereas the inhibition of torpor behaviour continued for about a week. Ultradian rhythms of activity are a common feature of the circadian behaviour in small mammals [9,33]. The ultradian rhythm in locomotor activity is usually accompanied by ultradian variations of body temperature and metabolic rate as described in many species, such as rats, Djungarian hamsters and sheep, [6,18,28]. However, nothing is known about the generation of these ultradian oscillations. Our data clearly suggest that the autonomous nervous system is required for the expression of ultradian rhythmicity.

References

[1] C. Atgie, M. Nibbelink, L. Ambid, Sympathoadrenal activity and hypoglycemia in the hibernating garden dormouse, Physiol. Behav. 48 (6) (1990) 783–787.
[2] D. Blum, S. Torch, N. Lambeng, M. Nissou, A.L. Benabid, R. Sadoul, J.M. Verna, Molecular pathways involved in the neurotoxicity of 6-OHDA, dopamine and MPTP: contribution to the apoptotic theory in Parkinson's disease, Prog. Neurobiol. 65 (2) (2001) 135–172.
[3] R. Brus, M.E. Hess, D. Jacobowitz, Effect of 6-hydroxydopamine and thyroxine on chronotropic response to norepinephrine, Eur. J. Pharmacol. 10 (3) (1970) 323–327.
[4] B. Cannon, J. Nedergaard, Brown adipose tissue: function and physiological significance, Physiol. Rev. 84 (1) (2004) 277–359.
[5] P.R. Draskóczy, C.P. Lyman, Turnover of catecholamines in active and hibernating ground squirrels, J. Pharmacol. Exp. Ther. 155 (1) (1967) 101–111.
[6] C. Eastman, A. Rechtschaffen, Circadian temperature and wake rhythms of rats exposed to prolonged continuous illumination, Physiol. Behav. 31 (4) (1983) 417–427.
[7] R. Elvert, G. Heldmaier, Cardiorespiratory and metabolic reactions during entrance into torpor in dormice, *Glis glis*, J. Exp. Biol. 208 (Pt. 7) (2005) 1373–1383.
[8] F. Génin, M. Nibbelink, M. Galand, M. Perret, L. Ambid, Brown fat and nonshivering thermogenesis in the gray mouse lemur (*Microcebus murinus*), Am. J. Physiol. Regul. Integr. Comp. Physiol. 284 (3) (2002) 811–818.
[9] M.P. Gerkema, S. Daan, Ultradian rhythms in behaviour: the case of the common vole (*Microtus arvalis*), in: H. Schulz, P. Lavie (Eds.), Ultradian Rhythms in Physiology and Behavior, Springer Verlag, Berlin, 1985, pp. 11–31.
[10] L. Girardier, J. Seydoux, Le contrôle de la thermogenèse du tissu adipeux brun, J. Physiol. (Paris) 63 (21) (1971) 147–186.
[11] B.H. Harris, W.K. Milsom, Parasympathetic influence on heart rate in euthermic and hibernating ground squirrels, J. Exp. Biol. 198 (1995) 931–937.
[12] J.S. Hayward, C.P. Lyman, Non-shivering heat production during arousal from hibernation and evidence for the contribution of brown fat, in: K.C. Fisher (Ed.), Proc. III. International Symposium on Natural Mammalian Hibernation, Oliver and Boyd, Edinburgh, 1967, pp. 346–355.
[13] G. Heldmaier, Die Thermogenese der Mausohrfledermaus (*Myotis myotis*) beim Erwachen aus dem Winterschlaf, J. Comp. Physiol. 63 (1969) 59–84.
[14] G. Heldmaier, M. Klingenspor, M. Werneyer, B.J. Lampi, S.P. Brooks, K.B. Storey, Metabolic adjustments during daily torpor in the Djungarian hamster, Am. J. Physiol. 276 (5 Pt. 1) (1999) 896–906.
[15] G. Heldmaier, T. Ruf, Body temperature and metabolic rate during natural hypothermia in endotherms, J. Comp. Physiol. B 162 (8) (1992) 696–706.
[16] G. Heldmaier, R. Steiger, T. Ruf, Suppression of metabolic rate in hibernation, in: C. Carey, G. Florant, B.A. Wunder, B. Horwitz (Eds.), Life in the Cold, Ecological, Physiological and Molecular Mechanisms, Westview Press, Colorado, Oxford, 1993, pp. 545–548.
[17] G. Heldmaier, S. Steinlechner, Seasonal pattern and energetics of short daily torpor in the Djungarian hamster, *Phodopus sungorus*, Oecologia 48 (1981) 265–270.
[18] G. Heldmaier, S. Steinlechner, T. Ruf, H. Wiesinger, M. Klingenspor, Photoperiod and thermoregulation in vertebrates: body temperature rhythms and thermogenic acclimation, J. Biol. Rhythms 4 (2) (1989) 251–265.

[19] B.A. Horwitz, R.E. Smith, E.T. Pengelly, Estimated heat contribution of brown fat in arousing ground squirrels (*Citellus lateralis*), Am. J. Physiol. 214 (1968) 115–121.
[20] L. Janský, I. Hájek, Thermogenesis of the bat *Myotis myotis* Borkh, Physiol. bohemoslov. 10 (1961) 283–289.
[21] G. Jonsson, C. Sachs, Effects of 6-hydroxydopamine on the uptake and storage of noradrenaline in sympathetic adrenergic neurons, Eur. J. Pharmacol. 9 (2) (1970) 141–155.
[22] R.M. Kostrzewa, D.M. Jacobowitz, Pharmacological actions of 6-hydroxydopamine, Pharmacol. Rev. 26 (3) (1974) 199–288.
[23] C.P. Lyman, P.O. Chatfield, Mechanisms of arousal in the hibernating hamsters, J. Exp. Zool. 14 (1950) 491–512.
[24] C.P. Lyman, R.C. O'Brien, Autonomic control of circulation during the hibernating cycle in ground squirrels, J. Physiol. 168 (1963) 477–499.
[25] A. Mertens, O. Stiedl, S. Steinlechner, M. Meyer, Cardiac dynamics during daily torpor in the Djungarian hamster (*Phodopus sungorus*), Am. J. Physiol. Regul. Integr. Comp. Physiol. 294 (2) (2008) 639–650.
[26] W.K. Milsom, M.B. Zimmer, M.B. Harris, Regulation of cardiac rhythm in hibernating mammals, Comp. Biochem. Physiol. A Mol. Integr. Physiol. 124 (4) (1999) 383–391.
[27] W.K. Milsom, R.F. Burlington, M.L. Burleson, Vagal influence on heart rate in hibernating ground squirrels, J. Exp. Biol. 185 (1993) 25–32.
[28] E. Mohr, H. Krzywanek, Variations of core-temperature rhythms in unrestrained sheep, Physiol. Behav. 48 (3) (1990) 467–473.
[29] J.E. Morhardt, Heart rates, breathing rates and the effect of atropine and acetycholine on white-footed mice (*Peromyscus* sp.) during daily torpor, Comp. Biochem. Physiol. 33 (1970) 441–457.
[30] S. Morris, A.L. Curtin, M.B. Thompson, Heterothermy, torpor, respiratory gas exchange, water balance and the effect of feeding in Gould's long-eared bat *Nyctophilus gould*, J. Exp. Biol. 197 (1994) 309–335.
[31] S. Ortmann, G. Heldmaier, Regulation of body temperature and energy requirements of hibernating alpine marmots (*Marmota marmota*), Am. J. Physiol. Regul. Integr. Comp. Physiol. 278 (3) (2000) 698–704.
[32] P.G. Osborne, J. Sato, N. Shuke, M. Hashimoto, Sympathetic alpha-adrenergic regulation of blood flow and volume in hamsters arousing from hibernation, Am. J. Physiol. Regul. Integr. Comp. Physiol. 289 (2) (2005) 554–562.
[33] R. Refinetti, M. Menaker, The circadian rhythm of body temperature, Physiol. Behav. 51 (3) (1992) 613–637.
[34] H. Sell, Y. Deshaies, D. Richard, The brown adipocyte: update on its metabolic role, Int. J. Biochem. Cell Biol. 36 (11) (2004) 2098–2104.
[35] X. Song, G. Körtner, F. Geiser, Thermal relations of metabolic rate reduction in a hibernating marsupial, Am. J. Physiol. 273 (6 Pt. 2) (1997) 2097–2104.
[36] F. Strumwasser, Some physiological principles governing hibernation in *Citellus beecheyi*, Bull. Mus. Comp. Zool. 124 (1960) 285–320.
[37] S.J. Swoap, M.J. Gutilla, L.C. Liles, R.O. Smith, D. Weinshenker, The full expression of fasting-induced torpor requires beta 3-adrenergic receptor signalling, J. Neurosci. 26 (1) (2006) 241–245.
[38] S.J. Swoap, D. Weinshenker, Norepinephrine controls both torpor initiation and emergence via distinct mechanisms in the mouse, PLoS One 3 (12) (2008) e4038.
[39] J.W. Twente, J.A. Twente, Autonomic regulation of hibernation by *Citellus* and *Eptesicus*, in: L.C.H. Wang, J.W. Hudson (Eds.), Strategy in the Cold, Natural Torpor and Thermogenesis, Academic Press, New York, 1978, pp. 327–337.
[40] L.C.H. Wang, J.W. Hudson, Temperature regulation in normothermic and hibernating eastern chipmunks, *Tamias striatus*, Comp. Biochem. Physiol. A 38 (1971) 59–90.
[41] M.B. Zimmer, M.B. Harris, W.K. Milsom, Control of cardiac and ventilation frequencies during hibernation in ground squirrels, in: G. Heldmaier, M. Klingenspor (Eds.), Life in the Cold, Eleventh International Hibernation Symposium, Springer, Berlin, Heidelberg, New York, 2000, pp. 159–167.
[42] G.R. Zosky, The parasympathetic nervous system: its role during torpor in the fat-tailed dunnart (*Sminthopsis crassicaudata*), J. Comp. Physiol. B 172 (8) (2002) 677–684.

Cell Metabolism
Article

CB_1 Signaling in Forebrain and Sympathetic Neurons Is a Key Determinant of Endocannabinoid Actions on Energy Balance

Carmelo Quarta,[1,18] Luigi Bellocchio,[2,3,18] Giacomo Mancini,[4,18] Roberta Mazza,[1] Cristina Cervino,[1] Luzie J. Braulke,[6] Csaba Fekete,[7,8] Rocco Latorre,[9] Cristina Nanni,[10] Marco Bucci,[1,11] Laura E. Clemens,[6] Gerhard Heldmaier,[6] Masahiko Watanabe,[12] Thierry Leste-Lassere,[2,3] Marlène Maitre,[2,3] Laura Tedesco,[13,14] Flaminia Fanelli,[1] Stefan Reuss,[5] Susanne Klaus,[15] Raj Kamal Srivastava,[4] Krisztina Monory,[4] Alessandra Valerio,[13,16] Annamaria Grandis,[17] Roberto De Giorgio,[9] Renato Pasquali,[1] Enzo Nisoli,[13,14] Daniela Cota,[2,3] Beat Lutz,[4] Giovanni Marsicano,[2,3] and Uberto Pagotto[1,*]

[1]Endocrinology Unit and Centro di Ricerca Biomedica Applicata, Department of Clinical Medicine, University of Bologna, Bologna 40138, Italy
[2]INSERM U862 Neurocentre Magendie, Bordeaux 33077, France
[3]Université Bordeaux, Bordeaux 33077, France
[4]Institute of Physiological Chemistry
[5]Institute of Anatomy and Cell Biology
University Medical Center of the Johannes Gutenberg University Mainz, Mainz 55099, Germany
[6]Department of Biology Animal Physiology, Philipps University Marburg, Marburg 35032, Germany
[7]Department of Endocrine Neurobiology, Institute of Experimental Medicine, Hungarian Academy of Sciences, Budapest 1083, Hungary
[8]Division of Endocrinology, Diabetes, and Metabolism, Tupper Research Institute and Department of Medicine, Tufts Medical Center, Boston, MA 02111, USA
[9]Department of Clinical Medicine and Centro di Ricerca Biomedica Applicata
[10]Department of Nuclear Medicine, S. Orsola-Malpighi Hospital
University of Bologna, Bologna 40138, Italy
[11]Turku PET Centre, University of Turku, 20521 Turku, Finland
[12]Department of Anatomy, Hokkaido University School of Medicine, Sapporo 060-8638, Japan
[13]Integrated Laboratories Network, Center for Study and Research on Obesity, Department of Pharmacology, Chemotherapy, and Medical Toxicology, Università degli Studi di Milano, Milano 20129, Italy
[14]Istituto Auxologico Italiano, Milano 20145, Italy
[15]Department of Pharmacology, German Institute of Human Nutrition Potsdam-Rehbruecke, Nuthetal 14558, Germany
[16]Department of Biomedical Sciences and Biotechnologies, University of Brescia, Brescia 25123, Italy
[17]Department of Veterinary Morphophysiology and Animal Productions, University of Bologna, 40064 Ozzano dell'Emilia, Bologna 40138, Italy
[18]These authors contributed equally to this work
*Correspondence: uberto.pagotto@unibo.it
DOI 10.1016/j.cmet.2010.02.015

SUMMARY

The endocannabinoid system (ECS) plays a critical role in obesity development. The pharmacological blockade of cannabinoid receptor type 1 (CB_1) has been shown to reduce body weight and to alleviate obesity-related metabolic disorders. An unsolved question is at which anatomical level CB_1 modulates energy balance and the mechanisms involved in its action. Here, we demonstrate that CB_1 receptors expressed in forebrain and sympathetic neurons play a key role in the pathophysiological development of diet-induced obesity. Conditional mutant mice lacking CB_1 expression in neurons known to control energy balance, but not in nonneuronal peripheral organs, displayed a lean phenotype and resistance to diet-induced obesity. This phenotype results from an increase in lipid oxidation and thermogenesis as a consequence of an enhanced sympathetic tone and a decrease in energy absorption. In conclusion, CB_1 signaling in the forebrain and sympathetic neurons is a key determinant of the ECS control of energy balance.

INTRODUCTION

The endocannabinoid system (ECS) has emerged as a key player in both central and peripheral functions related to energy metabolism (Pagotto et al., 2006; Kunos et al., 2008). Initial studies based on the evidence that the cannabinoid receptor type 1 (CB_1) was exclusively present in the brain all attributed the ability of the ECS to modulate food intake to a central site of action (Pagotto et al., 2006). However, new evidence has accumulated, which suggests that the ECS might regulate energy balance not exclusively at central sites. In fact, CB_1 receptors and their ligands were also found in several peripheral organs (Pagotto et al., 2006; Kunos et al., 2008). Consequently, it has emerged that CB_1 might control body weight by food intake-independent mechanisms. Complete deletion of CB_1 in mice (CB_1-KO) led to decreased fat mass, reduced body weight, and resistance to develop obesity (Cota et al., 2003; Ravinet Trillou et al., 2004). In addition, beneficial food intake-independent effects on metabolism were demonstrated by using CB_1 antagonists

Cell Metabolism
CB_1 Receptors and Energy Metabolism

(Ravinet Trillou et al., 2004). Recent studies suggested that the sustained body weight loss induced by CB_1 antagonists after the initial decrease in food intake might be explained by an effect of the drugs on energy expenditure. Blockade of CB_1 in obese animals induces an array of pharmacological effects, including stimulation of lipolysis and fatty acid oxidation (Herling et al., 2008). However, the anatomical location of the CB_1 receptors involved in these functions is still under discussion (Kunos et al., 2009). This is an important point because rimonabant, the first CB_1 antagonist used for the treatment of obesity, has been recently withdrawn from the market due to psychiatric side effects (Akbas et al., 2009). The generation of CB_1 antagonists selectively acting at peripheral organs could be a promising way to preserve the metabolic effects of CB_1 blockade without causing side effects due to CB_1 inhibition in neural circuits regulating mood and anxiety (McElroy et al., 2008; LoVerme et al., 2009). Nevertheless, the identification of the anatomical site(s) where the ECS exerts its effects on energy balance and metabolism is mandatory before further screening for potentially more selective and safer drugs. Thus, in order to single out the major anatomical sites underlying the ECS-dependent regulation of energy balance and metabolism, we studied conditional mutant mice (CaMK-*CB$_1$*-KO mice) characterized by a CB_1 deletion in forebrain neurons (Marsicano et al., 2003) and compared their phenotype to that of conventional *CB$_1$*-KO (Marsicano et al., 2002) and of mice treated with the CB_1 antagonist rimonabant.

RESULTS

Anatomical Characterization of CB_1 Expression in CaMK-*CB$_1$*-KO Mice

CaMK-*CB$_1$*-KO conditional mutant mice were obtained using the Cre/loxP system by crossing *CB$_1$*$^{flox/flox}$ mutants with CaMKIIα-iCre transgenic mice (Casanova et al., 2001; Marsicano et al., 2003). CaMKIIα-iCre mice express the recombinase in the great majority of adult forebrain neurons, with the exclusion of cortical GABAergic interneurons (Casanova et al., 2001). Importantly, brain regions known to control energy balance (e.g., the hypothalamus) do express the Cre recombinase in these mutant mice (Casanova et al., 2001).

As expected, the abundant expression of CB_1 mRNA in intrinsic neurons of the hypothalamus (Cota et al., 2003) (Figures 1A and 1B) was absent in CaMK-*CB$_1$*-KO mice (Figures 1A and 1B). In the hypothalamus, CB_1 protein was found mainly on axon terminals of both extrinsic and intrinsic neurons (Wittmann et al., 2007). Immunohistochemistry (IHC) revealed that the intensely CB_1-positive meshwork in the hypothalamus of CaMK-*CB$_1$*-WT was virtually absent in CaMK-*CB$_1$*-KO mice (Figures 1A and 1B).

The nucleus of the solitary tract (NTS) is one of the main funneling sites of energy balance regulation (Grill and Hayes, 2009). It receives inputs from both higher brain regions (as hypothalamus and cerebral cortex) and vagal ganglions (i.e., nodose ganglion) and regulates output efferents that control the functions of several peripheral organs modulating energy metabolism (Grill and Hayes, 2009). Similar to the hypothalamus, CB_1 receptors are present in both afferent and efferent neurons of the NTS (Tsou et al., 1998). Intrinsic NTS neurons of CaMK-*CB$_1$*-KO mice still expressed CB_1 mRNA, as revealed by double in situ hybridization (DISH) using glucagon-like peptide 1, a marker of NTS neurons (Figure 1C). However, no CB_1 protein was found in this region (Figure 1C). Thus, these data indicate that the afferent terminals in the NTS of CaMK-*CB$_1$*-KO mice do not contain CB_1 protein. Because CB_1 protein is expressed generally at presynaptic level, the preserved CB_1 mRNA expression in intrinsic NTS neurons suggests that CB_1 protein at the axonal terminals of these neurons is present in mutant mice. CB_1 mRNA expression is preserved in both rostral and distal nodose ganglion (Figures 1D and 1F and Figure S1A available online) of CaMK-*CB$_1$*-KO, and CB_1 immunoreactivity is also unchanged in these mutant mice as compared to WT (Figure S1B). Thus, CB_1 signaling on vagal afferents to NTS and to the nodose ganglion is maintained in CaMK-*CB$_1$*-KO mice. CB_1 mRNA is also present in a subset of dopamine-β-hydroxylase (DBH)-expressing neurons of superior cervical sympathetic ganglia but is significantly reduced as compared to WT (Figure 1E). The neuroanatomical analysis was in agreement with QT-PCR data showing a nearly 60% reduction in the ratio between CB_1 and DBH mRNA expression in superior cervical ganglia of CaMK-*CB$_1$*-KO mice (data not shown). Conversely, CB_1 expression was preserved in nonneuronal peripheral organs (Figures 1F and 1G).

CaMK-*CB$_1$*-KO Mice Are Lean and Unresponsive to the Acute Action of the CB_1 Antagonist Rimonabant

The monitoring of body weight in mice maintained on standard diet (SD) revealed that CaMK-*CB$_1$*-KO mice had a significantly lower body weight than their WT (Figure 2A). However, when compared to complete *CB$_1$*-KO mice, the phenotype of conditional mutants was less pronounced (Figures 2B and 2C), suggesting that CB_1 expressed in forebrain and sympathetic neurons does not fully account for the lean phenotype observed in the complete *CB$_1$*-KO mice on SD.

The CB_1 antagonist rimonabant exerts profound CB_1-dependent effects on food intake, body weight, and lipid oxidation (Herling et al., 2008). To investigate whether these effects are dependent upon CB_1 in forebrain and sympathetic neurons, CaMK-*CB$_1$*-KO and WT littermates were treated with rimonabant. The administration of the CB_1 antagonist acutely reduced body weight and respiratory quotient (RQ) of CaMK-*CB$_1$*-WT mice, but not of CaMK-*CB$_1$*-KO mice (Figures 2D and 2E). Furthermore, because the effects of acute CB_1 blockade are particularly evident in stimulated conditions (Di Marzo et al., 2001), we evaluated rimonabant action on fasting-induced overeating in conditional mutant mice. After 24 hr of fasting, CaMK-*CB$_1$*-WT mice ate significantly more than CaMK-*CB$_1$*-KO mice (Figure 2F). Under these experimental conditions, rimonabant (3 mg/kg i.p.) significantly decreased food intake in CaMK-*CB$_1$*-WT, unlike in CaMK-*CB$_1$*-KO (Figure 2F). These data indicate that CB_1 expressed in forebrain and sympathetic neurons is an important mediator of the acute effects of rimonabant on food intake, body weight, and lipid oxidation.

CB_1 in Forebrain and Sympathetic Neurons Regulates Diet-Induced Obesity

To assess the role of CB_1 in diet-induced obesity (DIO), CaMK-*CB$_1$*-KO, complete *CB$_1$*-KO, and their WT littermates were maintained on a mild high-fat diet (HFD, 40% fat content) for 12 weeks.

Cell Metabolism
CB1 Receptors and Energy Metabolism

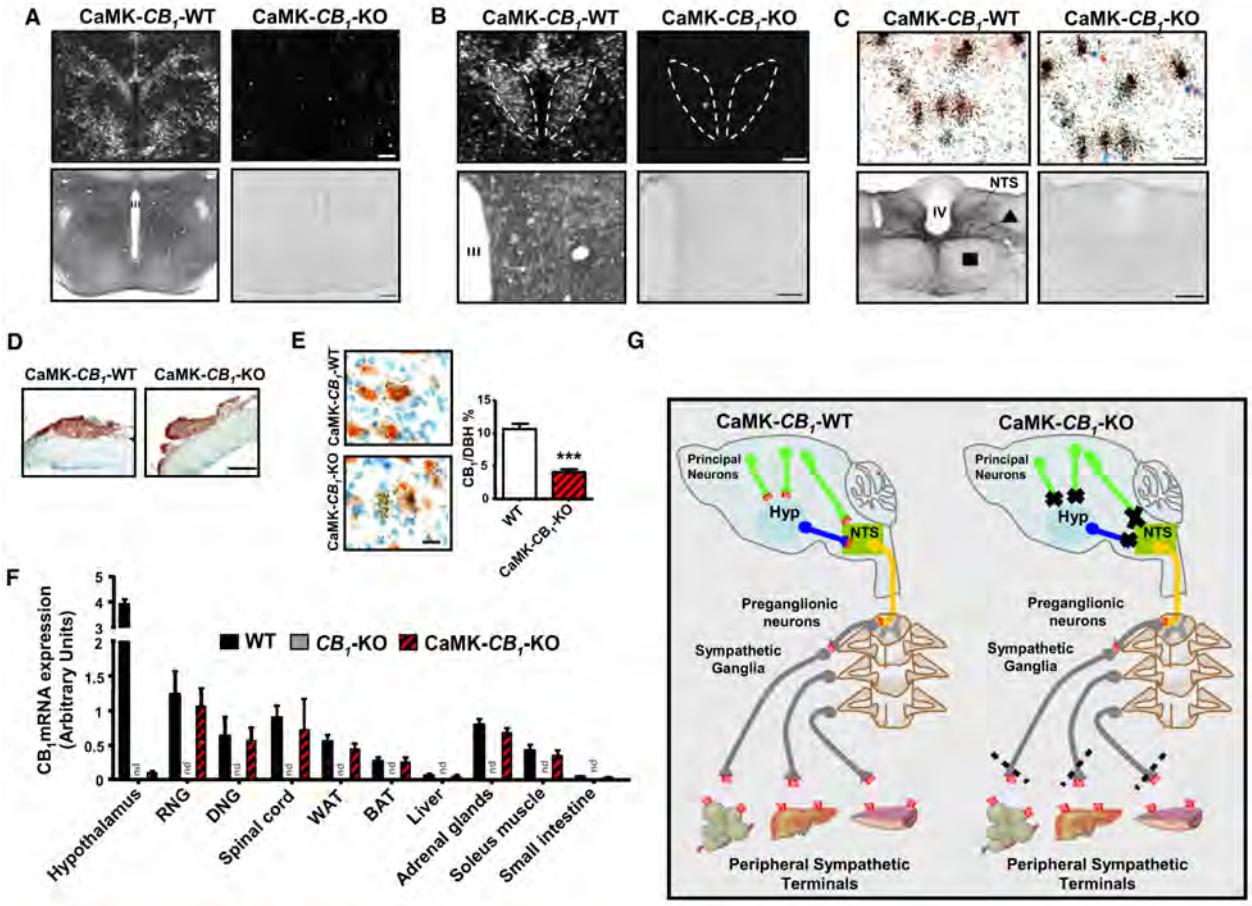

Figure 1. CB_1 mRNA and Protein Distribution in CaMK-CB_1-KO Mice

(A) CB_1 mRNA expression detected by ISH (top) and staining of CB_1 protein by IHC (bottom) in the whole hypothalamus. Scale bar, 200 μm.

(B) ISH (top) and IHC (bottom) for CB_1 in the paraventricular nucleus of the hypothalamus (PVN, encircled scattered lines in top panels). Scale bar, 50 μm. (III) third ventricle.

(C) (Top) DISH for CB_1 mRNA (black dots) and glucagon-like peptide 1 (GLP-1) mRNA (red color) in the nucleus of the solitary tract (NTS). Scale bar, 30 μm. (Bottom) CB_1 protein in the NTS. (Triangle) Dorsal motor nucleus of the vagus. (Square) Hypoglossal nucleus. (IV) Fourth ventricle. Scale bar, 200 μm.

(D) ISH for CB_1 mRNA (in red) in the nodose ganglia. Scale bar, 50 μm.

(E) DISH for CB_1 mRNA (black dots) and dopamine-β-hydroxylase (DBH) (red color) and QT-PCR analysis of the ratio CB_1/DBH mRNA expression in the superior cervical sympathetic ganglia. Scale bar, 1.5 μm; n = 4 ganglia per group; data are mean ± SEM. ***$p \leq 0.0005$.

(F) CB_1 mRNA expression by QT-PCR in the hypothalamus and in peripheral tissues of CaMK-CB_1-WT and KO mice (n = 6 per genotype). CB_1-KO mice organs are negative control. WAT, white adipose tissue; BAT, brown adipose tissue, RNG, rostral nodose ganglion; DNG, distal nodose ganglion; n.d., not detected. Data are mean ± SEM.

(G) Schematic representation of areas of CB_1 deletion in CaMK-CB_1-KO mice, referring to regions implicated in energy control. Presynaptic CB_1 protein is in red. Black crosses indicate CB_1 deletion. Dashed lines indicate reduced CB_1 expression. Hyp, hypothalamus; NTS, nucleus of the solitary tract.

See also Figure S1.

To study CB_1 expression in peripheral tissues after HFD, we analyzed, by QT-PCR, CB_1 mRNA levels in white adipose tissue (WAT), brown adipose tissue (BAT), and liver of CaMK-CB_1-KO and -WT. QT-PCR analysis in BAT and liver of CaMK-CB_1-WT mice revealed that CB_1 mRNA expression was increased in HFD, as compared to SD (Figure 3A). This increase remained significant only in the liver, but not in the BAT, of CaMK-CB_1-KO. No differences were detected in WAT of both CaMK-CB_1-KO and -WT mice on HFD compared to SD (Figure 3A).

Both CaMK-CB_1-KO and complete CB_1-KO mice had a significantly lower body weight than their WT under HFD (Figures 3B and 3C). However, when body weight was expressed as percentage of the initial weight, CaMK-CB_1-KO mice gained significantly less weight than WT or CB_1-KO mice (Figure 3D). Of interest, the weight gain of complete CB_1-KO was not different from WT. Furthermore, a chronic treatment with rimonabant (10 mg/kg; 32 days, daily) did not affect the body weight of CaMK-CB_1-KO mice under HFD, whereas it reduced body weight gain in CaMK-CB_1-WT (Figure 3E). A diet higher in fat content (60%, super HFD) caused a greater body weight gain in WT mice, but not in CaMK-CB_1-KO mice (Figures 3F and 3G). Thus, these data exclude that the resistant phenotype

Cell Metabolism
CB_1 Receptors and Energy Metabolism

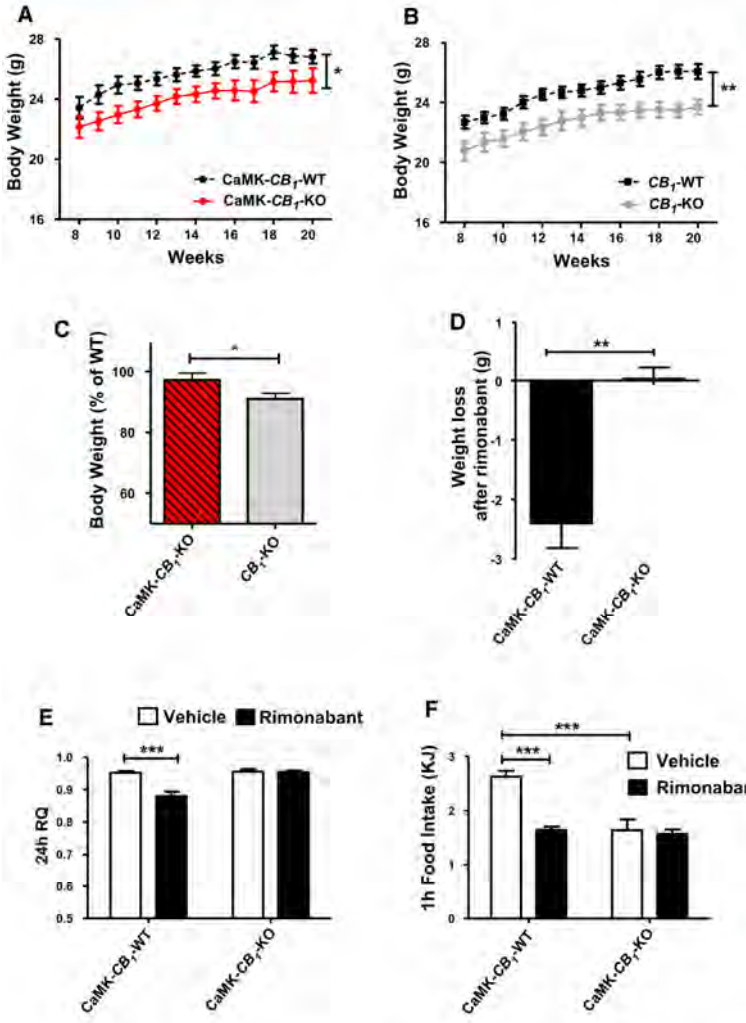

Figure 2. Characterization of CaMK-CB_1-KO Mice during Standard Diet

(A) Average body weight of CaMK-CB_1-WT (black circles) and CaMK-CB_1-KO mice (red circles) kept on SD for a period of 12 weeks (n = 18 per genotype). *p < 0.05.

(B) Average body weight of CB_1-WT mice (black circles) and complete CB_1-KO mice (gray circles) kept on SD for a period of 12 weeks (n = 18 per genotype). **p < 0.005.

(C) Body weight of CaMK-CB_1-KO and complete CB_1-KO mice, expressed as percentage of WT mice ± SEM. Values for CaMK-CB_1-WT and CB_1-WT were cumulated since not statistically different (black bar). Red dashed bar, CaMK-CB_1-KO; gray bar, CB_1-KO mice. *p < 0.05.

(D) Weight loss of CaMK-CB_1-WT mice (black bar) (n = 6) and CaMK-CB_1-KO (red dashed bar) (n = 5) 24 hr after rimonabant administration (10 mg/kg i.p.). **p < 0,005.

(E) Average 24 hr respiratory quotient (RQ) measured every hour for two days in CaMK-CB_1-WT mice (n = 7) and CaMK-CB_1-KO (n = 6). On the first day, animals were treated with vehicle; rimonabant treatment (10 mg/kg i.p.) started at the beginning of day 2. ***p < 0.0005. White bars, vehicle mice; black bars, rimonabant mice.

(F) Cumulative food intake within 1 hr after fasting of CaMK-CB_1-WT mice (black bars) and CaMK-CB_1-KO mice (white bars) treated with vehicle or rimonabant (3 mg/kg i.p.), respectively. n = 10 per genotype. ***p < 0.0005.

Data represent mean ± SEM.

observed in CaMK-CB_1-KO mice was displayed only under conditions of moderate DIO. Furthermore, we measured the total adiposity, hepatic steatosis (by hepatic triglyceride measurement), and plasma metabolic profile of CaMK-CB_1-KO, CB_1-KO, and their respective WT mice after 12 weeks of HFD. No significant difference was observed between WT littermates of CaMK-CB_1-KO mice and CB_1-KO mice, neither under SD nor under HFD (data not shown). Thus, WT values were cumulated to improve readability of the results. As shown in Figures 4A and 4B, chronic HFD did not significantly increase adipose tissue content in CaMK-CB_1-KO and CB_1-KO mice, as opposed to WT. Hepatic triglycerides content was significantly increased in WT animals after HFD administration, but not in CB_1-KO and CaMK-CB_1-KO mice (Figure 4C). The plasma levels of leptin, insulin, glucose, free fatty acids (FFA), and triglycerides were significantly increased in WT animals, but not in CB_1-KO and CaMK-CB_1-KO mice, after the same HFD (Figure 4D). Total cholesterol increased in WT animals after HFD, but no significant changes were observed in either CB_1-KO or CaMK-CB_1-KO mice (Figure 4D). Altogether, these results suggest that CB_1 signaling in forebrain and sympathetic neurons plays an important role in body weight gain, fat accumulation, and metabolic alterations associated with chronic HFD consumption.

Metabolized Energy and Lipids Utilization under HFD Are Modulated by CB_1 in Forebrain and Sympathetic Neurons

CaMK-CB_1-KO and CB_1-KO mice under HFD showed a total food intake comparable to their WT controls (Figures 5A and 5B). Nevertheless, CaMK-CB_1-KO mice had a significantly lower feed efficiency than either WT or complete CB_1-KO mice (Figure 5C). Thus, CB_1 in forebrain and sympathetic neurons regulates the conversion of energy intake into fat accumulation and body weight gain. To analyze the mechanisms underlying the reduced feed efficiency of CaMK-CB_1-KO mice, we evaluated energy homeostasis. First, as compared to their WT littermates, CaMK-CB_1-KO mice exhibited a less-efficient absorption of energy, as indicated by the increase in the energy content of the feces (Figure 5D). CaMK-CB_1-KO mice and their WT littermates had comparable metabolic rate (Figure 5E) and body temperature (data not shown). Conversely, the RQ was significantly reduced in the mutant animals during the night, the active period of mice (Figure 5F). No difference in night and day food intake was found between CaMK-CB_1-KO and CaMK-CB_1-WT mice (data not shown), thus allowing us to exclude that a different amount of food ingested in the dark period influenced the RQ. As in SD (Figure 2E), the acute administration of rimonabant in HFD reduced RQ in CaMK-CB_1-WT mice, but not in CaMK-CB_1-KO mice (Figure 5G).

Cell Metabolism
CB_1 Receptors and Energy Metabolism

CB_1 in Forebrain and Sympathetic Neurons Regulates BAT Functions and Thermogenesis

Low feed efficiency may be also explained by increased BAT thermogenic and mitochondrial activities. Of note, peroxisome proliferator-activated receptor γ coactivator 1α (PGC-1α), nuclear respiratory factor-1 (NRF-1), mitochondrial transcription factor A (Tfam) (master regulators of mitochondrial biogenesis), and cytochrome c (Cyt c) and cytochrome c oxidase IV (COX IV) (two mitochondrial proteins involved in oxidative phosphorylation) mRNA levels, as well as mitochondrial DNA amount and citrate synthase activity (biomarkers of mitochondrial mass and function), were significantly increased in BAT of CaMK-*CB_1*-KO as compared to WT (Figure 6A). Western blot analysis confirmed the QT-PCR data. In fact, an increase in PGC-1α, COX IV, and Cyt c protein levels in the BAT of CaMK-*CB_1*-KO mice, as compared to WT mice, was observed (Figure S2A). Furthermore, mRNA levels of uncoupling protein 1 (UCP-1) were significantly increased in BAT of CaMK-*CB_1*-KO mice, as compared to WT mice (Figure 6A), suggesting an increased thermogenic capacity in the conditional mutant mice. To test this hypothesis, we exposed HFD-fed CaMK-*CB_1*-KO mice to a thermal challenge. Body temperature and O_2 consumption were significantly higher in CaMK-*CB_1*-KO mice than in CaMK-*CB_1*-WT mice after cold exposure (+6°C) (Figures 6B and 6C), thus suggesting that the lack of CB_1 in the forebrain neurons improves the thermogenic responses and increases energy expenditure. In vivo positron emission tomography (PET) analysis revealed that the uptake of 2-deoxy-2-[^{18}F]fluoro-D-glucose (^{18}F-FDG) was markedly increased in cold-exposed HFD-fed CaMK-*CB_1*-KO mice, as compared to CaMK-*CB_1*-WT mice (Figures 6D and 6E). Moreover, rimonabant treatment increased the ^{18}F-FDG uptake in CaMK-*CB_1*-WT mice, but not in CaMK-*CB_1*-KO mice (Figure 6E). These data strongly suggest that the activation of neuronal CB_1 signaling modulates BAT thermogenesis during HFD and that CB_1 in forebrain and sympathetic neurons has a major role in the regulation of this function.

CB_1 in Forebrain and Sympathetic Neurons Regulates Energy Balance by Modulating the Sympathetic Tone

To determine the mechanism leading to the energy balance changes observed in CaMK-*CB_1*-KO mice under HFD, we investigated the activity of the sympathetic nervous system (SNS). HFD-fed CaMK-*CB_1*-KO mice had a marked increase in plasma norepinephrine (NE) levels, as compared to WT (no changes in plasma epinephrine and dopamine; data not shown), and similar data were obtained in complete *CB_1*-KO mice (Figure 6F). To further substantiate whether the changes in BAT metabolism were due to increased SNS activity, we investigated the uptake of the PET tracer ^{11}C-meta-hydroxyephedrine (a NE analog) (Thackeray et al., 2007) into the BAT of WT, CaMK-*CB_1*-KO, and *CB_1*-KO mice. Similar increases in tracer uptake were observed in both CaMK-*CB_1*-KO and *CB_1*-KO mice as compared to WT at 24°C, suggesting an increased NE turnover in this tissue (Figure 6G). Consistently, WT mice chronically treated with rimonabant exhibited an increase in BAT NE turnover, as compared to vehicle-treated WT mice (Figure 6H). Moreover, a greater difference in tracer uptake was observed in both conditional and complete KO mice, as compared to WT, under hypothermia (+6°C) (Figure 6G). Altogether, these data suggest that the increased thermogenesis of CaMK-*CB_1*-KO mice is caused by an increased SNS activity in the BAT, implying that CB_1 receptors located in principal forebrain and sympathetic neurons play a key regulator role on peripheral SNS activity. This finding was further substantiated by the in vivo analysis of FDG uptake and ex vivo analysis of mitochondrial activity in the BAT of cold-exposed (+6°C) animals after sympathetic denervation. In vivo small animal PET data demonstrated that the higher thermogenic function of the BAT of CaMK-*CB_1*-KO mice is completely abolished after both chemical (6-OH-dopamine, 6-OH-DA) and surgical sympathectomy (Figure 6E). Moreover, the increase in BAT thermogenesis caused by rimonabant administration is also completely lost after sympathectomy (Figure 6E). Ex vivo analysis of mitochondrial activity in cold-exposed animals after chemical sympathectomy was in agreement with PET data showing that the improved mitochondrial and thermogenic functions of the BAT of CaMK-*CB_1*-KO were lost after sympathectomy (Figure S2B). Altogether, these results demonstrate that an increased NE-mediated sympathetic tone is responsible for the higher thermogenesis in CaMK-*CB_1*-KO mice.

DISCUSSION

This study demonstrates that CB_1 receptors expressed in forebrain and sympathetic neurons play a pivotal role in the regulation of energy balance, which is particularly evident in DIO. Several results support this conclusion: (1) Systemic administration of rimonabant, which antagonizes both neuronal and non-neuronal CB_1, does not affect body weight, food intake, and energy control in CaMK-*CB_1*-KO mice, both under SD or HFD; (2) Whereas CaMK-*CB_1*-KO mice show a milder lean phenotype than *CB_1*-KO mice under SD, their metabolic profile and fat content become indistinguishable after prolonged exposure to HFD; and (3) CaMK-*CB_1*-KO mice are resistant to DIO because of increased thermogenesis and overactivity of the SNS.

The anatomical characterization of CB_1 expression in CaMK-*CB_1*-KO mice demonstrates that this animal model lacks CB_1 protein in glutamatergic forebrain-projecting neurons in the hypothalamus and in the NTS while still preserving the receptor on distal terminals of NTS neurons and on peripheral organs. However, CaMK-*CB_1*-KO mice have a partial deletion of CB_1 in the sympathetic ganglia. Thus, the observed phenotype is the result of the reduced ECS signaling at the level of CB_1 expressed in the forebrain and/or sympathetic neurons.

Our data also show that CB_1 receptors in these locations exert an important role in the control of the metabolic plasmatic profile and hepatic steatosis in DIO. However, this could be secondarily related to the resistance to body weight gain of CaMK-*CB_1*-KO mice and not due to a direct control by CB_1 receptors expressed at these sites. For this reason, our data do not rule out that peripheral CB_1 blockade could directly improve peripheral metabolism, as recently demonstrated (Nogueiras et al., 2008; Osei-Hyiaman et al., 2008; Cota et al., 2009).

Of interest, the overall food intake of conditional mutant mice in HFD is similar to that of WT controls, suggesting that CB_1 receptors control energy balance by other mechanisms than food intake. Indeed, our data show that reduced CB_1 signaling at forebrain and sympathetic neurons counteracts the weight

Cell Metabolism
CB1 Receptors and Energy Metabolism

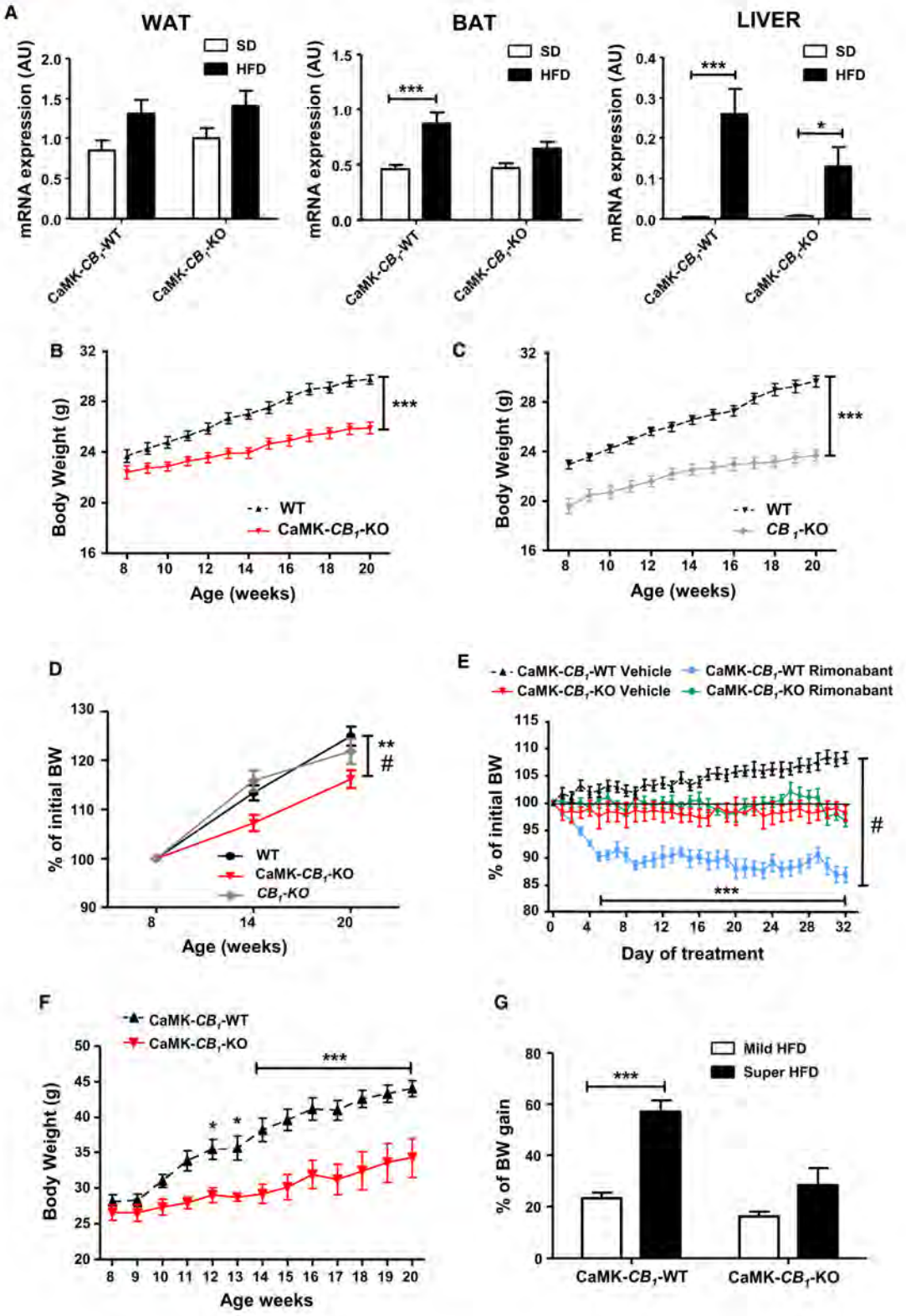

Cell Metabolism
CB_1 Receptors and Energy Metabolism

gain associated to HFD due to a reduction of metabolized energy and stimulation of lipid oxidation. Thus, blockade of CB_1 signaling at these sites is necessary to induce lipid oxidation, a phenomenon observed during chronic treatment with CB_1 antagonists (Herling et al., 2008).

Furthermore, CaMK-*CB*$_1$-KO mice display upregulated mitochondrial biogenesis and enhanced thermogenic activity in the BAT. These data are in agreement with previous studies demonstrating that CB_1 blockade promotes energy dissipation through mitochondrial heat production in the BAT, activation of futile cycles, and restoration of mitochondrial biogenesis in WAT of HFD-fed mice (Jbilo et al., 2005; Tedesco et al., 2008). Of note, the increased fatty acid oxidation and the elevation of several indexes of cellular energy dissipation seem to account for the lower feed efficiency observed in CaMK-*CB*$_1$-KO mice. Thus, the present findings suggest that CB_1 receptors on forebrain and sympathetic neurons play a necessary role in the ECS modulation of energy balance.

Our data demonstrate that CB_1 receptors regulate energy balance by modulating the SNS. Indeed, we found an elevated sympathetic noradrenergic tone in CaMK-*CB*$_1$-KO mice and an increased NE turnover in the BAT of CaMK-*CB*$_1$-KO mice, suggesting that enhanced SNS activity is the factor responsible for the increased functional activity of the BAT in CaMK-*CB*$_1$-KO mice. This conclusion is substantiated by two observations: (1) During acute exposure to cold, a condition stimulating thermogenesis via SNS activation, CaMK-*CB*$_1$-KO displayed a higher NE turnover of BAT and increased BAT functional activity, and they preserved their metabolic rate and body temperature; and (2) The increased BAT functional activity is lost in CaMK-*CB*$_1$-KO mice after both chemical and surgical sympathectomy.

The second important finding of this study is the demonstration that rimonabant modulates SNS activity and energy metabolism mainly through CB_1 expressed in forebrain and sympathetic neurons. Indeed, rimonabant-induced BAT thermogenesis under cold exposure was comparable to that observed in untreated CaMK-*CB*$_1$-KO mice. Moreover, sympathectomy reduced BAT activity of both CaMK-*CB*$_1$-KO and WT mice treated with rimonabant. This last observation is in agreement with recent data showing that the effects of rimonabant on energy expenditure and thermogenesis are attenuated by BAT denervation (Verty et al., 2009).

Exposure to HFD stimulates ECS activity by enhancing endocannabinoids production (Kunos et al., 2008). Due to the inhibitory effects of CB_1 signaling, the HFD-induced activation of the ECS likely dampens neuronal pathways controlling SNS activity, leading to decreased SNS activity that, in turn, favors energy storage and fat accumulation. Conversely, in CaMK-*CB*$_1$-KO mice, the reduced ECS signaling at the level of forebrain and/or sympathetic neurons favors SNS overactivity, thus leading to the lean phenotype observed, particularly under HFD. Considering that HFD increases general ECS activity, a possible interpretation of our data is that, in conditions of excessive energy intake, CB_1 signaling in forebrain and/or sympathetic neurons is particularly involved in limiting SNS overactivation during DIO. Importantly, the activation of presynaptic CB_1 receptors is known to inhibit norepinephrine release and consequently reduce sympathetic "tone" onto peripheral tissues (Kunos et al., 2008); therefore, it is possible that CB_1 reduction in sympathetic ganglia is the factor leading to the increased sympathetic activation in the mutant mice. However, an alternative possibility is that central CB_1 signaling might indirectly regulate sympathetic activity through descending pathways. Further studies using mutant mice with exclusive and complete deletion of CB_1 in sympathetic ganglia will reveal the relative contribution of central nervous system versus SNS endocannabinoid signaling in the control of peripheral energy metabolism.

Finally, we have also demonstrated that deletion of CB_1 in forebrain and sympathetic neurons influences CB_1 expression in peripheral organs. CaMK-*CB*$_1$-KO mice, as opposed to WT mice, did not increase CB_1 expression in the BAT after HFD. This supports the existence of a "vicious ECS cycle," in which CB_1 signaling might promote itself in pathological conditions, thus contributing to the worsening of the disease.

The present findings might have an important impact on clinical practice. CB_1 receptor antagonists have been recently proposed as antiobesity agents and have been successfully tested in humans in relation to their ability to reduce body weight and improve several metabolic parameters (Scheen, 2008; Addy et al., 2008). However, their clinical use has been recently halted by the European Medicines Agency for the increased incidence of psychiatric side effects (Akbas et al., 2009) due to their action on CB_1 located in brain areas regulating mood and response to stress. Therefore, the selective targeting of peripheral CB_1 antagonists unable to cross the blood brain barrier is the next

Figure 3. Phenotype of CaMK-*CB*$_1$-KO Mice during High-Fat/Super High-Fat Diet

(A) CB_1 mRNA expression by QT-PCR in the white adipose tissue (WAT), brown adipose tissue (BAT), and liver of CaMK-*CB*$_1$-WT and CaMK-*CB*$_1$-KO mice fed with SD (white columns) or HFD (black columns). n = 7 per genotype and diet. AU, arbitrary units.

(B) Body weight of CaMK-*CB*$_1$-WT (black triangles) and CaMK-*CB*$_1$-KO mice (red triangles) during the 12 weeks of HFD. n = 24 per genotype. ***p < 0.0005.

(C) Body weight of *CB*$_1$-WT mice (n = 25) (black triangles) and complete *CB*$_1$-KO mice (n = 20) (gray diamonds) during the 12 weeks of HFD. ***p < 0.0005.

(D) Weight gain expressed as percentage of initial weight in CaMK-*CB*$_1$-KO (red triangles), complete *CB*$_1$-KO (gray diamonds), and their WT (black circles). **p < 0.005 CaMK-*CB*$_1$-KO versus WT mice; #p < 0.05 CaMK-*CB*$_1$-KO versus *CB*$_1$-KO. The values of the CaMK-*CB*$_1$-WT and *CB*$_1$-WT were cumulated, since not statistically different.

(E) Weight change expressed as percentage of initial weight in mice daily treated with rimonabant (10 mg/kg i.p.) for 32 days. (Black triangles) CaMK-*CB*$_1$-WT vehicle (n = 6). (Red triangles) CaMK-*CB*$_1$-KO vehicle (n = 5). (Blue squares) CaMK-*CB*$_1$-WT rimonabant (n = 7). (Green circles) CaMK-*CB*$_1$-KO rimonabant (n = 6). #p < 0.0005 CaMK-*CB*$_1$-WT rimonabant versus CaMK-*CB*$_1$-WT vehicle; ***p < 0.0005 CaMK-*CB*$_1$-WT rimonabant versus CaMK-*CB*$_1$-KO rimonabant.

(F) Body weight of CaMK-*CB*$_1$-WT (black triangles) and CaMK-*CB*$_1$-KO mice (red triangles) during 12 weeks of super HFD (n = 5 per genotype).

(G) Weight gain in CaMK-*CB*$_1$-WT and CaMK-*CB*$_1$-KO mice fed with mild HFD (40% of fat) (white bars) or super HFD (60% of fat) (black bars). *p < 0.05; ***p < 0.0005.

Data represent mean ± SEM.

Cell Metabolism
CB_1 Receptors and Energy Metabolism

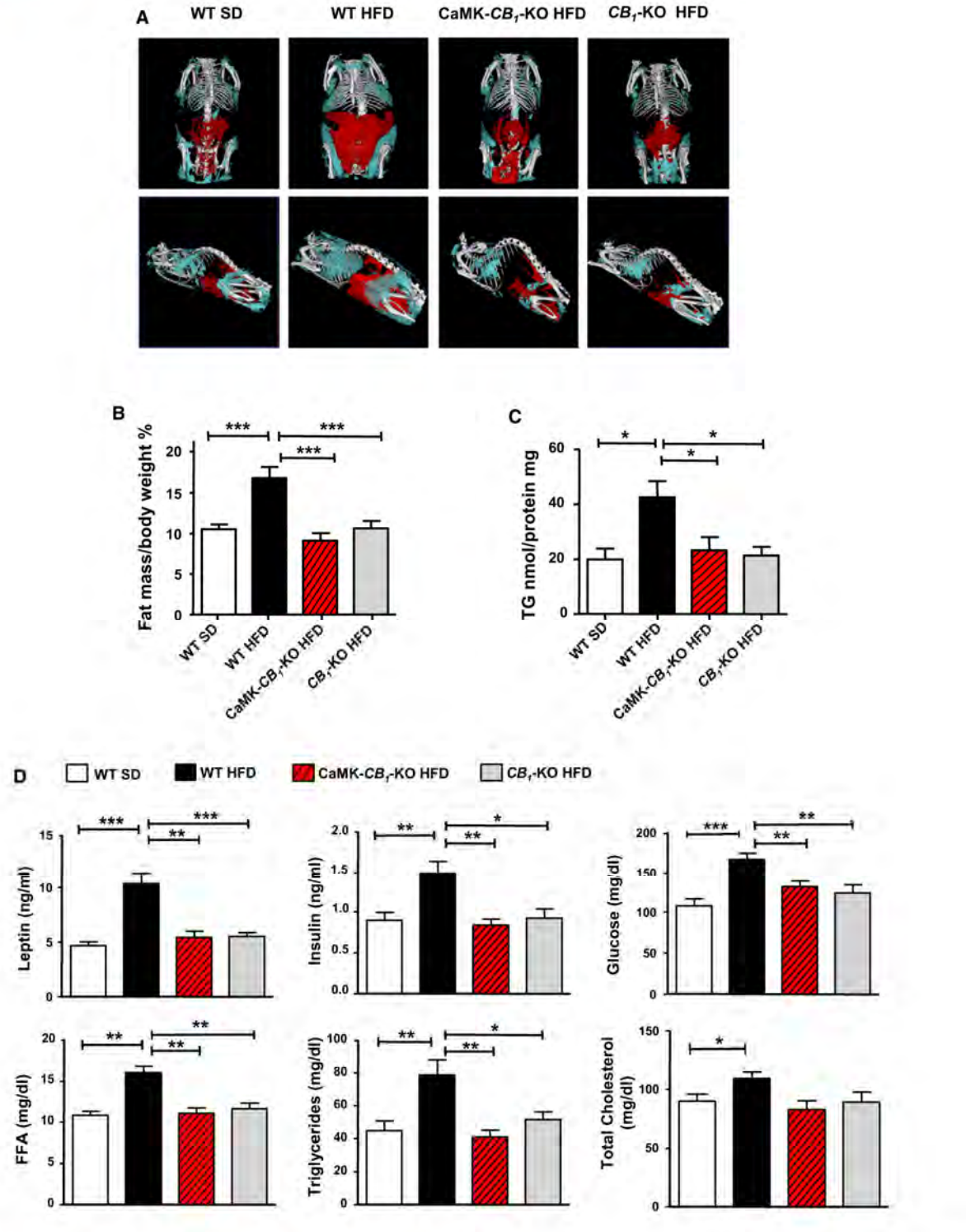

Figure 4. Characterization of CaMK-CB_1-KO Mice during High-Fat Diet

(A) Three-dimensional visualization of skeleton, visceral adipose tissue (red), and subcutaneous adipose tissue (blue) from in vivo micro-CT images of a WT on SD, WT on HFD, CaMK-CB_1-KO on HFD, and complete CB_1-KO on HFD, respectively. (Top) Frontal views. (Bottom) Lateral views.

(B) Quantification of total fat content (as percentage of body weight) by in vivo micro-CT analysis in WT mice fed on SD (white bar, n = 15), WT mice fed on HFD (black bar, n = 16), CaMK-CB_1-KO mice fed on HFD (red dashed bar, n = 11), and complete CB_1-KO mice on HFD (gray bar, n = 13). ***$p < 0.0005$.

Cell Metabolism
CB1 Receptors and Energy Metabolism

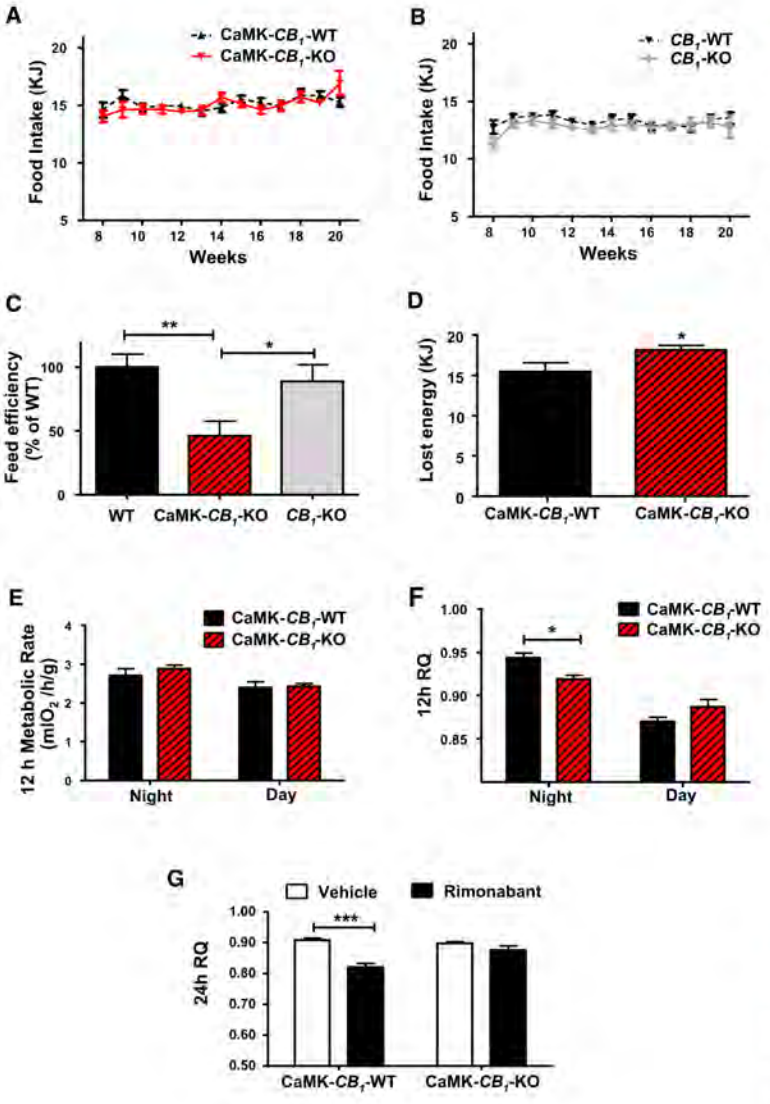

Figure 5. Energy Homeostasis in CaMK-CB_1-KO Mice on High-Fat Diet

(A) Food intake of CaMK-CB_1-WT (black triangles) and CaMK-CB_1-KO mice (red triangles) during the 12 weeks of HFD (n = 24 per genotype).

(B) Food intake of CB_1-WT (n = 25) (black triangles) and CB_1-KO mice (n = 20) (gray diamonds) during the 12 weeks of HFD.

(C) Feed efficiency of WT (black bar), CaMK-CB_1-KO (red dashed bar), and complete CB_1-KO mice (gray bar) during the 12 weeks of HFD (n = 20 per genotype). $^*p < 0.05$; $^{**}p < 0.005$. Data are expressed as percentage of WT. The values of the CaMK-CB_1-WT and CB_1-WT mice were grouped since not statistically different.

(D) Daily energy loss (24 hr energy content by bomb calorimetry). CaMK-CB_1-WT (n = 6, black bar) and CaMK-CB_1-KO (n = 7, dashed red bar) fed with HFD. $^*p < 0.05$.

(E) Metabolic rate at night (7:00 PM–7:00 AM) and during the day (7:00 AM–7:00 PM) in CaMK-CB_1-WT (n = 5, black bar) and CaMK-CB_1-KO mice (n = 6, dashed red bar) on HFD.

(F) Average RQ at night (7:00 PM–7:00 AM) and during the day (7:00 AM–7:00 PM) in CaMK-CB_1-WT (n = 5, black bar) and CaMK-CB_1-KO mice (n = 6, dashed red bar) on HFD. $^*p < 0.05$.

(G) Average RQ measured every hour for two days in CaMK-CB_1-WT (n = 7) and CaMK-CB_1-KO (n = 6) fed with HFD. On the first day, animals were treated with vehicle; rimonabant treatment (10 mg/kg i.p.) started at the beginning of day 2. $^{***}p < 0.0005$. White bars, vehicle-treated mice; black bars, rimonabant-treated mice.

Data represent mean ± SEM.

predictable step in order to minimize side effects and, at the same time, retain the favorable metabolic actions due to CB_1 inhibition at the level of the adipose tissue, liver, skeletal muscle, and endocrine pancreas (Kunos et al., 2009). Our results point to a key role of CB_1 expressed in forebrain neurons and sympathetic terminals in the control of energy metabolism but leave open the possibility that nonblood brain barrier-penetrating drugs (McElroy et al., 2008; LoVerme et al., 2009), acting at presynaptic CB_1 receptors on peripheral neurons and thereby on nonneuronal peripheral organs, may importantly contribute to reduce the negative effect of the overactivation of the ECS described in association with obesity and related disorders.

EXPERIMENTAL PROCEDURES

Animals

Male CB_1-KO mice, CaMK-CB_1-KO mice (CB_1 receptor deletion in neurons expressing the Ca^{2+}/calmodulin-dependent kinase IIα), and their WT littermates were genotyped as described (Marsicano et al., 2002; Monory et al., 2006). Mutant animals were in a mixed genetic background, with a predominant C57BL/6N contribution (seven backcrosses). Mice were housed in individual cages under conditions of controlled temperature (24°C) and illumination (12 hr light/12 hr dark cycle) in the DIMORFIPA animal facilities, University of Bologna, Italy. All of the procedures were approved by the Central Veterinary Office of Bologna University in accordance with the European Community (86/609/EEC) guidelines for the care and use of laboratory animals. Animals were fed either with a mouse SD containing 12.3 KJ/g (11% fat, 19% protein, 70% carbohydrate; Dr. Piccioni Lab, Gessate, Milano, Italy), with an HFD having 18.9 KJ/g (40% fat, 15% protein, 45% carbohydrate; Dottor Piccioni Lab), or with a super HFD (SHFD) having 21.3 KJ/g (60.3% fat, 18.4% protein, 21.3% carbohydrate; TD.06414 Harlan Teklad, Italy). Eight-week-old mice were placed on HFD or SHFD or were maintained on SD. Body weight was measured twice a week starting at 8 weeks until 20 weeks of age (when not mentioned otherwise).

(C) Hepatic triglycerides (TG) content in WT mice fed with SD (white bar, n = 7), WT on HFD (black bar, n = 6), CaMK-CB_1-KO on HFD (red dashed bar, n = 8), and CB_1-KO on HFD (gray bar, n = 8). $^*p < 0.05$.

(D) Hormonal profile in WT mice fed with SD (white bar), WT on HFD (black bar), CaMK-CB_1-KO on HFD (red dashed bar), CB_1-KO on HFD (gray bar). Leptin, insulin, and FFA: n = 20 per genotype and diet. Triglycerides and total cholesterol: n = 12. Glucose: n = 12. $^{***}p < 0.0005$; $^{**}p < 0.005$; $^*p < 0.05$.

Data in (B)–(D) represent mean ± SEM. The values of the CaMK-CB_1-WT and CB_1-WT in SD or HFD were cumulated in (B) and (C) since not statistically different.

Cell Metabolism
CB_1 Receptors and Energy Metabolism

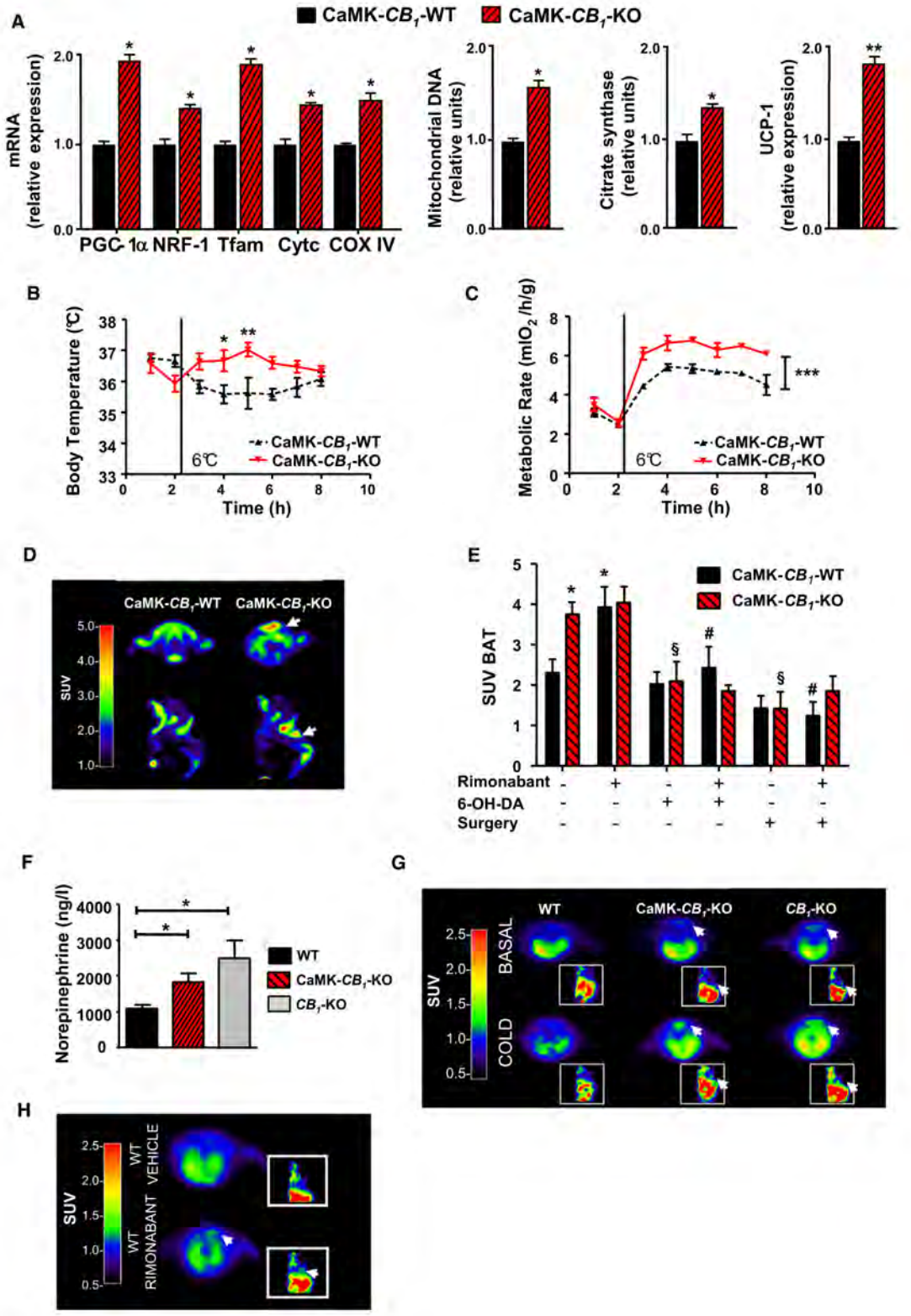

Cell Metabolism

CB$_1$ Receptors and Energy Metabolism

In Situ Hybridization

All tissues were derived from mice on SD. In situ hybridization (ISH) and DISH were performed using a radioactive or a nonradioactive (dig-labeled) CB$_1$-specific riboprobe and a nonradioactive (dig-labeled) GLP-1 in the hypothalamus, NTS, and nodose ganglia or a dopamine β-hydroxylase (DBH)-specific riboprobe in superior cervical sympathetic ganglia (Marsicano and Lutz, 1999) (see Supplemental Information).

IHC and Immunofluorescence

Polyclonal goat antibody (ab) (1:900) against the C-terminal 31 amino acids (443–473) of mouse CB$_1$ was used to stain hypothalamus and brainstem (Fukudome et al., 2004), and a polyclonal rabbit antiserum (1:300) against the last 73 amino acid residues of rat CB$_1$ (Wager-Miller et al., 2002) was used to stain nodose ganglion (generous gift of Dr. K. Mackie, Indiana University, Bloomington, IN). The specificity of the CB$_1$ antibodies was described elsewhere (Makara et al., 2007; Wager-Miller et al., 2002). Anti-tyrosine hydroxylase rabbit polyclonal ab (1:2000; Chemicon-Millipore, Temecula, CA 92590) detecting adrenergic nerve fibers was used in BAT. Biotinylated donkey anti-goat IgG (1:500; Jackson Lab, West Grove, PA) for hypothalamus and brainstem and rhodamine (TRITC)-conjugated affine pure donkey anti-rabbit IgG (1:200 Jackson ImmunoResearch) for BAT were used as secondary abs. For double-labeling immunofluorescence of nodose ganglia, a goat polyclonal anti-HuC/D (a panneuronal marker) (Santa Cruz Biotechnology, Inc. CA 95060) was used. As secondary abs, donkey anti-mouse IgG conjugated to fluorescein isothiocyanate (FITC) and rhodamine (TRITC)-conjugated (Jackson ImmunoResearch) (both at 1:500) were used (see Supplemental Information).

RNA Isolation and Real-Time PCR Analysis

RNA was isolated from tissues on SD or HFD (when indicated) mice and was analyzed as described (Tedesco et al., 2008) (see Supplemental Information). Primer sequences are in Table S1.

Immunoblot Analysis

The following antibodies were used: anti-PGC-1α (1: 1000, Cell Signaling), anti-COX IV (1:500, Molecular Probes), anti-Cyt c (1:500, BD Bioscience), anti-UCP-1 (1:1000, Calbiochem), and anti-GAPDH (1:20000 Histo-Line Laboratories) (see Supplemental Information).

Food Intake and Feed Efficiency

Food intake of mice allowed to food and water ad libitum was measured twice a week starting at 8 weeks until 20 weeks of age. Feed efficiency was calculated over the 12 weeks of diet as body weight gained per unit of energy intake (g/KJ). For the other studies on food intake, see Supplemental Information.

Hormone and Metabolite Assays

Plasma leptin was measured by Mouse Leptin RIA kit ML-82k (Millipore Corporation), insulin by Rat Insulin RIA kit RI-13K (Millipore Corporation), FFA by a colorimetric method (Wako Chemicals, Richmond, VA), triglycerides and total cholesterol by spectrophotometric enzymatic test (Roche Diagnostics, Mannheim, Germany), and glucose by the Breeze glucometer (Bayer). Plasma catecholamines were determined by high-performance liquid chromatography (Grossi et al., 1991). Blood for cathecolamines determination was obtained from nonanesthetized animals via surgically implanted intracardiac catheters. Haepatic lipids were extracted in chloroform/methanol 2:1 (0.01% BHT) and analyzed by BV-K622-100 kit (BoVision, Mountain View, CA).

In Vivo Quantification of Adipose Tissue

Mice were placed under anesthesia with 5% sevoflurane and oxygen supplementation (1 l/min) and scanned in an in vivo microcomputed tomography (micro-CT) scanner (eXplore Locus, GE, Milwaukee) at an isometric resolution of 90 μm (see Supplemental Information).

Energy Expenditure

Animals were kept individually in type II Makrolon cages inside a climate chamber. RQ and metabolic rate data were collected every hour in animals with free access to food and water. Some experiments were performed in two consecutive days. On day 1, mice were studied in their physiological conditions at ambient temperature. At the beginning of the light phase of day 2, mice were treated with rimonabant (10 mg/kg i.p.). Experiments under cold conditions were performed with an initial period of acclimation of the mice in the chambers (at 24°C for 3 hr), followed by a lowering of chambers temperature to 6°C (see Supplemental Information).

Telemetric Recording of Body Temperature

Animals were i.p. implanted with calibrated temperature transmitters (Mini-Mitter, Model X, Sunriver, Oregon, accuracy 0.1°C) under ketamine-hydrochloride anesthesia (50 mg*kg^{-1}) and 1%–2% isoflurane. The detection of the transmitter signals was accomplished by a radio receiver and processed by a microcomputer system.

Food and Feces Energy Content

Energy content of food and energy loss via the feces were determined using bomb calorimetry (IKA-Calorimeter C 5000, IKA-Werke GmbH & Co. KG, Staufen, Germany).

Mitochondrial DNA Analysis and Citrate Synthase Activity

Mitochondrial DNA analysis was performed and citrate synthase activity was measured as described in Tedesco et al., 2008.

Figure 6. Increased Thermogenesis and Sympathetic Tone in CaMK-*CB$_1$*-KO on High-Fat Diet

(A) Mitochondrial biogenesis and UCP1 mRNA levels in BAT of CaMK-*CB$_1$*-WT (black bars) and CaMK-*CB$_1$*-KO mice (dashed red bars) fed with HFD. PGC-1α, NRF-1, Tfam, COX IV, Cyt c mRNA level, and mitochondrial DNA amounts were analyzed by QT-PCR. CaMK-*CB$_1$*-WT: n = 7; CaMK-*CB$_1$*-KO: n = 8. **p < 0.005 versus CaMK-*CB$_1$*-WT mice.

(B) Body temperature in CaMK-*CB$_1$*-WT (black triangles) (n = 5) and CaMK-*CB$_1$*-KO mice (red triangles) (n = 6) on HFD during 6 hr of cold exposure (+6°C). *p < 0.05; **p < 0.005.

(C) Metabolic rate in CaMK-*CB$_1$*-WT (black triangles) (n = 5) and CaMK-*CB$_1$*-KO mice (red triangles) (n = 6) on HFD during 6 hr at +6°C. ***p < 0.0005.

(D) Representative PET image showing ^{18}F-FDG accumulation in the soprascapular BAT (arrows) of a CaMK-*CB$_1$*-WT and CaMK-*CB$_1$*-KO mouse at +6°C. (Top) Axial section. (Bottom) Sagittal section.

(E) Quantification of ^{18}F-FDG uptake (SUV) in the soprascapular BAT of CaMK-*CB$_1$*-WT (black bar) and CaMK-*CB$_1$*-KO mice (dashed red bar) under HFD after cold exposure and different treatments. The cohorts were composed of mice treated with: vehicle (n = 12 WT, n = 9 KO), vehicle + 6-0H-DA (n = 6 WT, n = 6 KO), vehicle + surgically denervation (n = 6 WT, n = 6 KO). For each cohort, the analysis was repeated on the same mice after rimonabant treatment. *p < 0.05 versus CaMK-*CB$_1$*-WT vehicle; §p < 0.05 versus CaMK-*CB$_1$*-KO vehicle; #p < 0.05 versus CaMK-*CB$_1$*-WT rimonabant.

(F) Plasma norepinephrine levels in WT (black bar, n = 12), CaMK-*CB$_1$*-KO (dashed red bars, n = 7), and *CB$_1$*-KO mice (gray bar, n = 9) on HFD. *p < 0.05 versus WT. The values of the CaMK-*CB$_1$*-WT and *CB$_1$*-WT mice were grouped since not statistically different.

(G) Representative PET image showing the uptake of ^{11}C-meta-hydroxyephedrine in the BAT (arrow) of WT (n = 4), CaMK-*CB$_1$*-KO (n = 4), and *CB$_1$*-KO (n = 3) mice in basal state and after cold exposure.

(H) Representative PET image showing ^{11}C-meta-hydroxyephedrine uptake (at 24°C) in the BAT (arrow) of WT mice chronically treated with vehicle or rimonabant (10 mg/kg) for 32 days.

Radioactive counts in (D), (G), and (H) are expressed as standard uptake values (SUV); smaller insets in (G) and (H) represent sagittal view. Data in (A–C), (E), and (F) represent mean ± SEM. See also Figure S2.

Cell Metabolism
CB_1 Receptors and Energy Metabolism

Small Animal PET Studies

For ^{18}F-FDG studies, 20-week-old mice were imaged in two different sessions. In the first, 8 hr fasted mice were placed at 24°C and i.p. treated with a vehicle solution; 1 hr later, mice were moved to a cold chamber (6°C) for 3 hr. Mice were then lightly anesthetized (gas sevofluorane), injected with ^{18}F-FDG (15 MBq), allowed to awake, and placed in a cold chamber for 1 hr (phase of tracer uptake). Scans were performed with a PET system (Explore Vista, GE) in animals treated with vehicle (3% DMSO, 1% Tween80 in saline solution) or vehicle + sympathetic denervation and repeated after 5 days of stabilization in the same animals treated with rimonabant (10 mg/kg i.p.). Control mice after sympathectomy (vehicle of 6-hydroxydopamine hydrobromide [6-OH-DA] and sham-operated mice) did not present different values of FDG uptake compared to WT mice treated with the vehicle of rimonabant (data not shown); thus, they were not included in the analysis.

For ^{11}C-meta-hydroxyephedrine studies, PET scan started immediately after the tracer injection (20 MBq) in the tail vein of anaesthetized animals. Imaging was first performed on 20-week-old animals at 24°C and then repeated (after 5 days) in the same animals exposed to cold (6°C) for 3 hr. Data for accumulation of ^{18}F-FDG and ^{11}C-meta-hydroxyephedrine on small animal PET images were expressed as standard uptake values (SUV) representing radioactive counts per gram of tissue, divided by injected dose of radioactivity per gram of animal weight. To correctly identify BAT uptake of the tracers, a CT reference image was coregistered with the PET image for each scan as described in Galiè et al., 2007.

Sympathectomy

For the chemical sympathectomy, mice were i.p. treated with injections of 80 mg/kg of 6-OH-DA in 0.1% ascorbic acid or vehicle daily for 3 consecutive days. Surgical sympathectomy of BAT was performed by cutting each of the nerve bundles projecting into the left and the right soprascapular pads. For the sham-operated animals, the BAT and the nerves were exposed, but not transected. Animals were allowed to recover for 10 days before testing. For histological verification of denervation, see Figure S2C.

Statistics

Results are expressed as mean ± SEM. Statistical analysis was performed by unpaired two-tailed Student's t test or by analysis of variance (ANOVA) with appropriate posthoc tests. The software GraphPad Prism 5.0 was used. A p value less than 0.05 was considered statistically significant.

SUPPLEMENTAL INFORMATION

Supplemental Information includes Supplemental Experimental Procedures, two figures, and one table and can be found with this article online at doi:10.1016/j.cmet.2010.02.015.

ACKNOWLEDGMENTS

This research was supported by grants from: European Union (LSHM-CT-2003-503041 to U.P.), European Union REPROBESITY (FPVII-223713 to U.P., G. Marsicano, and B. Lutz); 2007 PRIN from MIUR (to U.P. and E.N.); FIRB 2003 RBNE03KZRJ_002 (to R.P.); Avenir Program of INSERM (to D.C. and G. Marsicano); in part by the DFG (to B. Lutz); the European Foundation for the Studies of Diabetes (EFSD) (to G. Marsicano, B. Lutz, and D.C.), Fondation Bettencourt Schueller (to G. Marsicano); Bourse Ministerielle de Doctorat (to L. Bellocchio); Fondazione Cassa di Risparmio Bologna (to R.D.G.). We acknowledge Dr. K. Mackie (The Linda and Jack Gill Center for Biomolecular Science, Indiana University, Bloomington, IN) for the gift of polyclonal rabbit CB_1 antiserum and Dr. S. Boschi (Radiopharmacy, Department of Nuclear Medicine, S. Orsola-Malpighi Hospital, University of Bologna, Italy) for the synthesis of PET tracers.

Received: July 10, 2009
Revised: December 22, 2009
Accepted: February 26, 2010
Published: April 6, 2010

REFERENCES

Addy, C., Wright, H., Van Laere, K., Gantz, I., Erondu, N., Musser, B.J., Lu, K., Yuan, J., Sanabria-Bohórquez, S.M., Stoch, A., et al. (2008). The acyclic CB1R inverse agonist taranabant mediates weight loss by increasing energy expenditure and decreasing caloric intake. Cell Metab. *7*, 68–78.

Akbas, F., Gasteyger, C., Sjödin, A., Astrup, A., and Larsen, T.M. (2009). A critical review of the cannabinoid receptor as a drug target for obesity management. Obes. Rev. *10*, 58–67.

Casanova, E., Fehsenfeld, S., Mantamadiotis, T., Lemberger, T., Greiner, E., Stewart, A.F., and Schütz, G. (2001). A CamKIIalpha iCre BAC allows brain-specific gene inactivation. Genesis *31*, 37–42.

Cota, D., Marsicano, G., Tschöp, M., Grübler, Y., Flachskamm, C., Schubert, M., Auer, D., Yassouridis, A., Thöne-Reineke, C., Ortmann, S., et al. (2003). The endogenous cannabinoid system affects energy balance via central orexigenic drive and peripheral lipogenesis. J. Clin. Invest. *112*, 423–431.

Cota, D., Sandoval, D.A., Olivieri, M., Prodi, E., D'Alessio, D.A., Woods, S.C., Seeley, R.J., and Obici, S. (2009). Food intake-independent effects of CB1 antagonism on glucose and lipid metabolism. Obesity (Silver Spring) *17*, 1641–1645.

Di Marzo, V., Goparaju, S.K., Wang, L., Liu, J., Bátkai, S., Járai, Z., Fezza, F., Miura, G.I., Palmiter, R.D., Sugiura, T., and Kunos, G. (2001). Leptin-regulated endocannabinoids are involved in maintaining food intake. Nature *410*, 822–825.

Fukudome, Y., Ohno-Shosaku, T., Matsui, M., Omori, Y., Fukaya, M., Tsubokawa, H., Taketo, M.M., Watanabe, M., Manabe, T., and Kano, M. (2004). Two distinct classes of muscarinic action on hippocampal inhibitory synapses: M2-mediated direct suppression and M1/M3-mediated indirect suppression through endocannabinoid signalling. Eur. J. Neurosci. *19*, 2682–2692.

Galiè, M., Farace, P., Nanni, C., Spinelli, A., Nicolato, E., Boschi, F., Magnani, P., Trespidi, S., Ambrosini, V., Fanti, S., et al. (2007). Epithelial and mesenchymal tumor compartments exhibit in vivo complementary patterns of vascular perfusion and glucose metabolism. Neoplasia *9*, 900–908.

Grill, H.J., and Hayes, M.R. (2009). The nucleus tractus solitarius: a portal for visceral afferent signal processing, energy status assessment and integration of their combined effects on food intake. Int. J. Obes. (Lond.) *33* (*Suppl 1*), S11–S15.

Grossi, G., Bargossi, A.M., Lucarelli, C., Paradisi, R., Sprovieri, C., and Sprovieri, G. (1991). Improvements in automated analysis of catecholamine and related metabolites in biological samples by column-switching high-performance liquid chromatography. J. Chromatogr. *22*, 273–284.

Herling, A.W., Kilp, S., Elvert, R., Haschke, G., and Kramer, W. (2008). Increased energy expenditure contributes more to the body weight-reducing effect of rimonabant than reduced food intake in candy-fed wistar rats. Endocrinology *149*, 2557–2566.

Jbilo, O., Ravinet-Trillou, C., Arnone, M., Buisson, I., Bribes, E., Péleraux, A., Pénarier, G., Soubrié, P., Le Fur, G., Galiègue, S., and Casellas, P. (2005). The CB1 receptor antagonist rimonabant reverses the diet-induced obesity phenotype through the regulation of lipolysis and energy balance. FASEB J. *19*, 1567–1569.

Kunos, G., Osei-Hyiaman, D., Liu, J., Godlewski, G., and Bátkai, S. (2008). Endocannabinoids and the control of energy homeostasis. J. Biol. Chem. *283*, 33021–33025.

Kunos, G., Osei-Hyiaman, D., Bátkai, S., Sharkey, K.A., and Makriyannis, A. (2009). Should peripheral CB(1) cannabinoid receptors be selectively targeted for therapeutic gain? Trends Pharmacol. Sci. *30*, 1–7.

LoVerme, J., Duranti, A., Tontini, A., Spadoni, G., Mor, M., Rivara, S., Stella, N., Xu, C., Tarzia, G., and Piomelli, D. (2009). Synthesis and characterization of a peripherally restricted CB1 cannabinoid antagonist, URB447, that reduces feeding and body-weight gain in mice. Bioorg. Med. Chem. Lett. *19*, 639–643.

Makara, J.K., Katona, I., Nyíri, G., Németh, B., Ledent, C., Watanabe, M., de Vente, J., Freund, T.F., and Hájos, N. (2007). Involvement of nitric oxide in depolarization-induced suppression of inhibition in hippocampal pyramidal cells during activation of cholinergic receptors. J. Neurosci. *27*, 10211–10222.

Cell Metabolism
CB_1 Receptors and Energy Metabolism

Marsicano, G., and Lutz, B. (1999). Expression of the cannabinoid receptor CB1 in distinct neuronal subpopulations in the adult mouse forebrain. Eur. J. Neurosci. *11*, 4213–4225.

Marsicano, G., Wotjak, C.T., Azad, S.C., Bisogno, T., Rammes, G., Cascio, M.G., Hermann, H., Tang, J., Hofmann, C., Zieglgänsberger, W., et al. (2002). The endogenous cannabinoid system controls extinction of aversive memories. Nature *418*, 530–534.

Marsicano, G., Goodenough, S., Monory, K., Hermann, H., Eder, M., Cannich, A., Azad, S.C., Cascio, M.G., Gutiérrez, S.O., van der Stelt, M., et al. (2003). CB1 cannabinoid receptors and on-demand defense against excitotoxicity. Science *302*, 84–88.

McElroy, J., Sieracki, C., and Chorvat, R. (2008). Non-brain penetrant CB1 receptor antagonists as novel treatment of obesity and related metabolic disorders. Obesity (Silver Spring) *16* (*Suppl. 1*), S47.

Monory, K., Massa, F., Egertová, M., Eder, M., Blaudzun, H., Westenbroek, R., Kelsch, W., Jacob, W., Marsch, R., Ekker, M., et al. (2006). The endocannabinoid system controls key epileptogenic circuits in the hippocampus. Neuron *51*, 455–466.

Nogueiras, R., Veyrat-Durebex, C., Suchanek, P.M., Klein, M., Tschöp, J., Caldwell, C., Woods, S.C., Wittmann, G., Watanabe, M., Liposits, Z., et al. (2008). Peripheral, but not central, CB1 antagonism provides food intake-independent metabolic benefits in diet-induced obese rats. Diabetes *57*, 2977–2991.

Osei-Hyiaman, D., Liu, J., Zhou, L., Godlewski, G., Harvey-White, J., Jeong, W.I., Bátkai, S., Marsicano, G., Lutz, B., Buettner, C., and Kunos, G. (2008). Hepatic CB1 receptor is required for development of diet-induced steatosis, dyslipidemia, and insulin and leptin resistance in mice. J. Clin. Invest. *118*, 3160–3169.

Pagotto, U., Marsicano, G., Cota, D., Lutz, B., and Pasquali, R. (2006). The emerging role of the endocannabinoid system in endocrine regulation and energy balance. Endocr. Rev. *27*, 73–100.

Ravinet Trillou, C., Delgorge, C., Menet, C., Arnone, M., and Soubrié, P. (2004). CB1 cannabinoid receptor knockout in mice leads to leanness, resistance to diet-induced obesity and enhanced leptin sensitivity. Int. J. Obes. Relat. Metab. Disord. *28*, 640–648.

Scheen, A.J. (2008). CB1 receptor blockade and its impact on cardiometabolic risk factors: overview of the RIO programme with rimonabant. J. Neuroendocrinol. *20* (*Suppl 1*), 139–146.

Tedesco, L., Valerio, A., Cervino, C., Cardile, A., Pagano, C., Vettor, R., Pasquali, R., Carruba, M.O., Marsicano, G., Lutz, B., et al. (2008). Cannabinoid type 1 receptor blockade promotes mitochondrial biogenesis through endothelial nitric oxide synthase expression in white adipocytes. Diabetes *57*, 2028–2036.

Thackeray, J.T., Beanlands, R.S., and Dasilva, J.N. (2007). Presence of specific 11C-meta-Hydroxyephedrine retention in heart, lung, pancreas, and brown adipose tissue. J. Nucl. Med. *48*, 1733–1740.

Tsou, K., Brown, S., Sañudo-Peña, M.C., Mackie, K., and Walker, J.M. (1998). Immunohistochemical distribution of cannabinoid CB1 receptors in the rat central nervous system. Neuroscience *83*, 393–411.

Verty, A.N., Allen, A.M., and Oldfield, B.J. (2009). The effects of rimonabant on brown adipose tissue in rat: implications for energy expenditure. Obesity (Silver Spring) *17*, 254–261.

Wager-Miller, J., Westenbroek, R., and Mackie, K. (2002). Dimerization of G protein-coupled receptors: CB1 cannabinoid receptors as an example. Chem. Phys. Lipids *121*, 83–89.

Wittmann, G., Deli, L., Kalló, I., Hrabovszky, E., Watanabe, M., Liposits, Z., and Fekete, C. (2007). Distribution of type 1 cannabinoid receptor (CB1)-immunoreactive axons in the mouse hypothalamus. J. Comp. Neurol. *503*, 270–279.

3. VERÖFFENTLICHTE KONGRESSBEITRÄGE

PM_PH_1.31 Seite 167

Thyronamine - a novel hormone controlling glucose metabolism

Braulke, Luzie ; Klingenspor, Martin & Heldmaier, Gerhard

Philipps-University Marburg, Department of Biology, Marburg, Germany

3-Iodothyronamine is a derivate of thyroid hormone (TH) occuring naturally as a result of deiodination and decarboxylation. In vitro it is a potent agonist of the G protein-coupled trace amine receptor TAR1. The physiological role of thyronamine is not known. Treatment of mice with thyronamine caused a profound hypothermia, bradycardia and reduced cardiac output, effects which are opposite to the role of TH. Since the Djungarian hamster Phodopus sungorus shows spontaneous hypothermia and hypometabolism in the winter acclimatized state we investigated the influence of thyronamine on metabolic rate (MR), body temperature (T_b) and respiratory quotient (RQ) in this species. Thyronamine treated hamsters showed a rapid decrease in MR and T_b, and displayed an instant reduction in RQ from 0.92 to 0.7 for at least ten hours and then the hamsters returned to their normal RQ of 0.92. The massive decrease in RQ concludes that metabolic pathways are rerouted from carbohydrate to lipid utilisation in response to thyronamine. This assumption is supported by the fact that thyronamine treated animals developped ketonuria 12 hours post-injection. We propose that thyronamine has the potential to play a critical role for the balance between glucose and lipid utilization in vivo.

ACTION OF 3-IODOTHYRONAMINE: CAN TORPOR BE INDUCED BY METABOLIC INHIBITORS?

Braulke, Luzie & Heldmaier, Gerhard

Philipps-University Marburg, Marburg, Germany

3-Iodothyronamine (T1AM) is a derivative of thyroid hormone (TH) occurring naturally as a result of deiodination and decarboxylation. In vitro it is a potent agonist of the G protein-coupled trace amine receptor TAR1. The physiological role of thyronamine is unknown. Treatment of mice with thyronamine caused a profound hypothermia, bradycardia and reduced cardiac output, effects which are opposite to the role of TH and resemble those during torpor and hibernation. This suggests that thyronamine may act as a metabolic inhibitor during torpor. Therefore we investigated the influence of thyronamine on metabolic rate (MR), body temperature (T_b) and respiratory quotient (RQ) in the natural torpidator *Phodopus sungorus* and compared this response with natural torpor bouts. Thyronamine treated hamsters showed a rapid decrease in MR and T_b, and displayed an instant reduction in RQ from 0.92 to 0.7 for at least ten hours, indicating a rapid switch from carbohydrate to lipid utilization. The rates of entrance into and recovery from this hypometabolic state and especially the massive and long lasting decrease in RQ in response to thyronamine do not reflect the changes observed during spontaneous daily torpor. Furthermore, the effects caused by thyronamine were more pronounced in summer acclimated hamsters as compared to winter acclimated hamsters, although summer acclimated hamsters never become torpid when fed ad libitum. We conclude that thyronamine simply blocks the utilization of glucose but does not activate the same pathways for metabolic depression which are involved in spontaneous daily torpor.

P PH.21 – EN Seite 196

The onset of spontaneous daily torpor in *Phodopus sungorus* depends upon the sympathetic nervous system

Luzie Braulke, Gerhard Heldmaier

Biologie/ Tierphysiologie, Philipps-Universität Marburg

Entrance into torpor is characterized by a rapid reduction of metabolic rate, heart rate and ventilation. It is still an open question how the autonomic nervous system is involved in the initiation of a torpor bout. The large depression of cardiac and respiratory activity suggests a dominance of parasympathetic activity. If this is true a vagal blockade by Atropine should inhibit or decrease spontaneous torpor occurrence. If primarily the SNS is involved, sympathectomy by 6-Hydroxydopamine (6-OHDA) should have the same effect. Hence we compared the influence of Atropine and 6-OHDA on torpor behaviour. Body temperature of *Phodopus sungorus* was recorded continuously. As soon as hamsters displayed torpor regularly either PNS or SNS was blocked by either of the two antagonists. Vagal blockade by s.c. implants delivering Atropine for 21 days did not affect the occurrence of daily torpor at all. The sympathetic inhibition by 6-OHDA injection however resulted in a complete disappearance of ultradian rhythmicity and torpor for at least four days. These results conclude that the onset of daily torpor requires an intact signalling of the sympathetic nervous system.

4. DANKSAGUNG

Die Seiten 86-87 (Danksagung) enthalten persönliche Daten. Sie sind deshalb nicht Bestandteil der Online-Veröffentlichung.

Die Seiten 86-87 (Danksagung) enthalten persönliche Daten. Sie sind deshalb nicht Bestandteil der Online-Veröffentlichung.

5. LEBENSLAUF

Die Seiten 88-89 (Lebenslauf) enthalten persönliche Daten. Sie sind deshalb nicht Bestandteil der Online-Veröffentlichung.

Die Seiten 88-89 (Lebenslauf) enthalten persönliche Daten. Sie sind deshalb nicht Bestandteil der Online-Veröffentlichung.

6. EIGENANTEIL

Ich versichere, daß ich meine Dissertation

Regulation des Energiehaushalts von Kleinsäugern unter besonderer Berücksichtigung saisonaler Stoffwechseladaptionen des Dsungarischen Zwerghamsters, *Phodopus sungorus*.

selbständig, ohne unerlaubte Hilfe angefertigt und mich dabei keiner anderen als der von mir ausdrücklich bezeichneten Quellen und Hilfen bedient habe.

Die Dissertation wurde in der jetzigen oder einer ähnlichen Form noch bei keiner anderen Hochschule eingereicht und hat noch keinen sonstigen Prüfungszwecken gedient.

Marburg, den 12. Juli 2010 _____

(Luzie Julia Braulke)